Phase Separation Dynamics of Aqueous Thermo-responsive Polymer Solutions Studied by a Laser-induced Temperature Jump Method Combined with Transient Photometry

（レーザー温度ジャンプ型過渡透過光計測法による
温度応答性高分子水溶液の相分離ダイナミクスの研究）

By

Takanori Tada

A dissertation submitted in partial fulfillment of the requirements for the degree of
Doctor of Philosophy

Graduate School of Chemical Sciences and Engineering

HOKKAIDO UNIVERSITY
Sapporo, Japan

March 2016

Acknowledgements

I am extraordinarily fortunate in the support I have received on the path to this accomplishment.

The present study has been carried out under the direction of Dr. Noboru Kitamura, professor at the Laboratory of Analytical Chemistry and Photochemistry, Graduate School of Chemical Sciences and Engineering, Hokkaido University.

I would like to express my sincere appreciation to my supervisor, Dr. Noboru Kitamura for his guidance, suggestions of problems, numerous valuable comments, and his critical reading of the manuscript. I deeply appreciate the working environment that he provided and educating me during April 2011 – March 2016.

I am likewise grateful to Dr. Kazuki Sada, professor at the Laboratory of Material Chemistry, Graduate School of Chemical Sciences and Engineering, Dr. Yasuchika Hasegawa, professor at the Laboratory of Advanced Materials Chemistry, Graduate School of Engineering, Hokkaido University and Atsushi Miura, associate professor at the Laboratory of Analytical Chemistry and Photochemistry, Graduate School of Chemical Sciences and Engineering, Hokkaido University for their valuable comments and suggestions for the improvement of the thesis.

I am also deeply grateful to Dr. Yasuyuki Tsuboi, Professor at the Laboratory of Analytical Chemistry, Department of Chemistry, Graduate School of Science, Faculty of Science, Osaka City University. He continuously guided and encouraged me throughout the thesis. I will forever appreciate his mental support and opportunities to meet with impressive researchers.

Many thanks to the following people and organization for helping the thesis:

Prof. Kazuki Sada and Dr. Shogo Amemori, Graduate School of Chemical Sciences and Engineering, Hokkaido University, for measurements of number average molecular weight and their distribution of PNIPAM samples.

Prof. Sadamu Takeda, Dr. Yoshiyuki Kageyama and Mr. Tomonori Ikegami, Graduate School of Chemical Sciences and Engineering, Hokkaido University, for measurements of heat capacity changes during phase transition/separation of aqueous PNIPAM solutions.

Prof. Koichi Ute and Dr. Tomohiro Hirano, Graduate School of Advanced Technology and Science, Institute of Technology and Science, Faculty of Engineering, Tokushima University, for providing syndiotactic-rich PNIPAM samples and helpful discussion on the phase separation mechanisms of aqueous stereo-controlled PNIPAM solutions.

Dr. Yukiteru Katsumoto, Department of Chemistry, Faculty of Science, Fukuoka University, for providing isotactic-rich PNIPAM samples and valuable feedback in the phase separation mechanisms of aqueous stereo-controlled PNIPAM solutions.

Prof. Johan Hofkens, Prof. Hiroshi Uji-i, Dr. Karel Goossens, Department of Chemistry, Faculty of Science, KU Leuven, for their kind acceptance of an immature master student to study at Hofkens's laboratory and measurements of microscopic polymer structures in the solutions of aqueous PNIPAM solutions.

A Research Fellowship of the Japan Society for the Promotion of Science for Young Scientists and Japan Student Services Organization Short Visit Program financially supported me.

I would like to thank the members of the Laboratory of Analytical Chemistry and Photochemistry, Graduate School of Chemical Sciences and Engineering, Hokkaido University and the Advanced Laboratory of Analytical Chemistry, Department of Chemistry, Graduate School of Science, Faculty of Science, Osaka City University for sharing their ideas and supporting me. In particular, I thank Dr. Tatsuya Shoji for the stimulating discussions, daily care, and all the fun we have had in the last six years. For the last two years, my sincere thank also goes to Dr. Taka-aki Asoh, who gave me precious advice regarding my study and my daily life.

Most importantly, I owe my deepest gratitude to my family for their endless support and constant encouragement. They always treat me with their gentle patience.

Abstract

Poly(*N*-isopropylacrylamide) (PNIPAM) is a well-known thermoresponsive polymer. In aqueous solution, PNIPAM shows drastically change of its conformation upon temperature elevation above a critical solution temperature. Such conformational changes in solution directly lead to changes in the solubility of the polymer, resulting in phase separation of the polymer solution. Although there has been wealth of observations of the structural changes upon thermal phase separation of an aqueous PNIPAM solution, little is known about the dynamic behaviors of phase separation such as the time scales of the phase separation processes. For precise understanding of fundamental mechanisms of phase separation of aqueous thermoresponsive polymer solutions, it is indispensable to reveal the phase separation dynamics quantitatively. Also, such dynamic study will promote applications of the polymers to smart materials such as drug delivery systems. In this thesis, the phase separation rates in aqueous PNIPAM solutions and the factors regulating the phase separation rate are investigated by means of a laser-induced temperature jump technique combined with transient transmittance-photometry techniques. The phase separation rate of an aqueous PNIPAM solution was investigated as a function of the following three important factors: the PNIPAM concentration, the molecular weight of PNIPAM, and the stereoregularity of PNIPAM. Three main conclusions in the present study are summarized:

1) Phase separation of an aqueous PNIPAM solution is accelerated with increasing the polymer concentration (chapter 3).
2) There is an optimum molecular weight of PNIPAM for rapid phase separation in an aqueous solution (chapter 3).
3) Phase separation in an aqueous solution is accelerated by setting a high stereoregularity of PNIPAM (chapter 4 and 5).

The dynamic aspects of the phenomena are well correlated with the satic aspects. Entanglements of the polymer chains formed at a high polymer concentration play an important role in the phase separation dynamics: the phase separation time constant levels-off at a certain concentration value. Phase separation of aqueous highly syndiotactic-rich PNIPAM solutions becomes considerably fast when the polymer chains are entangled below the critical temperature. Cooperative dehydration of PNIPAM in an aqueous solution, defined by simultaneous dissociation of the bound water molecules from the sequential polymer chains, and subsequent formation of intrapolymer hydrogen bondings also result in rapid phase separation of an aqueous highly syndiotactic-rich PNIPAM solution. Furthermore, it has been demonstrated that formation of microscopic inter-chain networks even below the critical temperature in an aqueous isotactic-rich PNIPAM solution is the origin of rapid phase separation in the solution.

By accumulating the knowledge about the phase separation dynamics as a function of the primary structures of a polymer in solution, it would be possible to develop a new model predicting the phase separation rate based on the fundamental structural and solution properties of a thermo-responsive polymer. The present study and further investigation of the phase separation dynamics as a function of various primary factors controlling phase separation will open new channels toward the design and development of stimuli-responsive-polymer-based smart materials.

Table of Contents

List of Tables

List of Figures

List of Abbreviations

ANS	8-anilino-1-naphthalensufonic
CCD	Charge-coupled-device
cw	continuous wave
DLS	Dynamic light scattering
DPSS	Diode pumped solid state
DSC	Differential scanning calorimetry
FCS	Fluorescence correlation spectroscopy
HD-TG	Heterodyne transient grating
IR	Infrared
LCST	Lower critical solution temperature
N. A.	Numerical aperture
PDEA	Poly(*N*,*N*-diethylacrylamide)
PEPD	1-Phenylethyl phenyldithioacetate
PMVE	Poly(methylvinylether)
PNIPAM	Poly(*N*-isopropylacrylamide)
PNNPAM	Poly(*N*-*n*-propylacrylamide
RAFT	Reversible addition-fragmentation chain transfer
SEC	Size exclusion chromatography
SMI	Single molecule fluorescence imaging
TIRF	Total internal reflection
T_c	Clouding point
UCST	Upper critical solution temperature
VDP	(3-(2-propenyl)- 9-(4-*N*,*N*-dimethylaminophenyl)phenanthrene
YAG	Yttrium aluminum garnet

Chapter 1| Back ground and introduction

1.1 General introduction

The impact of synthetic organic polymers on our everyday lives is not to be overestimated, since these are, in many cases, indispensable and are widely used in automobiles, electronics, buildings, textiles, food packaging, (bio-) medical applications, personal care products, sports leisure items [1]–[8], and so on. The properties of a synthetic organic polymer depend on its molecular weight, stereoregularity and its higher-order structure, which originates from monomers with specific chemical structures [9]–[11]. The higher-order structures of some polymers with specific primary structures can be varied by external stimuli such as temperature, light, electric or magnetic fields, or ionic strength [12]–[17]. Among the available stimuli-responsive polymers, thermoresponsive polymers have attracted much attention because of the ease with which their chemical and physical properties can be finely tuned.

Thermoresponsive polymers are defined as those whose conformation changes radically in response to a small change in temperature. Generally, such conformational changes in solution lead directly to changes in the solubility of the polymer, resulting in phase separation of the polymer solution [17]–[21]. Such macroscopic changes in thermoresponsive polymers have prompted the development of intelligent or smart materials [22]–[29].

Poly(*N*-isopropylacrylamide) (PNIPAM) whose structure is shown in Figure 1-1 is a well-known thermoresponsive polymer. Although there has been a wealth of observations of the structural changes upon thermal phase separation in aqueous PNIPAM solutions, little is known about the dynamic behavior of phase separation. As an example, even the time scales for phase separation processes in aqueous PNIPAM solutions still remain unclear because of the lack of an experimental technique to make measurements on these time scales. For a precise understanding of the fundamental mechanisms of phase separation in aqueous thermoresponsive polymer solutions, a quantitative evaluation of the phase separation dynamics is absolutely necessary. Also, such dynamic studies will promote applications of the polymers to smart materials such as artificial

organs [30], actuators [31] and drug delivery systems [25], [32]–[38]. In this thesis, the phase separation rates in aqueous thermoresponsive polymer solutions and the factors regulating the phase separation rate are investigated by means of a laser-induced temperature (T)-jump technique combined with transient transmittance-photometry techniques.

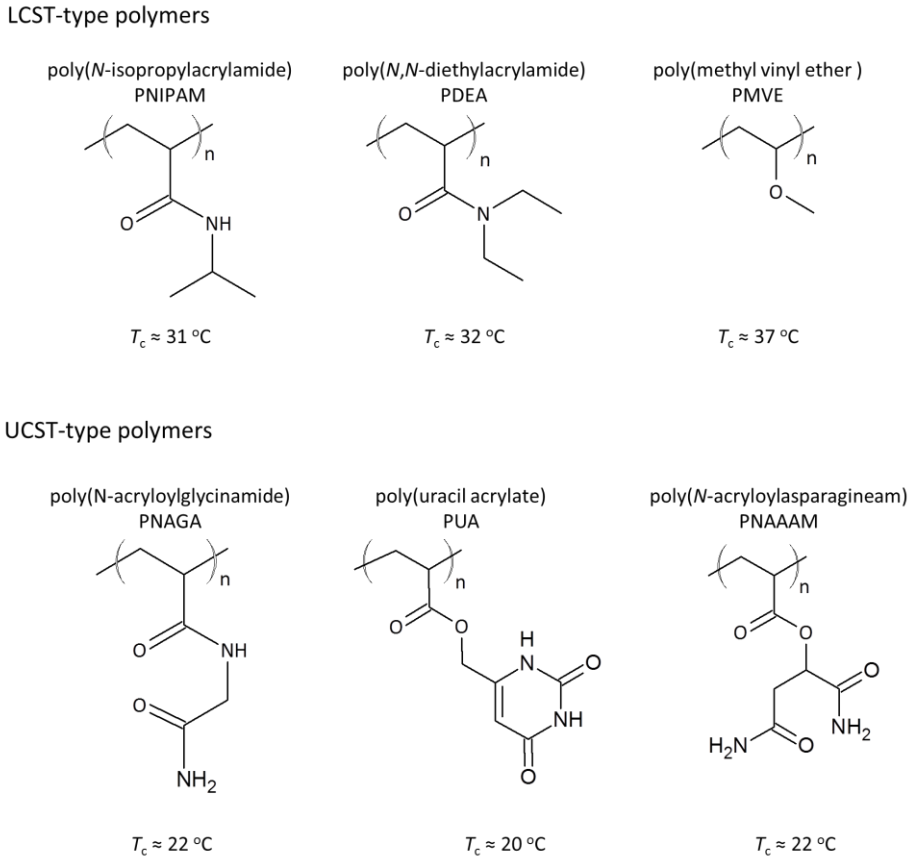

Figure 1-1. Typical examples of thermoresponsive polymers exhibiting lower critical solution temperature (LCST)-type and upper critical solution temperature (UCST)-type behavior in water.

1.2 LCST and UCST behavior

1.2.1 Turbidity change

Whereas large parts of small molecules are soluble in solvents at ambient temperature, some synthetic polymer solutions exhibit thermally induced phase separation as shown in Figure 1-2. Typical examples of such synthetic organic polymers are displayed in Figure 1-1 [17], [21], [39]–[43]. Some thermoresponsive polymers, such as PNIPAM, undergo phase transitions from a coil structure to a

globular structure at certain temperatures. In solution, such polymers have a lower critical solution temperature (LCST: T_{LCST}). Below T_{LCST}, the polymer solution is transparent since the coil structure of the polymer is likely to be soluble in solution, while the solution becomes turbid above T_{LCST} owing to the low solubility of the globular structure of the polymer in solution. Another type of thermoresponsive polymer in solution exhibits an upper critical solution temperature (UCST: T_{UCST}). In contrast to LCST-type polymers, the globular structures of UCST-type polymers in solution are insoluble below T_{UCST} while those with coil structures are soluble above T_{UCST}. Therefore, the LCST or UCST behavior of a polymer solution can be easily confirmed by the turbidity of the solution as shown in Figure 1-2.

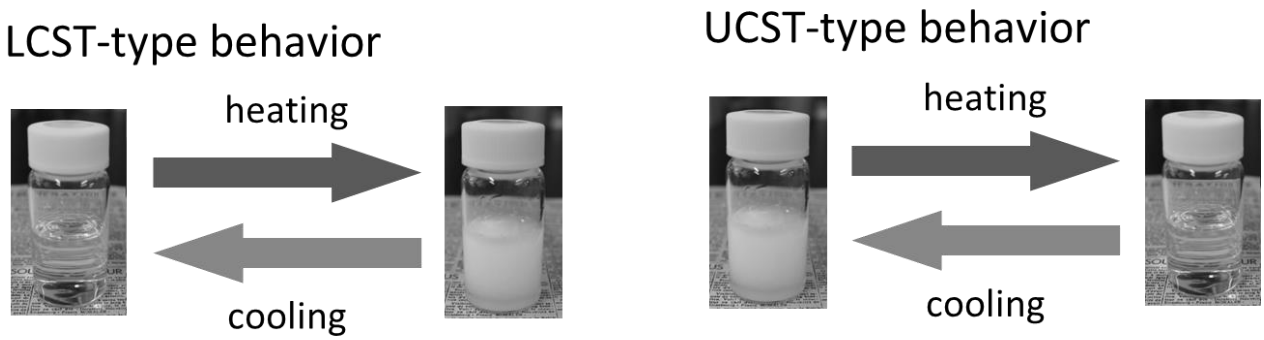

Figure 1-2. Changes in optical transparency of aqueous LCST-type and UCST-type polymer solutions upon heating and cooling.

1.2.2 Classification of thermoresponsive polymers

The LCST behavior of a polymer solution can be viewed phenomenologically as the inverse of the UCST behavior and both behaviors are characterized by polymer chain collapses or phase separation with a change in temperature. However, the physical basis of LCST-type phase separation is quite different from that of UCST-type phase separation. According to the second law of thermodynamics, the most stable phase has the lowest Gibbs free energy G at a given temperature T and pressure P. Three terms contribute to the change in the Gibbs free energy ΔG_m when mixing a polymer with a solvent, the change in the internal energy ΔU_m, which is related to the intermolecular attraction, the volume of the mixture ΔV_m, and the entropy change ΔS_m upon mixing. Thus

$$\Delta G_m = \Delta U_m + P\Delta V_m - T\Delta S_m \qquad (1.1)$$

$$= \Delta H_m - T\Delta S_m \qquad (1.2)$$

where ΔH_m is the enthalpy change upon mixing. Whereas UCST phase separation is explained by the enthalpy change, the LCST phase separation is driven by the entropy change.

As shown in Figure 1-1, LCST-type and UCST-type thermoresponsive polymers have different structural features. For example, non-ionic amphiphilic polymers such as poly(*N*-isopropylacrylamide) (PNIPAM) [17], [39], poly(methylvinylether) (PMVE) [44]–[46] and poly(*N*,*N*-diethylacrylamide) (PDEA) [47]–[53] are well-known as LCST-type thermoresponsive polymers. The hydrophilic part in the amphiphilic polymer interacts strongly with water molecules and increases its solubility in water. The hydrophobic part contributes to the negative entropy change upon mixing, and the hydrophobic attraction between the hydrophobic parts plays a role in minimizing the entropic loss of the system. The total negative entropy change upon heating becomes larger than the enthalpy of the hydrogen bonding, and the change in ΔG_m becomes positive, causing shrinking of the polymer chain and phase transition. Therefore, the balance between the hydrophilic part for solubilization and the hydrophobic part for aggregation is important to the LCST-type phase separation behavior in water. The change in the hydrophilic-hydrophobic energy balance upon heating causes phase separation of the solution by dehydration of the polymer.

The hydrophilic-hydrophobic energy balance depends on the stereoregularity of the polymer. A schematic illustration for the stereoregularities of vinyl polymers of the type $[(CH_2)\text{-}(CHR)]_n$ is shown in Figure 1-3. As shown in Figure 1-3a, if the skeletal bonds are in the *trans* conformation and lie in the plane of the paper, the *R* groups on successive asymmetric carbons projecting on the same side define a meso diad and perpetuation of this configuration leads to an isotactic polymer. Assignment of a configuration *d* to the asymmetric carbons in this figure is arbitrary. If one of the asymmetric carbons of the diad is in the *d* configuration and other is in *l*, the diad is racemo (Figure 1-3b) and regular alternation of the *d* and *l* centers along the chain defines a syndiotactic polymer. Random occurrence of *d* and *l* centers along the chain leads to an atactic polymer, as shown in Figure 1-3c. The effect of stereoregularity on the properties of polymers has

long been recognized, with such basic differences as in the glass transition temperature [54]–[56], crystallization [57]–[60], and solubility [61]–[64].

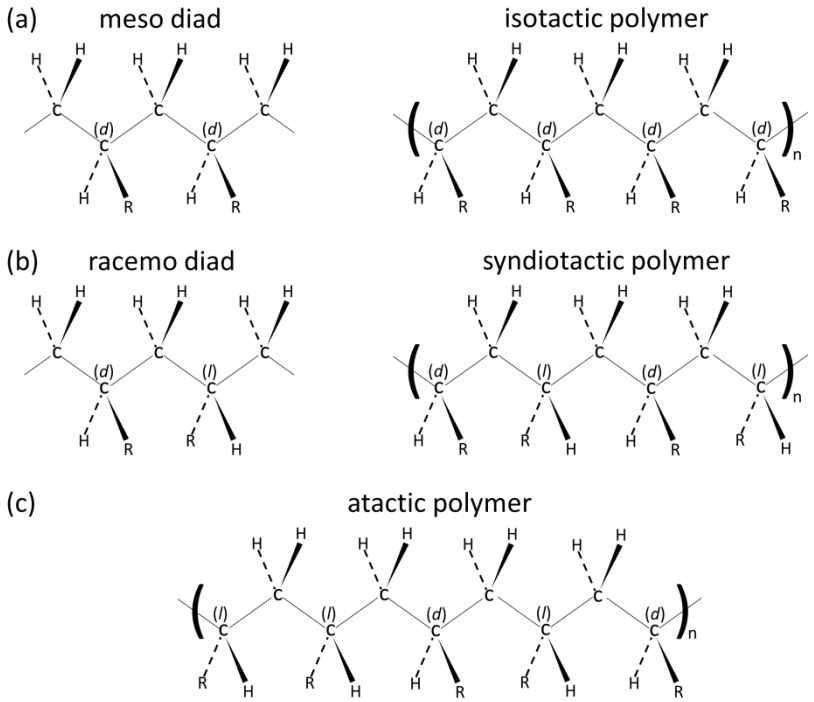

Figure 1-3. Schematic illustration of the definition of the stereoregularity of an asymmetric chain of the type $[(CH_2)\text{-}(CHR)]_n$.

On the other hand, UCST-type thermoresponsive polymers in solution show strong polymer-polymer interactions on the basis of hydrogen bonding and/or Coulomb interactions in many cases. According to eq. 1-2, UCST-type polymers should have positive ΔH_m and ΔS_m values. This suggests that stronger polymer-polymer and solvent-solvent interactions compared to polymer-solvent interactions are required for positive ΔH_m. The hydrophobic part, which induces the large negative entropic change upon mixing, is less dominant for UCST-type polymers showing positive ΔS_m. Therefore, UCST-type polymers generally have hydrophilic characteristics and strong hydrogen bond forming groups such as amide [40], carboxylic acid [41], ureido [42], and uracil groups [43]. Hydrogen bonds and electrostatic interactions are stabilized in less polar solvents. Thus, UCST behavior is scarcely observed in aqueous media (especially under physiological conditions), because both the hydrogen bonds and electrostatic interactions between the polymer chains are destabilized by water and salts. Therefore, polymers exhibiting LCST-type behavior have been

studied more extensively compared to those exhibiting UCST-type behavior.

1.2.3 Structural changes upon phase separation in an aqueous solution of a LCST-type polymer

The complete LCST-type phase separation process observed typically for an aqueous PNIPAM solution consists of 4 steps as shown in Figure 1-4. i) At (or below) room temperature, the polymer chains are homogeneously dissolved in water, taking hydrated coiled-structures [65]–[73] and, hence, the solution is transparent. ii) Upon a temperature rise above the critical temperature (≈ 32 °C), the polymer chains become dehydrated by dissociation of the hydrogen bonds [65]–[68], [70]–[72], iii) leading to a phase transition from coil to globular structures (coil-globule transition) [41], [74]–[76]. This critical temperature is called the lower critical solution temperature (LCST). iv) The globules aggregate with one another due to the hydrophobic interaction and free mutual diffusion in water [77]–[80]. Consequently, the solution undergoes phase separation into polymer rich domains and water rich domains [66], [70]. This phase-separated solution is turbid due to light scattering by such micro-domains.

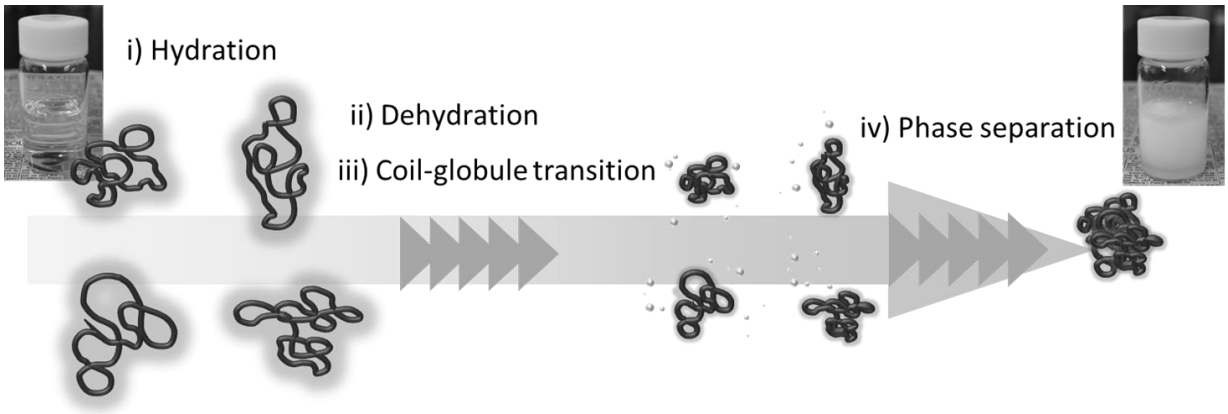

Figure 1-4. Schematic illustration of the phase separation mechanism of an aqueous PNIPAM solution.

1.3 Studies on the phase separation dynamics of aqueous solutions of thermoresponsive polymers

1.3.1 Studies on the phase separation dynamics with low time resolution

The phase separation mechanisms of aqueous PNIPAM solutions have been extensively studied using various methods to reveal the static properties of polymers, such as structural changes to the polymer chain. In contrast to the wealth of observations underlying the broad structural changes of the polymer chain, there have been fewer reports on the dynamics of the phase separation processes.

Van Mele et al. investigated the phase separation dynamics of an aqueous PNIPAM solution in a modulated temperature DSC study [81]. They measured the time necessary for the formation of an aggregate of PNIPAM upon a temperature change. They indicated that the phase separation processes took place on time scales of <100 s and that the phase mixing, which they defined as the phase transition from a dehydrated aggregate to a hydrated coil upon cooling of the solution below the LCST, was slower than that of the phase separation. Yushmanov et al. studied the phase separation dynamics of an aqueous PNIPAM solution based on ^{1}H NMR spectroscopy combined with a T-jump technique [82]. Their study demonstrated that the coil-globule transition and subsequent interpolymer aggregation upon heating was completed within a few seconds. Although their study provided an insight into the phase separation dynamics, the time resolution of the experimental technique was not sufficiently high to follow the phenomena, because the T-jump was done by electrical heating and was of the order of 350 ms. Liu et al. investigated the dynamics of the coil-globule transition of an aqueous solution of PNIPAM copolymerized with 4-(1-pyrenyl) butyl acrylate using a stopped-flow technique [83]. They found that the chain collapse upon phase transition proceeded in two steps: First, formation of small locally collapsed nuclei on the chain, and second, subsequent compaction of the chain. These steps were characterized by two time constants, $\tau_{fast} \approx 12$ and $\tau_{slow} \approx 270$ ms, respectively. Note that the stopped-flow technique has been widely used to study the kinetics of micellar formation and protein folding with a time resolution of

a few milliseconds, though, it cannot detect a chemical event faster than ≈ 1 ms. In order to investigate the phase separation processes of an aqueous PNIPAM solution, the time resolution of the technique should be much shorter than milliseconds.

1.3.2 Studies on phase separation dynamics based on a laser-induced T-jump technique with high time resolution

A few studies have succeeded in measuring phase separation dynamics based on laser-induced T-jump techniques with high time resolutions. Suzuki and Tanaka demonstrated that the thermoresponsive volume phase transition of cross-linked PNIPAM could be induced by UV light irradiation through the absorption of a 488 nm laser beam by a dye chromophore covalently linked to the polymer backbone [84]. Tsuboi et al. developed a laser-induced temperature-jump technique, by which phase separation of an aqueous PNIPAM solution was triggered by irradiation of an infrared pulsed laser beam to the sample solution [85], [86]. This technique is particularly important since the time resolution of the method is as high as ≈ 10 ns as described in §2.1.1. Furthermore, it can induce phase separation of an aqueous PNIPAM solution without the need of photosensitive dopants (chemical reagents) for light absorption.

A few groups have also developed T-jump techniques with high time resolutions using photo-thermal sensitizers (dye) as light absorbers. Katayama et al. employed a laser-induced T-jump technique combined with a heterodyne transient grating (HD-TG) method to investigate the phase separation and phase mixing processes of aqueous PNIPAM solutions [87]. The HD-TG method detects the photophysical dynamics of a solution, such as the thermal diffusion, via refractive index changes of the solution. They estimated the time constants for the coil-globule transition and the phase separation to be ≈ 100 μs and several tens of ms, respectively. It should be noted that the time scales for thermal diffusion and coil-globule transition are similar to each other, leading to low accuracy for the time constant. Wu et al. also used a laser-induced T-jump method combined with fluorescence spectroscopy [88], [89]. They employed 8-anilino-1-naphthalensufonic acid as a

fluorescent hydrophobic/hydrophilic probe [90], [91] and observed transient changes in the *fluorescence intensity* upon a T-jump, following which they proposed that the phase transition/separation processes involved multiple steps: the formation of pearls (i.e., locally contracting segments) with a time constant (τ_{pearls}) of ≈ 0.02 ms and merging/coarsening of the pearls with a time constant, $\tau_{merging}$ ≈ 0.2 ms. Figure 1-5 shows schematic illustrations of their study and the mechanism of the coil-globule transition. Although in their studies they estimated the time constants of the multi-stepwise coil-globule transition, their conclusion is still controversial, since transient fluorescence intensity changes are affected by various factors such as the temperature rise and light scattering and, accordingly, it is difficult to interpret the origin of the signal changes [92]–[94].

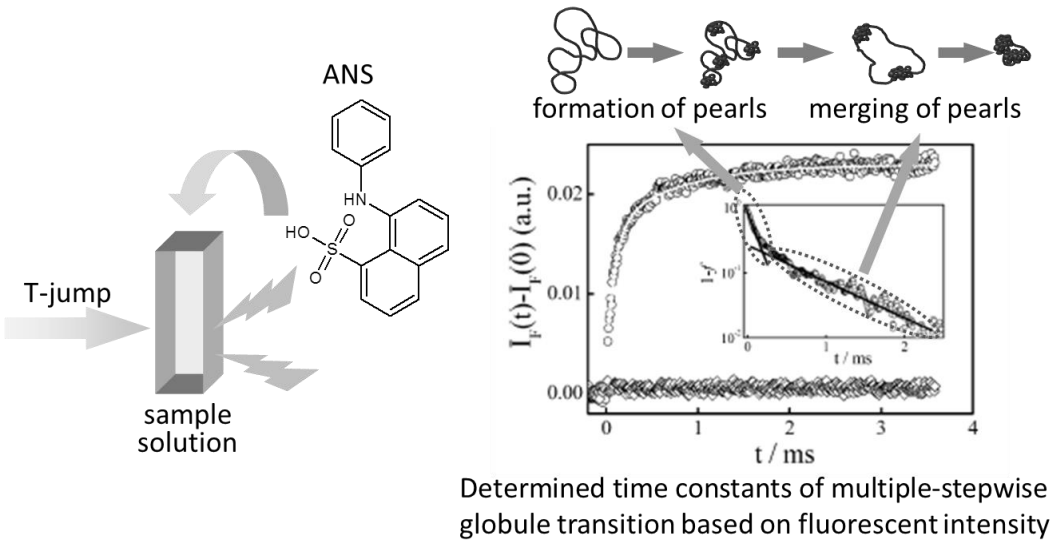

Figure 1-5. Schematic illustration of a laser-induced T-jump study on the coil-globule transition in an aqueous PNIPAM solution based on the fluorescence intensity change of 8-anilino-1-naphthalensufonic acid (ANS) added to the solution upon transition [88], [89]. The graph shows the time dependences of the fluorescence intensity changes of ANS after a T-jump with and without PNIPAM. The inset shows a semilogarithmic plot of (1 - *f*) vs time (t), where *f* is defined as $[I_F(t) - I_F(0)]/[I_F(\infty) - I_F(0)] = 1 - A \exp(-t/\tau_{fast}) - (1 - A) \exp(-t/\tau_{slow})$. Reprinted with permission from the American Chemical Society.

On the other hand, Tsuboi et al. developed two techniques based on a laser-induced T-jump technique, by which one can determine the time constants of the coil-globule transition[85] and the phase separation of aqueous thermoresponsive polymer solutions [86]. The main advantage of the

technique is the clarity of the origin of the signals: the technique detects the dynamic Stokes shift of a fluorescence probe (Figure 1-6) or transient changes in the optical transmittance (Figure 1-7) caused by the coil-globule transition or the phase separation of aqueous thermoresponsive polymer solutions, respectively. As shown in Figure 1-7, in practice, an aqueous solution absorbs infrared light pulses (λ = 1200 nm) through the overtone band of the O-H stretching vibrations of water and, accordingly, the temperature of the irradiated volume in the sample solution can be raised within the time scale of the incident laser pulse width: nanosecond time scale ($\approx$ 10 ns). In this system, a representative temperature rise (ΔT) is 0.35 K at a laser fluence of 0.10 J cm^{-2} as estimated on the basis of the absorption of infrared laser light at 1200 nm. The laser pulse at 1200 nm directly excites the vibrational mode (O-H) of water molecules, and the temperature is raised by vibrational relaxation.

$$\Delta T = (I_{IR}/cL)(1 - e^{-2.303\alpha L}) \qquad (1\text{-}3)$$

In eq. (1-3), I_{IR} is the laser fluence ($J \cdot cm^{-2}$), c is the heat capacity of the medium ($J \cdot cm^{-3} \cdot deg^{-1}$), L is the heating path length, and α is the medium's absorbance per centimeter. Here, c = 4.2 $J \cdot cm^{-3} \cdot deg^{-1}$, L = 0.10 cm, I_{IR} = 0.10 J cm^{-2}, and α = 1.1 cm^{-1} [95]. The technique induces phase separation of an aqueous PNIPAM solution by changing the temperature of the sample solution.

Based on laser T-jump techniques such as this, Tsuboi et al. developed two methodologies. One is transient fluorescence spectroscopy (Figure 1-6). A fluorescence probe (3-(2-propenyl)-9-(4-*N*,*N*-dimethylaminophenyl)phenanthrene, VDP) with a spectrum that is very sensitive to the microenvironment is copolymerized with NIPAM (p(VDP-*co*-NIPAM)) [80], [96], [97]. The coil-globule transition of an aqueous p(VDP-*co*-NIPAM) (M_w = 30,000) solution changes the microenvironment around the probe. By observing the dynamic Stokes shifts of the fluorescence probe, they determined the time constant of the coil-globule transition of the solution to be 35 μs.

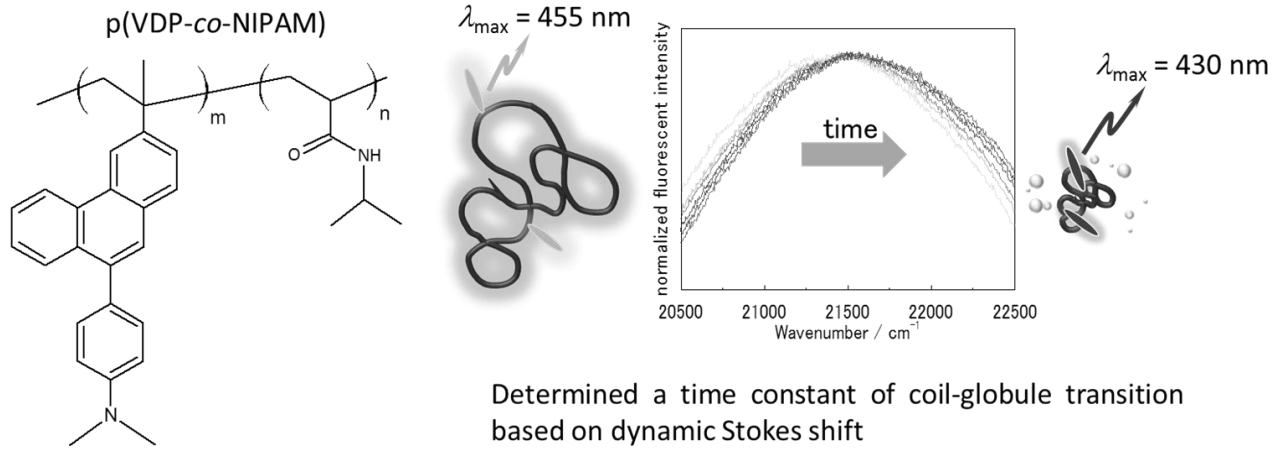

Figure 1-6. Structure of p(VDP-*co*-NIPAM) and microsecond-time-resolved dynamic Stokes shift of the fluorescence in an aqueous p(VDP-*co*-NIPAM) solution (1.0 wt.%) after a T-jump. The direction of the temporal evolution is indicated by the arrows in the figure. Reprinted with permission from Elsevier.

The other technique is the T-jump method combined with transient transmittance-photometry. This technique enables one to measure transient changes in optical transmittance caused by the turbidity change upon thermal phase separation of an aqueous PNIPAM solution. Based on the technique, one can determine the time constant of the phase separation (τ_{ps}) with high accuracy: several ms ~ several hundreds of ms. On the basis of these two techniques, Tsuboi et al. successfully observed the dynamic behaviors of the phase transition and phase separation processes of an aqueous PNIPAM solution separately in different time domains.

1.4 The aim of the thesis

The aim of this thesis is to identify the factors regulating the phase separation rate of aqueous thermoresponsive polymer solutions. To understand the fundamental mechanisms of phase separation, it is necessary to have a precise knowledge of both the static and dynamic aspects of the phenomena and to correlate them with each other. In this thesis, the phase separation rates of aqueous PNIPAM solutions are studied as a function of the following three important factors: the concentration, the molecular weight of the polymer, and the stereoregularity of PNIPAM. Their roles in controlling the phase separation behavior are studied using dynamic light scattering,

differential scanning calorimetry, and a single molecule fluorescence imaging technique. The experimental results obtained in this study will offer a better understanding of the phase separation dynamics and mechanisms. Furthermore, the study will provide a new avenue for the design and development of thermoresponsive-polymer-based smart materials whose response can be controlled via the fundamental properties of the polymers and polymer solutions.

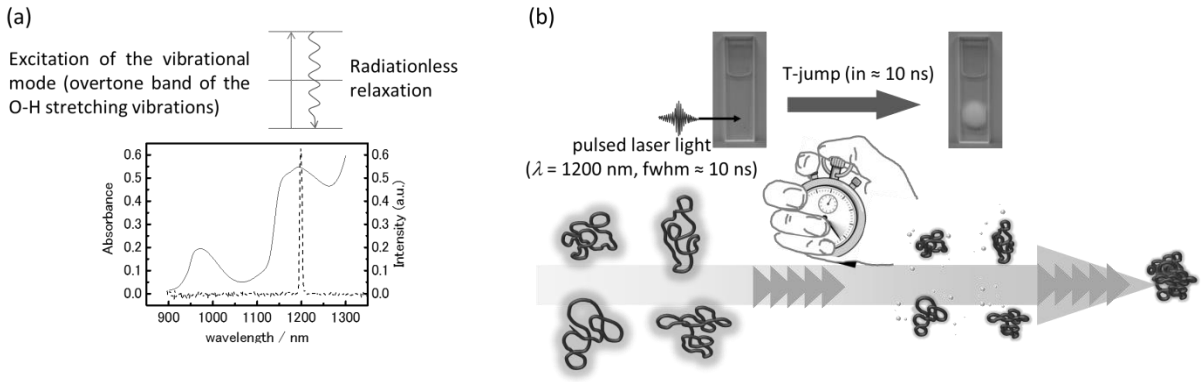

Figure 1-7. (a) Infrared absorption spectrum of water (solid line) and laser spectrum used in this thesis (dashed line) (Spectra Physics, PRO-130-10, λ = 1200 nm, fwhm ≈ 10 ns). An aqueous solution absorbs 1200 nm light through the overtone band of the O-H stretching vibrations of water and accordingly the temperature of the irradiated volume in the sample solution can be raised within the time scale of the incident laser pulse width: nanosecond time scale (≈ 10 ns). (b) Basic concept of the present study. Phase separation of the aqueous PNIPAM solution is triggered by irradiation with an infrared laser beam and the time constants of the phenomena are determined.

1.5 Contents of the thesis

In chapter 1, after presenting a general survey of the basic theory of LCST and UCST behaviors, the historical background of phase separation and the dynamics of aqueous PNIPAM solutions, the aim of the thesis is described.

In chapter 2, the experimental approaches are described. Two types of laser-induced T-jump technique are employed in this study. To induce photo-thermal phase separation of aqueous PNIPAM solutions, the following two techniques are applied; (i) a direct method in which water is heated by irradiating with infrared laser light and (ii) a dye-sensitized laser-heating method using a dye as a molecular heater.

In chapter 3, the effects of polymer concentration and the molecular weight of PNIPAM on

the phase separation dynamics are described. It was demonstrated that the phase separation of an aqueous PNIPAM solution is accelerated with increasing polymer concentration. Furthermore, it was revealed that there is an optimum molecular weight of PNIPAM for rapid phase separation. On the basis of evaluations of the intermolecular interactions between PNIPAM chains by dynamic light scattering measurements and the phase separation rates of polymer solutions, the phase separation behaviors are discussed in terms of a diffusion-controlled model.

In chapter 4, the phase separation dynamics of aqueous PNIPAM solutions with different polymer stereoregularities (atactic and isotactic-rich) were investigated. It was revealed that a slight increase in the isotacticity causes acceleration of the phase separation. Furthermore, the phase separation mechanisms of an aqueous isotactic-rich PNIPAM solution were revealed by means of a single molecule fluorescence imaging technique and fluorescence correlation spectroscopy. It was demonstrated that the origin of the acceleration of the phase separation is the formation of polymer networks below the LCST.

In chapter 5, the phase separation dynamics of aqueous PNIPAM solutions with different polymer stereoregularities, atactic and syndiotactic-rich PNIPAM, were investigated. The phase separation rates of aqueous highly syndiotactic-rich PNIPAM solutions become considerably faster when the solution polymer concentration is higher than a critical value. The phase separation mechanisms of aqueous syndiotactic-PNIPAM solutions are then discussed in terms of the hydrophobicity in the dehydrated state of the polymer based on the results obtained by differential scanning calorimetry and transmittance analysis as a function of temperature. The results obtained by dynamic light scattering (DLS) measurements on the polymer solutions are also discussed based on a diffusion-controlled aggregation model. These results demonstrate that the rapid phase separation of the polymer solution is due to the high hydrophobicity of the polymer chain originating from the cooperative formation of intrapolymer hydrogen bonding.

In chapter 6, a summary of the thesis and a future perspective on the phase separation dynamics of aqueous thermoresponsive polymer solutions are given.

Chapter 2| Experimental methods

2.1 Introduction

In this chapter, the experimental methods for the study on the phase separation dynamics of aqueous poly(*N*-isopropyl acrylamide) (PNIPAM) solutions are described. Two types of laser-induced temperature (T)-jump techniques were employed: (i) a direct method in which water as a solvent was heated using infrared laser light and (ii) a dye-sensitized laser-heating method using a dye as a molecular heater. The laser-induced T-jump methods mentioned above have been used to analyze the phase separation dynamics of aqueous PNIPAM solutions by observing the relaxation processes from the laser-induced heated solution to a thermally equilibrium state [98], [99]. Since heat is generated by absorption of a pulsed laser beam by water or a dye in a short time duration, the thermal relaxation processes of the solution can be observed with a high temporal resolution [98], [99]. Such techniques have been hitherto applied to the analysis of enzyme reaction mechanisms [100], protein folding–unfolding dynamics [101]–[105], and so forth [106]–[108]. A sample solution is directly heated by absorption of infrared light by water in the method (i), or indirectly heated by photo-thermal relaxation of exited dyes dissolved in a sample solution in the method (ii). If a laser pulse width is short enough, the solution temperature changes instantaneously. The heated solution temperature is relaxed to an equilibrium temperature due to thermal diffusion of heat in the solution, and the relaxation processes can be monitored in a time-resolved manner.

2.2 Experimental methods

2.2.1 Laser-induced T-jump technique combined with transient photometry

In the method (i), a 1200 nm laser pulse obtained by focusing a 1064 nm laser pulse (Spectra Physics, PRO-130-10, fwhm ≈ 10 ns) into a Raman shifter ($Ba(NO_3)_2$ crystal, Solar Laser, LZ221) was used as heating light. Since water (H_2O) has weak absorption (α: absorption coefficient ≈ 1.1 cm^{-1}) due to the overtone bands of the O–H stretching modes at λ = 1200 nm [95], a slight T-jump and subsequent homogeneous heating of a sample solution can be achieved in the irradiated

volume. Furthermore, a homogeneous T-jump is completed within the laser pulse width (≈ 10 ns), since the heating light pulse directly excites the molecular vibrations of a solvent (water). In this system, a representative temperature rise (ΔT) is 0.35 K at a laser fluence of 0.10 J cm^{-2} as estimated on the basis of absorption of infrared laser light by water at 1200 nm,

$$\Delta T = (I_{IR}/cL)(1 - e^{-2.303\alpha L}) \qquad (2\text{-}1)$$

where I_{IR} is the incident light intensity, c is the heat capacity of a medium ($J \cdot cm^{-3} \cdot deg^{-1}$), L is the length of a heating path, and α is the absorbance per centimeter of a medium. In this study, c = 4.2 $J \cdot cm^{-3} \cdot deg^{-1}$, L = 0.10 cm, I_{IR} = 0.10 J cm^{-2}, and α = 1.1 cm^{-1} [109].

In the method (ii), a small amount of crystal violet (Aldrich Co., Ltd., 0.50 mM) was added to a sample solution and a single pulse from a Nd^{3+}: YAG laser (Spectra Physics, PRO-130-10, λ = 532 nm, fwhm ≈ 8 ns) was focused to a sample cell as heating light at various fluence ranging from 0.10 to 0.48 $J \cdot cm^{-2}$. The dye molecules absorb 532 nm laser light and act as a molecular heater, converting light energy to heat with a high efficiency (≈100%) through rapid radiationless transition of the excited dye [101], [110]. The time scale for converting the light energy to the thermal energy is equal to the laser pulse width (8 ns) [101], [110]. The thermal diffusion length (l_{diff}) is given by,

$$l_{diff} = \sqrt{4Dt} \qquad 2\text{-}2$$

where D is the thermal diffusion coefficient in a medium and t is the diffusion time. In the present system, D in water is D = 0.15 $mm^2 \cdot s^{-1}$ and, therefore, l_{diff} is estimated to be l_{diff} = 70 nm within 8 ns. This value is much longer than the average distance between adjacent dye molecules in a solution (<0.2 nm). Therefore, it can be safely concluded that homogeneous heating of a sample solution is achieved before phase separation of an aqueous PNIPAM solution by using the T-jump method (ii).

In the methods (i) and (ii), a rapid T-jump is induced like a manner of a delta function in the time axis prior to phase separation of a sample solution. Therefore, the phase separation dynamics of a sample solution can be followed by the two methods. As pointed out in the relevant study [85], [87], since both methods (i) and (ii) have advantages and disadvantages when used in T-jump experiments, the two methods are employed in a complementary way in the present study as

described in chapter 5.

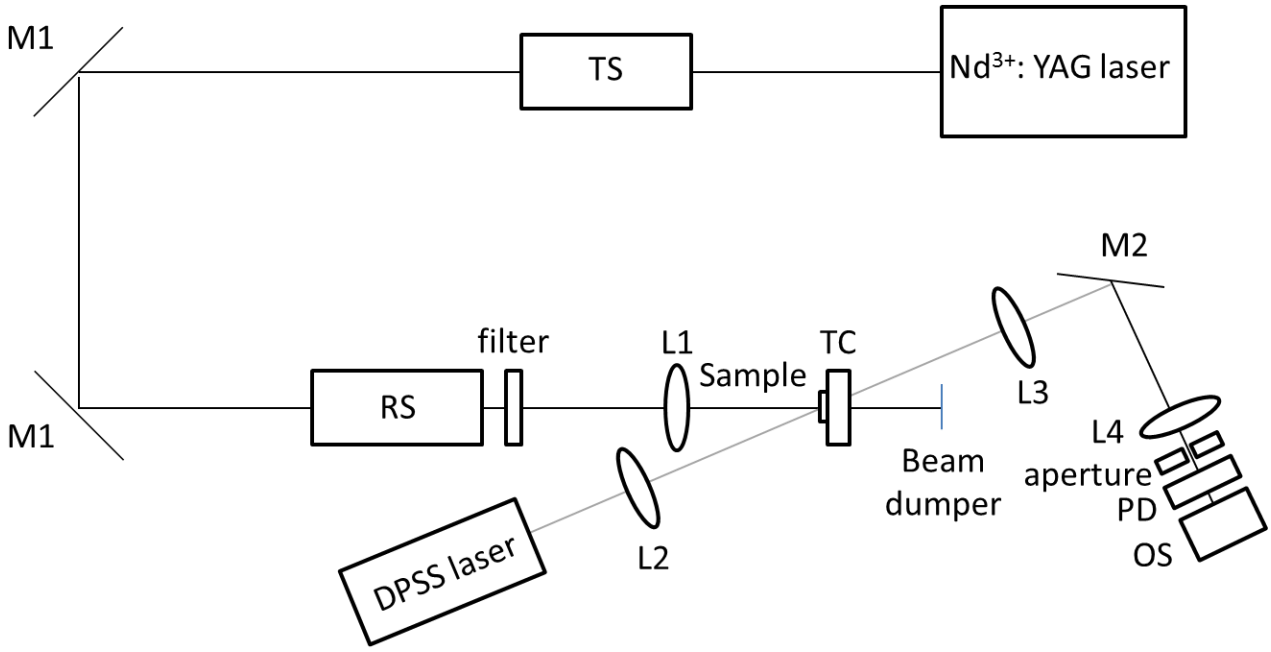

Figure 2-1. Schematic illustration of the optical setup for a laser-induced T-jump technique combined with transient photometry (method (i)). L1, L2, L3, L4; lens, M1; mirror with high reflectance at 1064 nm, M2; mirror with high reflectance at 532 nm, TS; telescope, RC; Raman shifter converting laser light from 1064 nm to 1200 nm, TC; temperature controller, PD; photodiode, OS; oscilloscope.

The instrumental setup is schematically shown in Figure 2-1. In the experiments (i) and (ii), a quartz cell with an optical path length of 1.0 mm was filled with an aqueous PNIPAM solution. The temperature of a sample solution before laser irradiation was maintained lower (0.2 K) than the cloud point (T_c) determined by the method described in §2.2.2 by using a temperature controller (Japan high tech Co., Ltd., PE-120). As probe light, the laser beam from a continuous-wave (cw) diode pumped solid state (DPSS) laser (GC Photonics Inc., GLML-30, λ = 532 nm) or cw semiconductor laser (NEOARK Co., Ltd., LDP-6935M, λ = 690 nm) in the experiment (i) or (ii), respectively, was introduced to the sample cell coaxially with the heating light beam. The diameter of heating light beam and probe light beam at the sample cell are 1.0 mm and 0.5 mm, respectively. Thus, sample is homogeneously heated in the probed area. These two laser beams were passed through an aperture and detected by using a combination of a fast response photodiode (Thorlabs,

Inc., DET210) and a digital storage oscilloscope (Teledyne LeCroy, Inc., wave Runner 104MXi, 1 GHz). In such an optical arrangement, the phase separation dynamics of a sample solution can be observed as temporal changes in the transmittance of the probe light due to the increase in the turbidity of the sample solution accompanied by phase separation. Each data point was normally averaged over 60 time measurements to improve the signal-to-noise ratio of the observed data. When the T-jump method (ii) is employed, the temperature rise (ΔT) in a sample solution can be controlled by adjusting the dye concentration and/or laser power, while the effects of the dye on the phase separation dynamics can be carefully examined as described in chapter 5.

2.2.2 Turbidimetry

The cloud point (T_c) of an aqueous PNIPAM solution was determined by turbidimetry. The optical transmittance curve of each aqueous PNIPAM solution was recorded at 532 nm (GC Photonics Inc., GLML-30) using a photodiode (Thorlabs, Inc., DET210) and a digital storage oscilloscope (Teledyne LeCroy, Inc., wave Runner 104MXi, 1 GHz). The temperature was controlled by a temperature controller (Japan high tech Co., Ltd., PE-120). The heating rate was set at 0.2 °C min^{-1}. T_c was defined as the temperature where the transmittance became 50%.

2.2.3 Other equipment

Dynamic light scattering (DLS) measurements were carried out to determine the size distributions of sample polymers in water at 25 °C using a model FDLS-300 (Otsuka Electronics Co., Ltd.). A 100 mW laser (λ = 532 nm) was used as an incident light beam for light scattering, and the scattering angle was set 90°. Differential scanning calorimetry (DSC) measurements were performed by a DSC micro calorimeter (Mettler-Toledo) with a cell volume of 100 μL at the heating rate of 1.0 ºC min^{-1} in the range of 25-40 ºC under elevated pressure (> 1.1 x 10^5 Pa). A single molecule fluorescence imaging technique (SMI) and fluorescence correlation spectroscopy (FCS) were introduced to investigate the microscopic solution structures of sample polymers in water. The

optical setups for these experiments are described in chapter 4. The details of sample preparations are described in each chapter.

Chapter 3| Concentration and molecular weight dependences of phase separation dynamics

3.1 Introduction

The most fundamental properties governing the phase separation behaviors of an aqueous thermoresponsive polymer solution are the concentration and molecular weight of the polymer as demonstrated by their effects on the cloud point (T_c) and the viscosity of the polymer solution [78], [111], [112] as well as on the hydration structure of the polymer [72], [113]. Aggregation of polymer chains in solution proceeds thorough the diffusion and collision of globules, and subsequent interpolymer entanglement. The concentration and molecular weight of a polymer play crucial roles in these processes. The average interpolymer distance related to the mutual diffusion time of the polymers in solution depends on the polymer concentration. When polymer chains overlap and interpenetrate with one another above a certain concentration (C_c) in solution, the initial structure of the polymer below T_c will be different from that below (C_c) due to the differences in the interpolymer interactions below and above C_c [89], [114], [115]. Also, above a polymer overlapping concentration (i.e., > C_c), it has been reported that polymer chains exhibit an extra process in phase separation which is ascribed to the disentanglement of the globules for further growth of the globules [89]. These findings indicate that the phase separation mechanisms of an aqueous thermoresponsive polymer solution depend strongly on the concentration and molecular weight of the polymer. Furthermore, the hydrophobic interactions between the polymer chains would become stronger with an increase in the molecular weight of the polymer [116], while it results in the decrease in the diffusion time of the polymer in solution. Therefore, it is intriguing to study the polymer concentration and molecular weight effects on the phase separation behaviors of an aqueous thermoresponsive polymer solution.

In this chapter, the polymer concentration and molecular weight dependences of the phase separation dynamics of aqueous poly(*N*-isopropyl acrylamide) (PNIPAM) solutions are described. On the basis of the evaluations of the intermolecular interactions between PNIPAM

chains by dynamic light scattering measurements and phase separation dynamics of the polymer solutions, the results are discussed in terms of a diffusion-controlled model.

3.2 Sample preparations and experimental

3.2.1 Preparation of 1-Phenylethyl phenyldithioacetate (PEPD)

PNIPAM samples employed in this study were prepared by living radical polymerization by using a reversible addition-fragmentation chain transfer (RAFT) agent [117]–[119]. 1-Phenylethyl phenyldithioacetate (PEPD) used as a RAFT agent whose structure was shown in Figure 3-1a was synthesized by the following procedures [120], [121]. Benzyl chloride (20 g, Wako Pure Chemicals Co., Ltd., > 98%) was added dropwise to a mixture of magnesium turnings (3.75 g, Wako Pure Chemicals Co., Ltd., > 99.5%)) in dry diethyl ether (100 ml, Wako Pure Chemicals Co., Ltd., > 99.5%). After ceasing the vigorous initial reaction, the solution was refluxed for 3 h to complete the reaction. The mixture was then cooled to room temperature and carbon disulfide (12.0 g, Wako Pure Chemicals Co., Ltd., > 99.0%) was added dropwise during 30 min and, then, the mixture was stirred at 0 °C for 2 h, affording a viscous yellow mixture. Ice water (100 mL) and a 30% aqueous hydrochloric acid solution (100 mL) were added to the mixture. The organic layer was extracted three times with cold 10 % aqueous sodium hydroxide (120 mL). The alkaline layer was extracted three times with diethyl ether. To the residual alkaline layer, 10 % aqueous hydrochloric acid solution (330 mL) was added and the aqueous phase was extracted three times with diethyl ether. The mixture was then poured into ice water (300 ml) and the aqueous portion was washed with diethyl ether for three times. Evaporation of the combined organic portions under reduced pressure afforded phenyldithioacetic acid. The acid was then reacted with styrene (9.0 g, Wako Pure Chemicals Co., Ltd., > 99.0%) in the presence of a small amount of toluene-*p*-sulfonic acid (Wako Pure Chemicals Co., Ltd., > 99.0%) in carbon tetrachloride (10 g, Wako Pure Chemicals Co., Ltd., > 99.5%). The crude product was then precipitated in cold methanol and recrystallized from methanol, affording fine yellow crystals. The ^{1}H NMR spectrum of the compound was recorded on a JEOL ECP-400

(400 MHz) as shown in Figure 3-1b.

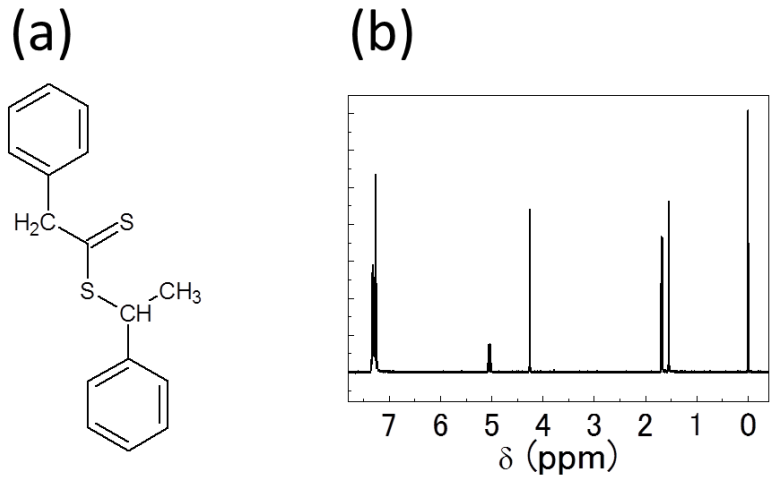

Figure 3-1. (a) Chemical structure and (b) ^{1}H NMR spectrum of 1-phenylethyl phenyldithioacetate (PEPD). ^{1}H NMR spectrum was measured in $CDCl_3$ (Wako Pure Chemicals Co., Ltd., >99.0%) (δ = 1.55 (s, water), δ = 1.67-1.69 (d, 3H, CH_3), δ = 4.26 (s, 2H, CH_2), δ = 5.01-5.08 (q 1H, CH), δ =7.23-7.35 (m, 10H, aromatic CH)).

3.2.2 Preparation of poly(N-isopropylacrylamide) (PNIPAM)

An *N*-isopropylacrylamide monomer (Wako Pure Chemicals Co., Ltd., > 98%) was recrystallized twice from *n*-hexane. 2,2'-Azobis(isobutyronitrile) (AIBN) (Wako Pure Chemicals Co., Ltd., > 98%) was recrystallized from methanol. Methanol (Wako Pure Chemicals Co., Ltd., > 99.8%) and toluene (Wako Pure Chemicals Co., Ltd., > 99.5%) were purified by distillation. Polymerizations were performed in methanol–toluene mixtures at 60 °C under the conditions of 2.23 M (= mol/dm^3) NIPAM as a monomer, 0.80 mM AIBN as an initiator, and 8.94 mM PEPD as a RAFT agent. The molecular weights of the polymers were controlled through the polymerization time as described in Table 3-1.

3.2.3 Characterizations of PNIPAM samples

The resulting polymers were purified by repeated reprecipitations from the acetone solution of the polymer to an enough amount of *n*-hexane. The number-averaged molecular weight (M_n) and the polydispersity (M_w/M_n) of the samples were determined by using size exclusion

chromatography (SEC) (HLC 8220 instrument (Tosoh Co., Ltd.), flow rate of 0.35 mL min^{-1} at 40 °C) equipped with TSK gels (Tosoh Co., Ltd., SuperHM-H) using *N*,*N*-dimethylformamide containing 0.1 M of LiBr (Wako Pure Chemicals Co., Ltd., > 99.0%) as an eluent. The SEC chromatograms shown in Figure 3-2 were calibrated with standard polystyrene samples (Polymer Laboratories, Amherst, MA). The hydrodynamic radius (R_h) of the polymer in water was determined by dynamic light scattering (DLS) (Otsuka Electronics Co., Ltd., FDLS-3000). The cloud points of the polymers in water (T_c) were evaluated by the same manner with those described in §2.2.2. The properties of the PNIPAM samples used in this study are summarized in Table 3-1. The specimens are abbreviated on the basis of M_n: For instance, PNIPAM with M_n = 62,000 is abbreviated as a-62.

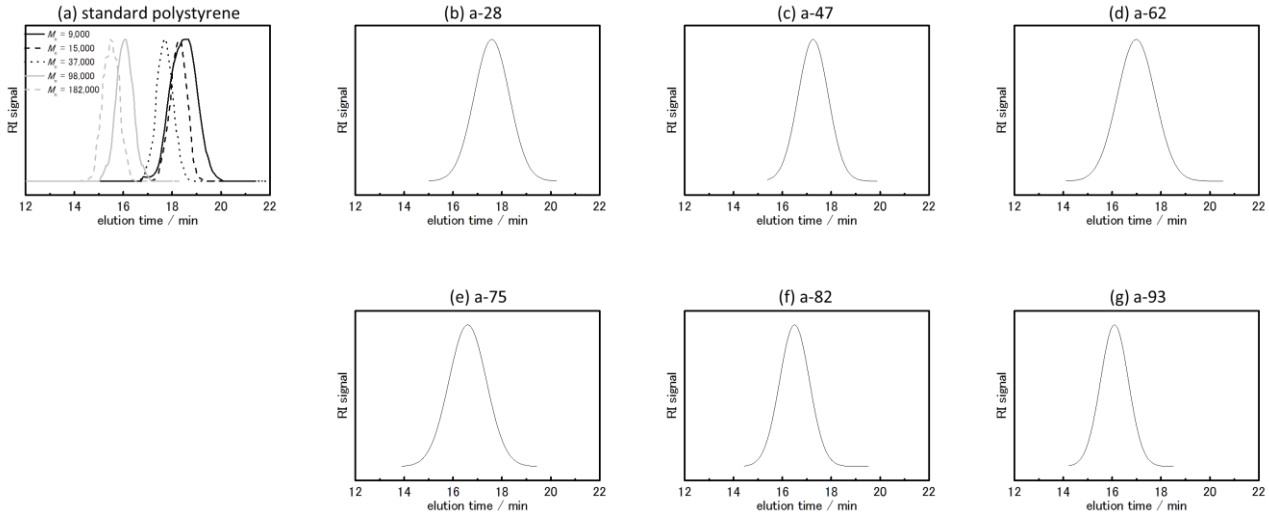

Figure 3-2. SEC chromatograms of (a) standard polystyrene samples (solid black line: M_n = 9,000, dashed black line: M_n = 15,000, doted black line: M_n = 37,000, solid gray line: M_n = 98,000, and dashed gray line: M_n = 182,00), (b) a-28, (c) a-47, (d) a-62, (e) a-75, (f) a-82, and (g) a-93. These chromatograms were measured at 40 °C using *N*,*N*-dimethylformamide containing 0.1 M of LiBr as an eluent.

Table 3-1. Fundamental properties of the sample polymers. M_w; weight-averaged molecular weight, M_n; number-averaged molecular weight, R_h; hydrodynamic radius in aqueous solution, T_c; cloud point.

Sample name	polymerization time (min)	M_n (1)	M_w / M_n (1)	R_h (nm) (2)	T_c(°C) (3)
a-28	90	28,000	1.3	13.2	31
a-47	120	47,000	1.1	15.4	32
a-62	180	62,000	1.5	16.2	32
a-75	300	75,000	1.4	16.8	32
a-82	420	82,000	1.2	17.8	32
a-93	600	93,000	1.1	17.9	32

(1) Determined by size exclusion chromatography (SEC) in a DMF solution.
(2) R_h; determined by dynamic light scattering (DLS) in a 0.10 wt% aqueous solution.
(3) Determined by turbidimetry in a 1.0 wt% aqueous solution.

3.3 Results and Discussion

3.3.1 Cloud points

Figure 3-3 shows the optical transmittance curves of aqueous (a) a-28 and (b) a-99 solutions as a function of temperature. The black and gray curves show the transmittance changes upon heating and cooling, respectively. As seen in Figure 3-3, the T_c value was the same irrespective of the molecular weight of the polymer in the range of M_n = 28,000 ~ 93,000. This tendency is in good agreement with the results reported previously [122]–[127].

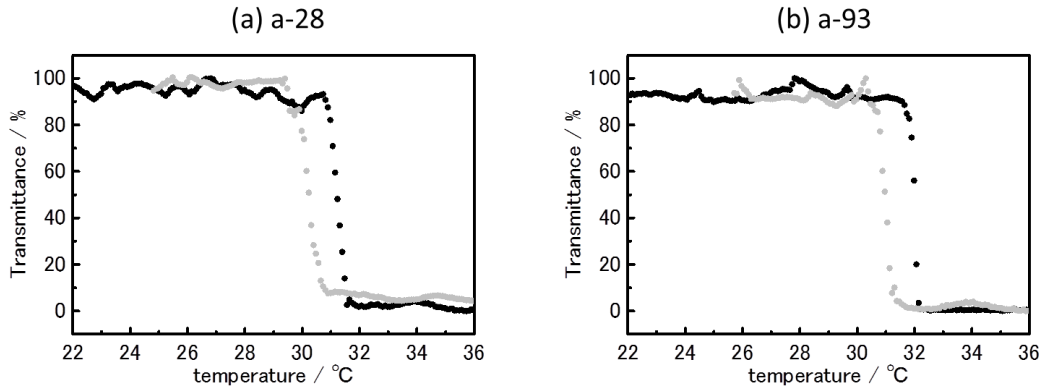

Figure 3-3. Temperature dependences of the optical transmittance at 532 nm observed for aqueous (a) a-28, and (b) a-93 solutions. The black and gray curves show the transmittance changes upon heating and cooling, respectively. Heating and cooling rate = 0.2 ^{o}C min^{-1}.

3.3.2 General aspects of phase separation dynamics

Figure 3-4 shows representative examples of the phase separation dynamics observed for a-47 in water at several concentrations ranging from 1.0 to 9.0 wt%, determined by the method (i) described in chapter 2. Phase separation of the polymer solution is triggered by a laser-induced T-jump. As clearly seen in the figure, the optical transmittance of the solution, $T(t)$, decays in time immediately after the T-jump, and reaches a quasi-equilibrium state within 200 ms, while it recovers in a longer time scale ($t \approx 1$ s) due to cooling of the solution. For a-47, phase separation of the solution proceeds in the order of several tens ~ several hundreds of ms depending on the polymer concentration, while that of phase mixing takes place over several hundreds of millisecond.

Each $T(t)$ curve in Figure 3-4 can be well fitted by a single exponential function in eq. (3-1),

$$T(t) = Aexp\left(-\frac{t}{\tau_{\mathrm{ps}}}\right) + B \qquad (3\text{-}1)$$

where τ_{ps} is the phase separation time constant and, A and B are the pre-exponential factors and the value corresponding to the minimum transmittance of the solution, respectively. Generally, A is observed to increase with an increase in the polymer concentration, since the turbidity of the

solution (i.e., optical transmittance) increases with the polymer concentration. Moreover, $T(t)$ becomes faster with increasing the polymer concentration, demonstrating that phase separation is faster at a higher polymer concentration.

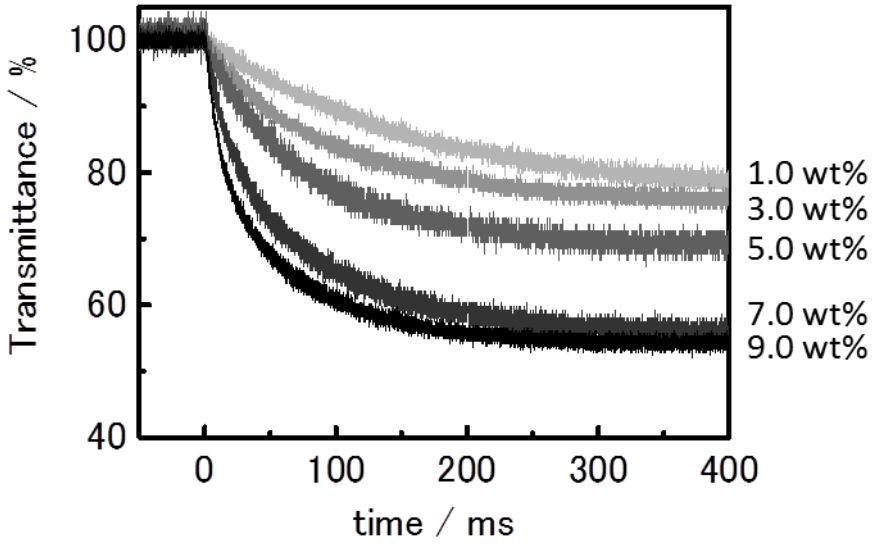

Figure 3-4. Representative curves of the time courses of the transient optical transmittance $T(t)$ as a function of the polymer concentration of a-47 (1.0–9.0 wt%) in water. The origin of the time scale (t = 0) is the time when the heating pulse reaches the cell.

3.3.3 Concentration dependence

By fitting the $T(t)$ data in Figure 3-4 by eq. (3-1), τ_{ps} was determined. The τ_{ps} value is plotted against the concentration of each sample as shown in Figure 3-5. The τ_{ps} value ranged from 200 to 40 ms, depending upon the concentration and the molecular weight of the polymer in water. For the concentration dependence of the τ_{ps} value (Figure 3-5a ~ f), similar behaviors with those of a-47 were observed irrespective of the molecular weight of the polymer. In each case, τ_{ps} decreases with increasing the polymer concentration and reaches a constant value at a certain concentration.

The origin of such characteristic behaviors in Figure 3-5 will be explained as follows. The phase separation processes of the solution consist of two processes that can be clearly distinguished in the time axis. Initially, the structural phase transition of the polymer from a hydrated coiled state to a dehydrated globular state takes place in a microsecond time scale. Subsequently, the dehydrated globules aggregate through diffusion and the hydrophobic interactions of the globules to form

polymer-rich domains. With increasing in the polymer concentration, the average interpolymer distance (*d*, average center-to-center distance between two polymer chains calculated based on the concentration) decreases and, therefore, the diffusion time for aggregation decreases as observed in Figure 3-5. A further quantitative analysis of the data is described in §3.3.5.

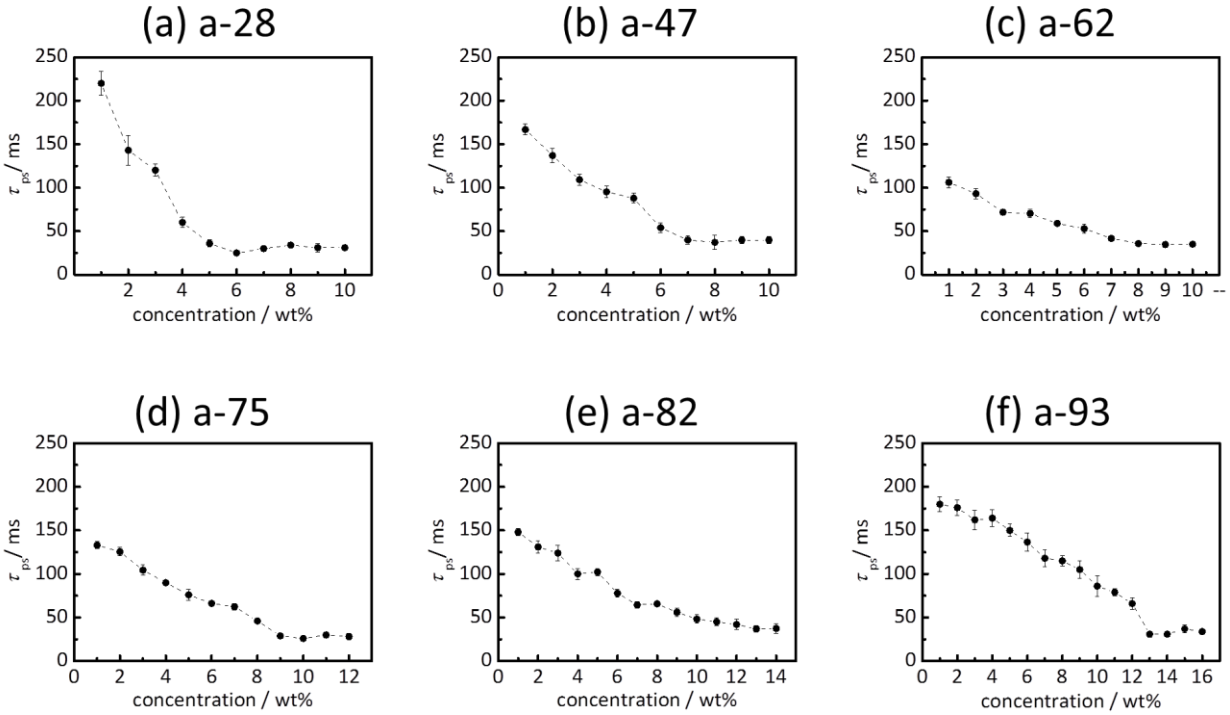

Figure 3-5 a-f. Relationships between τ_{ps} and the polymer concentration (in wt%) in water.

Table 3-2. Molecular weight effects on τ_c, C_c, and d at C_c.

Sample name	a-28	a-47	a-62	a-75	a-82	a-93
C_c (mM)	2.1	1.5	1.3	1.2	1.3	1.4
d (nm)	10	12	11	11	11	11
τ_c (ms)	25	40	36	29	45	31

As seen in Figure 3-5, the τ_{ps} value converges at a certain polymer concentration irrespective of the molecular weight of the polymer and, such specific τ_{ps} and polymer

concentration values are referred hereafter to τ_c and C_c, respectively, as summarized in Table 3-2, together with the relevant *d* values. As seen clearly in Table 3-2, the τ_c values are in the range of 25 ~ 45 ms. The decrease in the τ_{ps} value with an increase in the polymer concentration seen in Figure 3-5 could be ascribed to the interactions between the polymer chains through chain entanglement and/or aggregation of the polymers. To obtain information on polymer entanglement in solution, dynamic light scattering (DLS) measurements of the sample solutions were conducted to evaluate the hydrodynamic radii of the polymers: R_h. As the data on a-47 are shown in Figure 3-6, the DLS measurements exhibited a single peak at a low polymer concentration (1.0 ~ 6.0 wt%) indicating the absence of polymer entanglement, while those showed two peaks above 7.0 wt%, demonstrating formation of entangled polymers. The results indicate that the polymer chains above C_c are entangled with each other and, hence, phase separation of the solution proceeds without polymer diffusion. Therefore, τ_{ps} is independent of the concentration above C_c and converges to a certain value (≈ 40 ms).

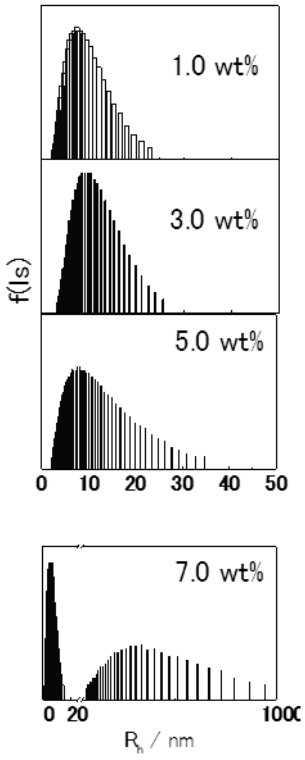

Figure 3-6. Typical examples of the concentration dependence of the hydrodynamic radius histogram observed for a-47 by dynamic light scattering measurements. The concentration of the sample solution is given in the figure.

3.3.4 Molecular weight dependence

The polymer molecular weight (M_w) effects on the phase separation dynamics are worth discussing on the basis of the data in Figure 3-5. In Figure 3-7, the τ_{ps} value determined below C_c is plotted against the molecular weight (M_n) of the polymer sample at several concentrations (0.4 ~ 1.4 mM). For the PNIPAM samples with high M_n (a-75, a-82, a-93), phase separation of the solution becomes faster with a decrease in M_n, while that becomes slower with a decrease in M_n for a-28, a-47, and a-62. Such behaviors were commonly observed irrespective of the polymer concentration below C_c as seen in the figure, demonstrating one of the important findings of the present study: appearance of an optimum molecular weight for phase separation of an aqueous PNIPAM solution.

The origin of the appearance of the optimum molecular weight value is as follows. With increasing M_n, the size of the globule also increases [78], leading to slow diffusion of the polymer

in solution and, hence, the slow rate of phase separation. Furthermore, since an increase in M_n accompanies that in the solution viscosity, this will contribute partly to slow phase separation [78]. By contrast, the reason for the opposite trend observed for PNIPAM samples with low M_n (a-28, a-47, a-62) is unclear in the present stage of the investigation. One possible reason for the behavior is as follows. For the lowest M_n PNIPAM sample (a-28), formation of a polymer-rich domain (i.e., phase separation) requires numerous collisions of the globules and, hence, phase separation should become slower. Another possible reason might be ineffective aggregation of the globules since the aggregates, even if produced, will be very likely to dissociate to the coil state due to the short polymer chains, resulting in slow phase separation [116].

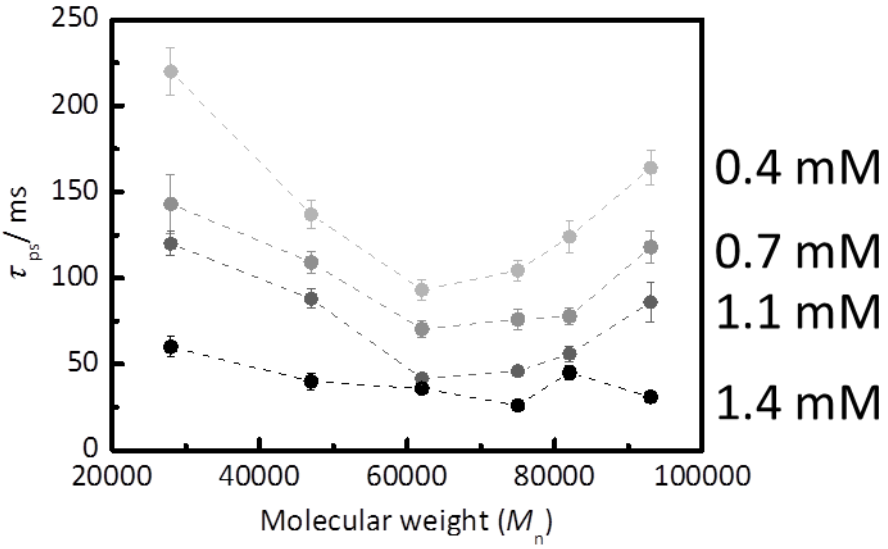

Figure 3-7. Molecular weight dependence τ_{ps}. τ_{ps} is plotted against the molecular weight of the polymer at several concentrations (0.4 − 1.4 mM).

3.3.5 Quantitative analysis

The τ_{ps} value ranging from 200 to 40 ms evaluated in the present study is worth discussing theoretically. Assuming a diffusion-controlled aggregation model, the molecular weight of a polymer aggregate (polymer-rich micro-domain) $<M_{agg}>$ including those of the polymer and water is given as a function of an aggregation time, *t*, as in eq. (3-2) [128], [129],

$$\left\langle M_{agg} \right\rangle = M_w \left(1 + \frac{4}{3} N_A \frac{kT}{\eta} \frac{C}{M_w} t \right) \qquad (3\text{-}2)$$

where N_A is the Avogadro number, k is the Boltzmann constant, T is temperature, η is the viscosity of a sample solution, and C is the concentration of an aqueous polymer solution. For instance, this equation can be applied to discuss the results on the a-47 sample solution (1.0 wt%), where the η value of the solution evaluated by a viscometer (Brookfield, cone/plate version) is 1.1 mPa·s. In this case, $<M_{agg}>$ is estimated to be 1.2×10^{10}.

On the other hand, the polymer weight composed of a single polymer-rich domain (assuming a droplet) M_{agg} is given by eq. (3-3),

$$M_{agg} = \frac{4}{3} \pi r^3 \times 10^{-12} \times C_{globule} \qquad (3\text{-}3)$$

where r is the radius of a polymer-rich domain (droplet) and $C_{globule}$ is the polymer concentration (wt%) in the domain. Wu et al. predicted the polymer density of a PNIPAM globule to be 0.20 g·mL^{-1}, which corresponding to $C_{globule}$ = 20 wt%, using a laser light scattering study. [130]

The growth rate is then given by eq. (3-4),

$$t = \frac{3}{4} \left(N_{glo} \times M_w - M_w \right) \frac{\eta}{N_A kTc} \qquad (3\text{-}4)$$

where N_{glo} is the number of the polymer chains composed of a single polymer-rich domain. Combining these relations, the average number of the polymer chains composed of a single polymer-rich micro-domain ($N_{glo} \sim <M_{agg}> / M_w$) is estimated to be 2000. Based on this value and putting the constant values in eq. (3-4), the growth time of a polymer-rich microdomain is estimated to be ≈ 15 ms. The calculated value is somewhat smaller than the τ_{ps} values observed in the

experiments (40 ~ 200 ms), suggesting that the aggregation of globules proceeds through numbers of collisions of globules; the aggregation is growth-controlled fashion.

3.4 Conclusions

In the present study, the phase separation dynamics and kinetics of aqueous PNIPAM solutions were investigated in terms of their concentration and molecular weight of the polymer. The τ_{ps} value decreased with increasing the polymer concentration and levelled-off at a certain constant value irrespective of the molecular weight of the polymer. The initial structure of the polymer chain before thermal phase separation also governs the phase separation dynamics. One of the important findings of the study is the observation of the optimal molecular weight for τ_{ps}. This finding provides a valuable insight to the development of PNIPAM-based functional materials showing quick thermo-response times. These characteristics can in part be interpreted by the growth-controlled aggregation model.

Chapter 4| Phase separation dynamics of aqueous isotactic-rich PNIPAM solutions

4.1 Introduction

In chapter 3, it was shown that the appropriate controls of the solution concentration and the molecular weight of poly(*N*-isopropyl acrylamide) (PNIPAM) allowed acceleration of the phase separation rate of the solution. Also, it was demonstrated that the structures of a PNIPAM polymer chain below the clouding temperature of the solution strongly reflected on the phase separation dynamics. In the case of the studies described in chapter 3, the polymer structures in solution before phase separation are governed by the interpolymer distance at a given PNIPAM concentration. Generally, the structures of a polymer in solution are also determined by the balance between the hydrophobicity and hydrophilicity of the polymer and, therefore, there are many reports on the synthetic polymers having various hydrophobic/hydrophilic parts in the main and/or side chains [131]–[136]. Recently, Katsumoto et al. demonstrated that the hydrophobic/hydrophilic balance of PNIPAM could be controlled by the stereoregularity of the polymer [61], which was very important for the present study.

On the basis of the development of the novel polymerization method for simultaneous controls of the molecular weight, its distribution, and stereoregularity of a polymer [118], some research groups have revealed that the phase separation behaviors of an aqueous PNIPAM solution are highly sensitive to the stereoregularity of PNIPAM. Ray et al. reported that the cloud points (T_c) of aqueous PNIPAM solutions became lower and an optical transmittance curve during heating the solution became broader with an increase in the meso diad content (isotactic-rich) in the polymer [64]. Katsumoto et al. investigated the partition coefficient of a NIPAM-dimer (DNIPAM) between water and chloroform, and demonstrated that DNIPAM with a meso configuration (m-DNIPAM) was more hydrophobic than that with a racemo configuration (r-DNIPAM) [61]. By means of small angle neutron scattering measurements, Nishi et al. demonstrated that isotactic-rich PNIPAM gradually aggregated with increasing temperature, while atactic PNIPAM suddenly associates with

each other around the phase separation temperature [137]. These reports strongly indicate that the phase separation processes are sensitive to the stereoregularity of PNIPAM.

In this chapter, the phase separation dynamics of aqueous solutions of PNIPAM with different stereoregularities (atactic and isotactic-rich) were investigated with the aid of a laser-induced T-jump technique. Furthermore, the phase separation mechanisms of an aqueous isotactic-rich PNIPAM solution were revealed by means of a single molecule fluorescence imaging technique and fluorescence correlation spectroscopy which could monitor the microscopic structures of the polymer in solution.

4.2 Sample preparations and experimental procedures

4.2.1 Sample preparations

PNIPAM samples were prepared by a stereospecific living radical polymerization using a reversible addition-fragmentation chain transfer (RAFT) agent and a Lewis acid catalyst [117]–[119]. 1-Phenylethyl phenyldithioacetate (PEPD) was synthesized with the similar manners to those described in chapter 3 [120], [121]. *N*-Isopropylacrylamide (NIPAM) (Wako Pure Chemicals Co., Ltd., > 98%) and 2,2'-azobis(isobuthyronitrile) (AIBN, Wako Pure Chemicals Co., Ltd., > 98%) were recrystallized from *n*-hexane and methanol, respectively. Scandium trifluoromethanesulfonate ($Sc(OTf)_3$, Aldrich Co. Ltd., 99%)) was used as received. Polymerizations were performed in methanol–toluene mixtures at 60 °C under the conditions of a 2.23 M (M = mol/dm^3) NIPAM monomer, 0.80 mM AIBN as an initiator, and 8.94 mM PEPD as a RAFT agent in the absence and the presence of $Sc(OTf)_3$ (Table 4-1). The resulting polymers were purified by repeated reprecipitations from the acetone solutions of the polymers to an enough amount of *n*-hexane.

Fluorescent labeled PNIPAM (Rh-m55) was synthesized by the analogous procedures to those described above in the presence of a rhodamine B derivative (acryloxyethyl thiocarbamoyl Rhodamine B) (Polysciences, Inc., the ratio of rhodamine B to NIPAM is 0.0001 in a monomer unit).

4.2.2 Characterizations of PNIPAM samples

The number-averaged molecular weights (M_n) and polydispersities (M_w/M_n) of the samples were determined by using size exclusion chromatography (SEC) (HLC 8220 instrument, Tosoh Co., flow rate of 0.35 mL min^{-1}) equipped with TSK gels (SuperHM-H (Tosoh Co.)) using *N*,*N*-dimethylformamide containing 0.1 M of LiBr as an eluent at 40 °C. The SEC chromatogram shown in Figure 4-1 was calibrated with standard polystyrene samples (Polymer Laboratories, Amherst, MA). The ^{1}H NMR spectra of the polymers in DMSO-d_6 at 140 °C were recorded on a JEOL ECP-400 spectrometer (400 MHz). The meso diad (*m*): racemo diad (*r*) ratios of the PNIPAM samples were determined based on the peak areas ratio of the methylene protons at 1.3 ppm and 1.7 ppm for the meso diad to that at 1.5 ppm for the racemo diad in the ^{1}H NMR spectra of the polymers. For examples, the ^{1}H NMR spectra of m-46 and m-55 are shown in Figure 4-2. Each peak is attributed as follows: methyl protons of the isopropyl group at δ = 1.1, methylene protons of the polymer backbone for the meso diad at δ = 1.3 and 1.7, methylene protons of the polymer backbone for the racemo diad at δ = 1.5, methine proton of the isopropyl group at δ = 3.8, and amide proton of the isopropyl group at δ = 6.7 [138]. The clouding points of the polymers in water (T_c) were evaluated by the same manner with those described in §2.2.2. Table 4-1 shows the data of the PNIPAM samples. The samples are abbreviated on the basis of the meso diad content in the polymers: For instance, PNIPAM with *m* = 50 is abbreviated as m-50.

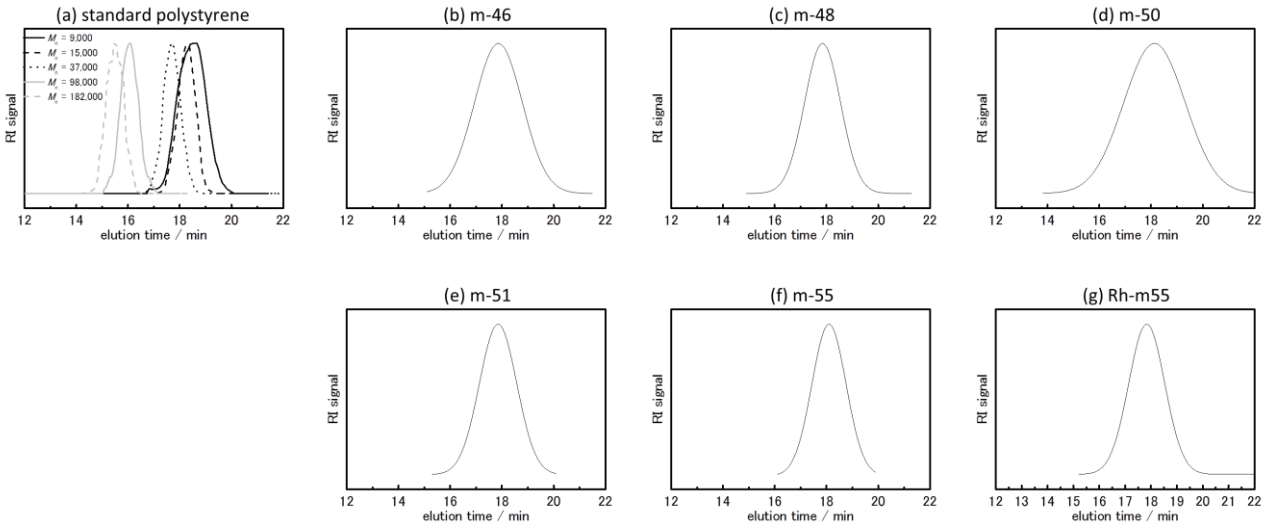

Figure 4-1. SEC chromatograms of (a) standard polystyrene samples (solid black line: M_n = 9,000, dashed black line: M_n = 15,000, doted black line: M_n = 37,000, solid gray line: M_n = 98,000, and dashed gray line: M_n = 182,00), (b) m-46, (c) m-48, (d) m-50, (e) m-51, (f) m-55 and (g) Rh-m55. These chromatograms were measured at 40 °C using *N*,*N*-dimethylformamide containing 0.1 M of LiBr as an eluent.

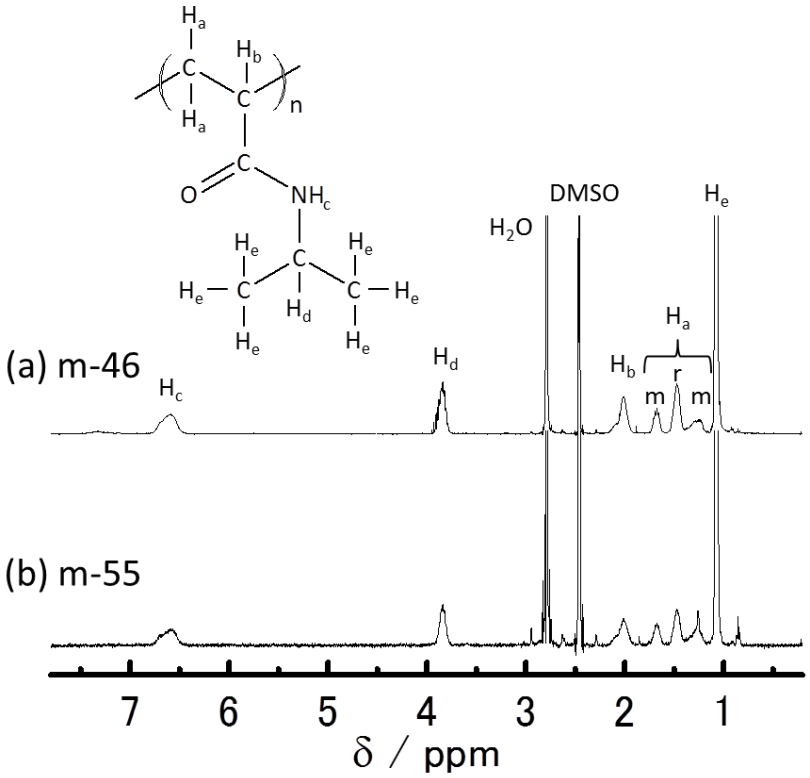

Figure 4-2. ^{1}H NMR spectra of PNIPAM samples prepared by RAFT polymerization in (a) the absence (m-46) and (b) presence of $Sc(OTf)_3$ (0.080 M) (m-55) in methanol/toluene (1/1,v/v) mixtures at 60˚C. These spectra were measured in DMSO-d_6 at 140 °C.

4.2.3 Dynamic light scattering (DLS)

The hydrodynamic radius (R_h) distributions of the polymers in water were measured by dynamic light scattering (DLS) (Otsuka Electronics, FDLS-3000).

4.2.4 Viscosity measurements

The viscosity of a sample polymer solution was measured by using a viscometer (Brookfield, cone/plate version).

4.2.5 Raman scattering measurements

Raman spectra were measured by confocal Raman microspectroscopy [139]. A cw Ar^+ laser beam (λ = 488 nm, Coherent, Innova 70) was used as an excitation light source for Raman scattering. The laser beam was introduced into an inverted optical microscope (Nikon, ECLIPSE TE300). A sample placed on the microscope stage was irradiated through an oil-immersion objective lens (N.A. = 1.30, plan Fluor). Raman- scattering light was passed through a pinhole with a diameter of 100 μm. After passing through the pinhole, Raman scattering light was passed through optical filters to cut off excitation and other stray light. Raman scattering light was detected by a cooled charge-coupled-device (CCD) camera (Andor Tec.) equipped with a polychromator (grating; 1200 grooves/mm).

Table 4-1. Fundamental properties of the sample polymers. M_w ; weight-averaged molecular weight, M_n ; number-averaged molecular weight, *m*: meso diad ratio, r: racemo diad ratio, T_c: cloud point.

Sample name	Lewis acid (M)	M_n [(1)]	M_w / M_n [(1)]	$m : r$ [(2)]	T_c(°C) [(3)]
m-46	–	29,000	1.8	46 : 54	32
m-48	0.025	29,000	1.3	48 : 52	31
m-50	0.050	20,000	2.8	50 : 50	31
m-51	0.057	29,000	1.1	51 : 49	30
m-55	0.080	19,000	1.4	55 : 45	28
Rh-m55	0.075	28,000	1.3	55 : 45	28

(1) Determined by size exclusion chromatography (SEC)

(2) Determined by ^{1}H NMR.

(3) Determined by turbidimetry for a 1.0 wt% aqueous solution.

4.2.6 Single molecule fluorescence imaging technique

For single molecule fluorescence imaging (SMI) and fluorescence correlation spectroscopy (FCS), a reporter fluorescent dye molecule, PDI-$(SO_4)_4$, whose structure was shown in Figure 4-3, in a dilute aqueous solution (concentration was 10^{-9}– 10^{-10} M) was used in the present study. The dye was supplied from Organica Feinchemie GmbH (Britterfield-Wolfen, Germany) and used without further purification.

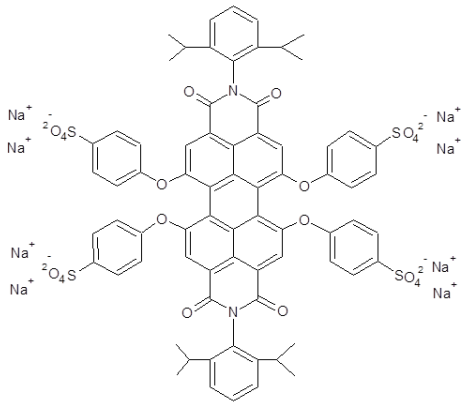

Figure 4-3. Chemical structure of a perylene diimide derivative (PDI-$(SO_4)_4$).

SMI was performed using a quasi-total-internal reflection fluorescence (quasi-TIRF) microscope [140]. A schematic illustration of the setup is shown in Figure 4-4. A 532 nm light beam from a diode-pumped solid state laser (JDS Uniphase Co., CDPS532M-50) was used for excitation. The laser beam was introduced into an inverted optical microscope (Olympus, IX71) equipped with an objective lens (x100, N.A.=1.30 Plan Fluorite, Olympus) and a cooled CCD camera (Princeton Instruments Inc., cascade 512B) through the objective lens off-center, however, not far enough for total-internal reflection. This alignment enables one to reduce dramatically the background noises in detecting fluorescence and to observe fluorescence from the dye sit at 5 μm above the glass substrate. The output from a diode-pumped solid state laser (continuous wave, 532 nm) is introduced into the quasi-TIRF microscope such that illumination is made in a wide-field mode, and the fluorescence from individual single reporter dye molecules can be detected with a cooled CCD camera.

4.2.7 Fluorescence correlation spectroscopy

For fluorescence correlation spectroscopy (FCS), a confocal microscope (Olympus, IX71) was employed and the fluorescence from the dye was detected by an avalanche photodiode (Perkin–Elmer, SPAD, SPCM-AQ 14). The microscope is equipped with a thermo-stage to control temperature of a sample solution.

The auto correlation curves observed experimentally were fitted by eqs. 4.1 and 4.2. Eqs. 4.1 and 4.2 were used to analyze the dye molecules moving at the same and different velocities, respectively.

$$G(t) = \frac{1}{N} \cdot \frac{1}{\left(1+\frac{t}{\tau_D}\right)} \cdot \frac{1}{\left(1+\frac{t}{\omega^2 \cdot \tau_D}\right)^{\frac{1}{2}}} \cdot \left[1 + \frac{T}{1-T} \exp\left(\frac{-t}{\tau_T}\right)\right] + offset \quad (4.1)$$

$$G(t) = \frac{1}{N} \cdot \left[f \frac{1}{\left(1+\frac{t}{\tau_{D1}}\right)} \cdot \frac{1}{\left(1+\frac{t}{\omega^2 \cdot \tau_{D1}}\right)^{\frac{1}{2}}} + (1-f) \frac{1}{\left(1+\frac{t}{\tau_{D2}}\right)} \cdot \frac{1}{\left(1+\frac{t}{\omega^2 \cdot \tau_{D2}}\right)^{\frac{1}{2}}} \right] \left[1 + \frac{T}{1-T} \exp\left(\frac{-t}{\tau_T}\right)\right] + offset \quad (4.2)$$

In eqs. 4.1 and 4.2, N is the average number of the fluorescent dye molecule in a confocal volume element, τ_{Dn} is the diffusion time of the dye molecule (in ms), f is the fraction of the dye molecule

diffusing with the time constant τ_{D1}, ω is the aspect ratio of the confocal volume (= w_z/w_{xy}), T is the fraction of the dye molecule in the excited triplet state, and τ_T is the relaxation time from the excited triplet state (in ms). To consider the contribution of the dark state of the dye to the fluorescence correlation functions, the relaxation time of the excited triplet state of the dye shoud be taken into account.

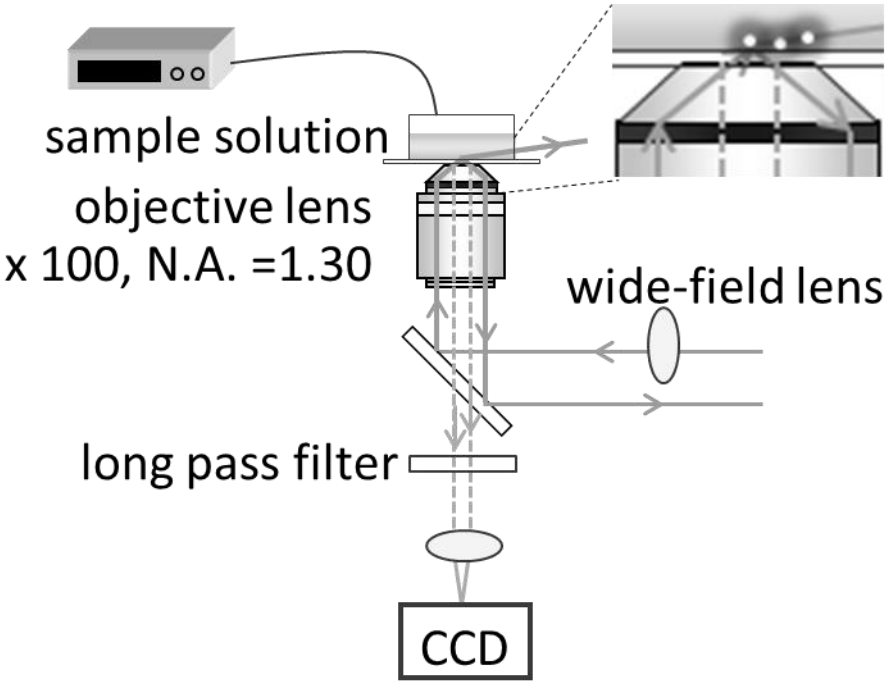

Figure 4-4. Schematic illustration of the optical setup for quasi-total-internal-reflection fluorescence microscopy.

4.3 Results and Discussion

4.3.1 Cloud points

Figure 4-5 shows the optical transmittance curves of aqueous (a) m-46, (b) m-51 and (c) m-55 solutions as a function of temperature. The black and gray curves show the transmittance changes upon heating and cooling, respectively. As seen in Figure 4-5, the T_c decreases with increasing the meso diad content in the polymer. Furthermore, the transmittance of the aqueous m-55 solution at around the clouding point gradually changed with temperature compared to that of

m-46 or m-52. These tendencies are in good agreement with the results reported previously [54], [137], [141]. Katsumoto et al. demonstrated that a NIPAM-dimer (DNIPAM) with a meso configuration was more hydrophobic than that with a racemo configuration by investigating the partition coefficient of DNIPAM between water and chloroform [61], resulting in the decrease in T_c with increasing the meso diad content in the polymer. Although the origin of the gradual changes in the transmittance curve with temperature in aqueous highly isotactic-rich PNIPAM solution at around the clouding point is still unclear, Nishi et al. have reported that an increase in the isotacticity of the polymer interfered the cooperative dehydration of the polymer, which is defined as simultaneous dissociation of the bound water molecules from the polymer, causing the gradual change in the transmittance with temperature [137].

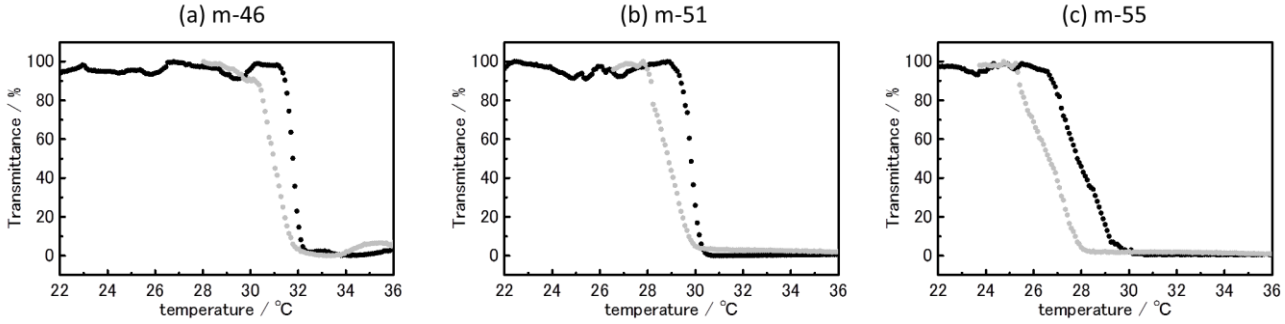

Figure 4-5. Temperature dependences of the optical transmittance at 532 nm observed for aqueous (a) m-46, (b) m-51, and (c) m-55 solutions. The black and gray curves show the transmittance changes upon heating and cooling, respectively. Heating and cooling rate = 0.2 ^{o}C min^{-1}.

4.3.2 The rates of phase separation

For a series of the different meso-content PNIPAM samples (m-46 ~ m-51), first, the phase separation dynamics was studied for similar molecular weight samples at the same concentration (1.0 wt%). Figure 4-6 shows the time courses of the optical transmittance, *T(t)*, after laser-induced T-jump by the method (i) described in §2.2.1. As seen clearly in the figure, $T(t)$ decreases immediately after the T-jump and reaches a quasi-equilibrium state after 200 ms with $T(t)$ being approached to a constant value, while it recovers at a longer time (t ~ 1 s) due to cooling of the solution. Each $T(t)$ curve can be well fitted with a single exponential function, $T(t) = A\,exp(-t/\tau_{ps}) +$

B, providing precise value of the phase separation time constant. The decay time of $T(t)$ gradually became faster with increasing the isotacticity of the polymer. In Figure 4-7, the phase separation time constants are plotted against the polymer concentrations of the m-46, m-48, m-50, and m-51 solutions. The figure clearly shows that, although the molecular weights and concentrations of the polymers are fixed almost constants, the polymer exhibits different phase separation dynamic behaviors with one another. With increasing the isotacticity of the polymer, the phase separation time constant becomes faster. At 5.0 wt%, as an example, the phase separation time constants of m-46, m-48, m-50, and m-51 were determined to be τ_{ps} = 120, 40, 15, and 6 ms, respectively. Note that the differences in the stereoregularity between these samples are very small. These results clearly indicate that the phase separation dynamics is very sensitive to the stereoregularity of PNIPAM and a slight increase in the isotacticity of the polymer results in dramatic acceleration of the phase separation time constant.

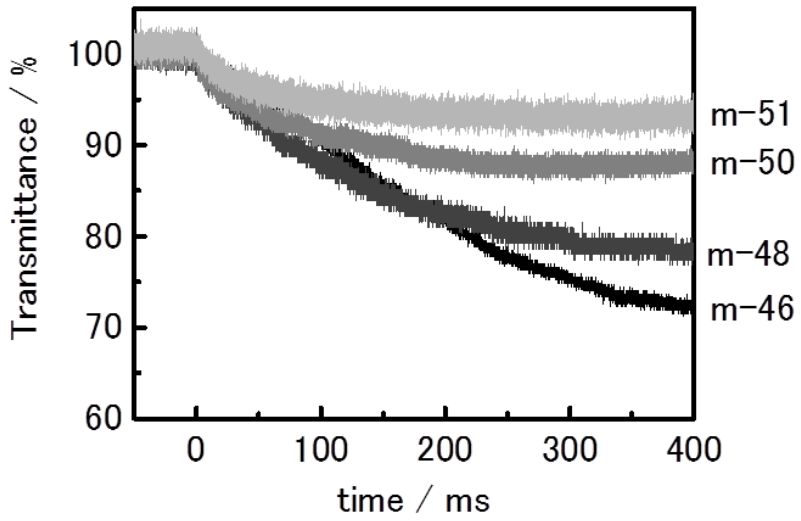

Figure 4-6. Typical examples of the time courses of the transient optical transmittance $T(t)$ observed for aqueous m-51, m-50, m-48 and m-46 solutions (1.0 wt%).

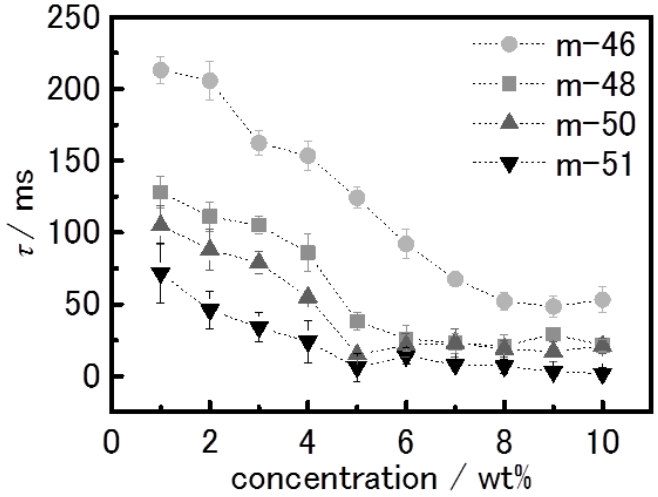

Figure 4-7. Phase separation time constants as a function of the concentration of the polymer (1.0 – 10 wt%) observed for aqueous m-51, m-50, m-48 and m-46 solutions. ●: m-46, ■: m-48, ▲: m-50, ▼: m-51.

The phase separation dynamics of aqueous PNIPAM solutions are correlated with the initial polymer state/structure in the solution before phase separation as described in chapter 3. For instance, the phase separation time constant observed for m-46 at a concentration above 8.0 wt% is the fastest among those of the samples studied (i.e., the fastest phase separation). Under the conditions, the m-46 sample in water shows interpolymer entanglement as confirmed by dynamic light scattering (DLS) as shown in Figure 4-8. In this case, the interpolymer entanglement is regarded as the origin of fast phase separation observed for m-46. In the isotactic-rich PNIPAM (m-50 and m-55) solutions, however, no such aggregate formation or molecular assembly in the solution before phase separation is observed by DLS measurements: see Figure 4-8. Such aggregation/assembly of the polymer chains due to the hydrophobic interactions presumably increases the mutual interactions between the polymer chains and affects the hydrated/dehydrated polymer structures, which should be reflected on the vibrational spectra of the aqueous PNIPAM solutions. In particular, the hydrated coils and dehydrated globules of PNIPAM can be distinguished by the Raman spectrum in 2800 ~ 3100 cm^{-1} on the basis of the CH_3 and CH_2 stretching vibrational modes [66], [139]. However, both m-46 and m-55 showed analogous vibrational spectra with one another as shown in Figure 4-9, implying no aggregate formation in the m-46 and m-55 solutions as

shown in Figure 4-8. On the other hand, the heterogeneity of a polymer solution such as aggregate formation would be presumably reflected on the solution viscosity. In practice, the viscosity of the m-55 solution (5.0 wt%) was somewhat higher than that of the m-46 solution (5.0 wt%): η = 3.9 mPa·s for *m-55* and η = 3.0 mPa·s for m-46. The solution heterogeneities observed by the viscosity measurements have been further revealed by a single molecule fluorescence imaging technique, as described in 4.3.2.

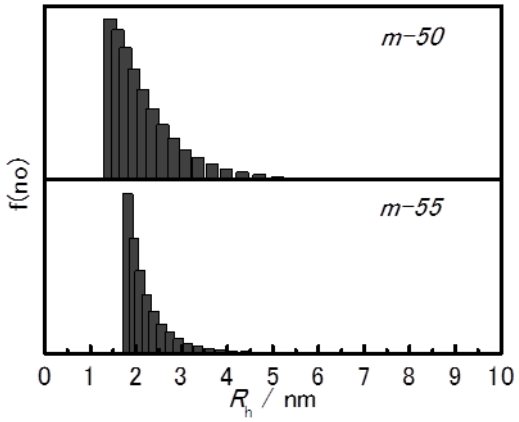

Figure 4-8. Hydrodynamic radius distributions of m-50 and m-55 in aqueous solutions (1.0 wt%) at room temperature.

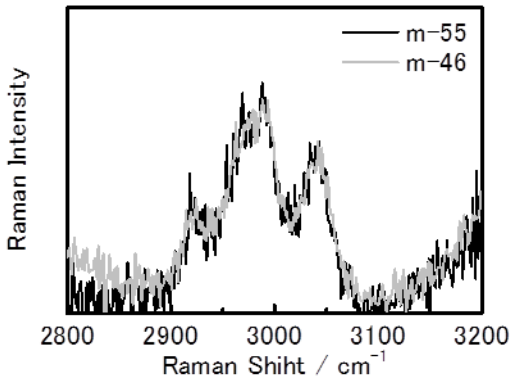

Figure 4-9. Raman spectra of aqueous m-46 and m-55 solutions (5.0 wt%) at room temperature. The observed peaks at 2923, 2967, 2983 and 3043 cm^{-1} are ascribed to those of the C-H stretching vibrations.

4.3.3 Single molecule fluorescence imaging (SMI)

To examine the microscopic polymer structures in the solutions, single molecule fluorescence imaging (SMI) experiments were conducted by adding a small amount of a perylene diimide derivative (PDI-$(SO_4)_4$, reporter dye molecule) to each sample solution. Due to the hydrophobicity of PDI-$(SO_4)_4$, the dye distributes preferentially to the polymer-rich domains or the vicinity of such domains. If the solution is a uniform and the polymer chains are homogeneously dissolved in the solution without aggregation, the dye should be homogeneously distributed in the solution and free from the polymer chains. On the other hand, if the polymer chains form small (nanometer- or micrometer-sized) polymer-rich domains and the solution has an inhomogeneous structure, such solution structures would be detected by SMI since such domains would be labeled by the reporter dye. By observing single molecule fluorescence from the polymer solution, one can obtain further detailed insight into the microscopic structures of the polymer solution.

Figure 4-10a shows the fluorescence images of PDI-$(SO_4)_4$ in an m-46 solution (5.0 wt%) at room temperature (below T_c). Neither bright spots corresponding to single molecule fluorescence nor a specific structure suggesting the inhomogeneity in the solution is seen in the images. This indicates that each reporter dye molecule is not trapped by any polymer domain and diffuses in the solution too fast to be traced. Therefore, it is concluded that the atactic PNIPAM is dissolved homogeneously and does not aggregate in water. Figure 4-10b shows the fluorescence images of PDI-$(SO_4)_4$ in an m-46 solution (5.0 wt%) at 34 ^oC (above T_c). In these images, several bright spots corresponding to individual dye molecules are observed. The observation of the fluorescence spots from single molecules means that diffusion of the dye molecules in water is suppressed, since they are bound to the polymer-rich-domains which diffuse slowly in water. The behaviors before/after phase separation can be interpreted within the accepted framework of PNIPAM physics: below T_c, PNIPAM polymer chains are dissolved homogeneously in water and, above T_c, those form aggregates, resulting in phase separation to the polymer-rich and water-rich domains in the solution.

Figure 4-10c shows the fluorescence images of PDI-$(SO_4)_4$ in an m-55 solution (5.0 wt%) at room temperature (below T_c). In contrast to the atactic sample (Figure 4-10a), many fluorescence spots can be seen, demonstrating that the translational motion of each individual dye molecule in the solution is suppressed. Importantly, this indicates that, even before phase separation of the solution at room temperature, the m-55 sample presumably forms polymer-rich domains in the solution, where the dye molecules are distributed to and bound in the domains. Thus, the formation of the interpolymer chain-networks in the isotactic-rich PNIPAM solutions below T_c is successfully proved by the single molecule fluorescence imaging experiments. Obviously, such polymer networks will accelerate phase separation in the isotactic-rich PNIPAM solutions.

The fluorescence images of PDI-$(SO_4)_4$ in an m-55 solution at 29 ^oC (above T_c) are shown in Figure 4-10d. In the images, numerous fluorescence spots from individual single molecules can be observed clearly, indicating that reporter dye molecules are bound to the polymer rich domains leading to suppression of rapid diffusion of the dye in the solution. What distinguishes the present results from those of the atactic polymer (m-46, Figure 4-10b) is that some dye molecules are *immobile* in the isotactic-rich PNIPAM solution. The center image in Figure 4-10d was taken 0.9 s after taking the left-sided image. Despite the long elapse time (Δt = 0.9 s), several dye molecules, marked by the circles in the image, do not diffuse and are immobilized in their original positions. This strongly demonstrates that diffusion of the polymer-rich domains in the solution is "frozen" after phase separation above T_c. Since such behavior has never been observed for the atactic PNIPAM samples, this is peculiar to the isotactic-rich PNIPAM samples. The growth of the inter-chain polymer networks formed at room temperature before phase separation is enhanced by elevating temperature after phase separation. In Figure 4-10e, each PDI-$(SO_4)_4$ fluorescence intensity distributions observed from an aqueous m-55 solution at 29 ^oC accumulated for 200 frames are shown, where the black areas correspond to the higher fluorescence intensity regions. This figure shows a frozen-gel-like structure. The polymer networks composed of the domains are fully observed in the whole image. These polymer networks are a kind of a physical gel, which has

been reported for a more highly isoctactic-rich PNIPAM (*m* : *r* = 65:35) by Nakano et al. [142].

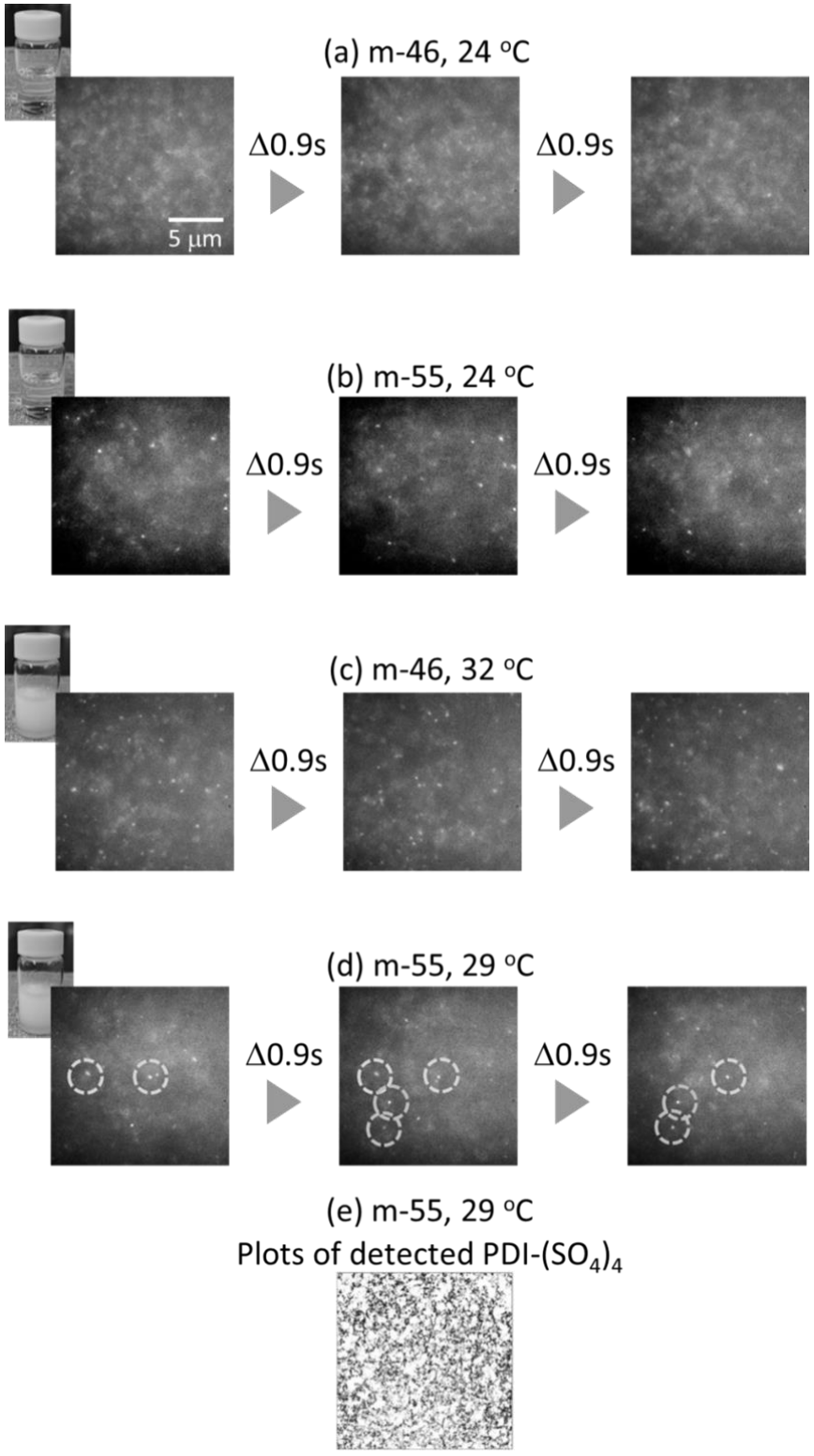

Figure 4-10. Fluorescence images of PDI-$(SO_4)_4$ in aqueous solutions of (a) m-46 at 24 °C, (b) m-55 at 24 °C, (c) m-46 at 32 °C, (d) m-55 at 29 °C. The concentrations of the polymers and PDI-$(SO_4)_4$ are 5.0 wt% and 10^{-10} M, respectively. Scale bar = 5 μm. (e) Fluorescence intensity distribution of PDI-$(SO_4)_4$ observed for an aqueous m-55 solution at 29 °C accumulated for 200 frames. The black color corresponds to the fluorescence.

For more precise experiments, single molecule fluorescence imaging experiments on an aqueous m-55 solution (5.0 wt%) were conducted by adding a small amount of Rh-m55 (0.70 nM) in the solution. As the results are shown in Figure 4-11, the analogous behaviors with those in Figure 4-10d were observed, confirming formation of the polymer network structures below T_c and a physical gel above T_c.

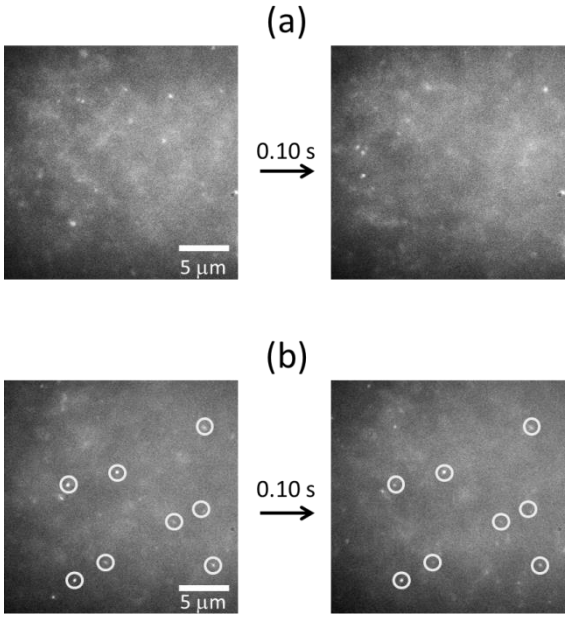

Figure 4-11. Fluorescence images of Rh-m55 (0.7 nM) in an aqueous solution of m-55 (5.0 wt %). The time interval between the left- and right-handed images is 0.1 s. Scale bar = 5 μm. Fluorescence spots that do not diffuse during the time interval are marked by the white circles. (a) At 24 °C (before phase separation). (b) At 32 °C (after phase separation).

4.3.4 Fluorescence correlation spectroscopy (FCS)

Fluorescence correlation spectroscopy (FCS) has frequently been applied for analyzing the phase separation behaviors of PNIPAM solutions [143]–[145]. For instance, Wang et al. synthesized fluorescence-labeled PNIPAM and performed FCS in water/ethanol mixtures to evaluate the hydrodynamic radius of the polymer and reported that the radius of the polymer depended upon the ethanol fraction in the solution [144]. Raccis et al. reported FCS for a grafted hydrogel film of PNIPAM to probe the mobility and inhomogeneity of the polymer [145]. In the present study, quantitative detection of multiple (double) diffusion components originated from the polymer networks and the gel like structures of the polymer was explored.

Figure 4-12a – d show the experimental correlation functions ($G(t)$) of PDI-$(SO_4)_4$ diffusing in aqueous m-46 (5.0 wt%) and m-55 solutions (5.0 wt%) before and after phase separation. The results obtained by the experiments are summarized in Table 4-2. Polymer network formation in an aqueous m-55 solution before and after phase separation was also verified by the FCS measurements. This provides the diffusion coefficients of the dye in the sample solutions. Before phase separation at 24 ^{o}C, only a single dye diffusion component with the diffusion coefficient of D = 96 $\mu m^2 s^{-1}$ was observed for the *m-46* solution (5.0 wt%) as shown in Figure 4-12a, which agreed with that determined in a homogeneous polymer solution. On the other hand, the *m-55* solution (5.0 wt%) before phase separation at 23 ^{o}C exhibited two dye diffusion components: D_1 = 175 $\mu m^2 s^{-1}$ and D_2 = 12 $\mu m^2 s^{-1}$ (Figure 4-12c). The obtained diffusion coefficients were transformed to hydrodynamic radius (R_h) of each domain by Einstein-Stokes equation (eq. 4.3).

$$R_h = \frac{kT}{6\pi\eta_0 D} \quad (4.3)$$

In eq. 4.3, k, T and η_0 are the Boltzmann constant, temperature and viscosity of solvent, respectively. In the case of the *m-55* solution before phase separation, R_h estimated from D_2 was 2.8 nm. This size is close to R_h (2.2 nm) of *m-55* chain measured by DLS as shown in Figure 4-8. These results indicate that the slow component (D_2) corresponds to that of the dye molecules bound to the polymer networks. After phase separation of the solution at 32 ^{o}C, the diffusion constants of both fast and slow components decreased to D'_1= 75 $\mu m^2 s^{-1}$ and D'_2 = 0.10 $\mu m^2 s^{-1}$, respectively, as seen in Figure 4-12d. The R_h of the domain estimated from D'_2 was 218 nm. The origin of the very large domain size can safely be ascribed to the frozen polymer networks (i.e., formation of a physical gel). It is worth pointing out that the small D'_2 value is in good agreement with the D values estimated by the SMI experiments for the PDI-$(SO_4)_4$ and Rh-m55 solutions: D = 0.16 $\mu m^2 s^{-1}$ for PDI-$(SO_4)_4$ and 0.023 $\mu m^2 s^{-1}$ for Rh-m55. Thus, the results obtained by FCS are consistent almost satisfactorily with those by SMI.

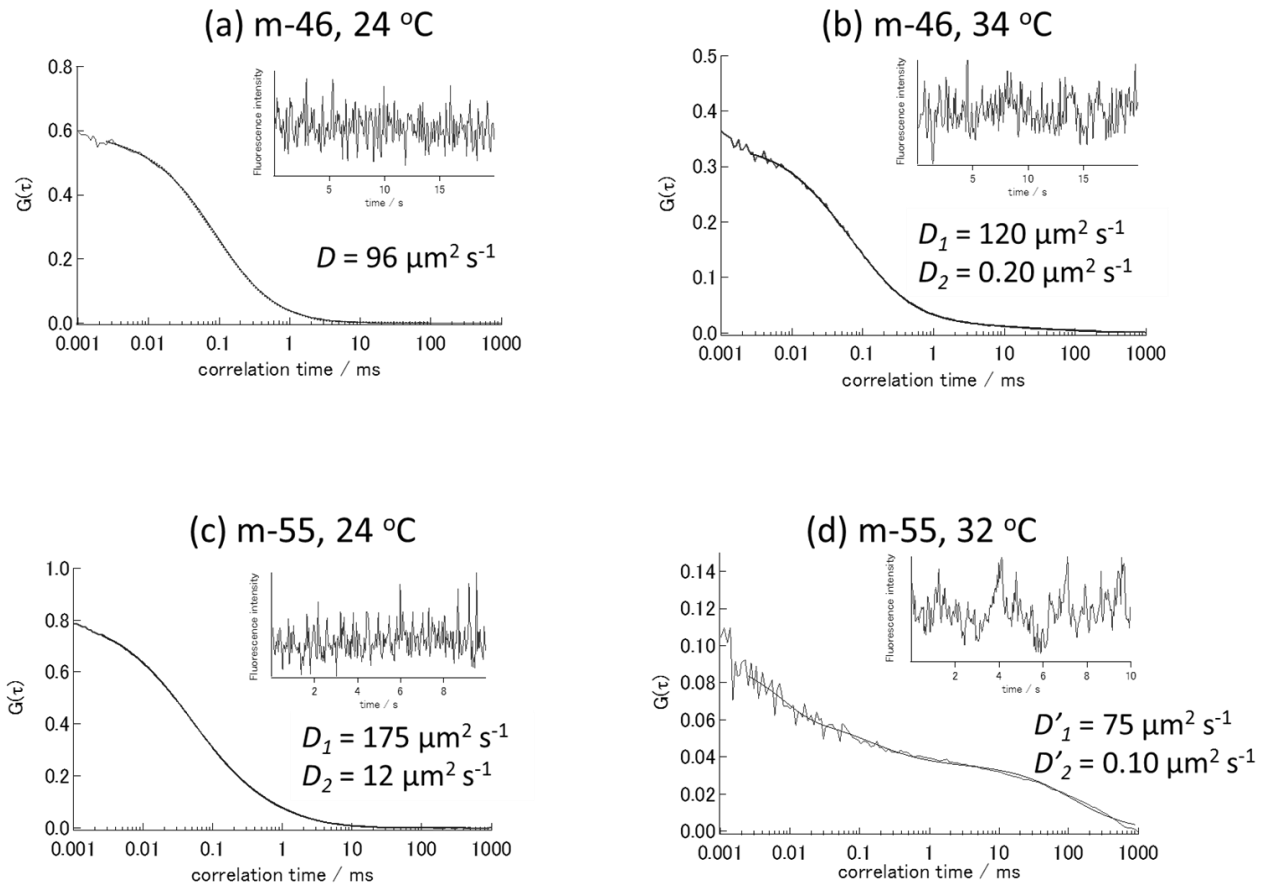

Figure 4-12. FCS correlation curves observed for PDI-$(SO_4)_4$ in aqueous solutions of (a) m-46 at 24 °C, (b) m-55 at 24 °C, (c) m-46 at 32 °C, and (d) m-55 at 29 °C. Solid curves: experimental curves. Dotted curves: fitting curves for single (a) and two dye diffusion components analysis based on $G(t)$ in Eqs. 4-1 and 4-2, respectively (b, c, and d).

Table 4-2. Diffusion coefficients of PDI-$(SO_4)_4$ in aqueous solutions of m-46 at 24 °C, m-55 at 24 °C, m-46 at 32 °C and m-55 at 29 °C.

Sample name	T (°C) [1]	N_{coop} [2]	D ($\mu m^2 s^{-1}$) [3]	R_h of domain (nm) [4]
m-46	24	1	96	0.23
	32	2	fast component 120	0.18
			slow component 0.20	110
m-55	24	2	fast component 175	0.13
			slow component 12	2.8
	29	2	fast component 75	0.29
			slow component 0.10	218

[1] Solution temperature, [2] Number of diffusion components, [3] Diffusion coefficient, [3] Hydrodynamic radius (R_h) estimated by eq. 4.3.

4.4 Conclusions

In this chapter, it has been shown that phase separation of aqueous PNIPAM solutions can be accelerated by a slight increase in the isotacticity of the polymer from *m* : *r* = 46:54 to *m*:*r* = 48~55: 52~45. For isotactic-rich PNIPAM (m-55), a single molecule fluorescence imaging (SMI) technique demonstrated formation of polymer networks even before phase separation of the polymer below T_c. Such polymer network formation has not previously been observed by Raman spectroscopy and dynamic light scattering measurements. Formation of the polymer networks is considered to be the origin of acceleration of phase separation in aqueous isotactic-rich PNIPAM solutions. Furthermore, “frozen” polymer networks similar to a physical gel were observed for isotactic-rich PNIPAM samples after phase separation. The results by FCS experiments satisfactorily corroborate with this model and provide important information. Although the

formation mechanisms of the polymer networks are complicated and still remain unclear, a precise control of the polymer stereoregularity will open new channels toward the design and development of stimuli-responsive-polymer-based smart materials.

Chapter 5| Phase separation dynamics of aqueous syndiotactic-rich PNIPAM solutions

5.1 Introduction

In chapter 4, it was demonstrated that the phase separation processes in aqueous poly(*N*-isopropyl acrylamide) (PNIPAM) solutions could clearly be accelerated by a slight increase in the isotacticity of the polymer. Furthermore, on the basis of a single molecule fluorescence imaging technique and fluorescence correlation spectroscopy introduced for the first time for the related researches, it was revealed that isotactic-rich PNIPAM produced microscopic inter-chain networks even below T_c in an aqueous solution, demonstrating that such polymer networks were the origin of rapid phase separation in aqueous isotactic-rich PNIPAMs solutions. These results suggest that the stereoregularity of PNIPAM is one of the most important factors regulating the phase separation characteristics.

Several research groups recently reported that streoregularity controls of PNIPAM affected the physical properties of the polymer such as a lower critical solution temperature (LCST), the solubility in water, and the aggregation mechanisms of phase separation [61]–[64], [141], [142]. It should be pointed out that a large portion of these studies have focused on the properties of aqueous isotactic-rich PNIPAM solutions. By contrast, the studies on the phase separation properties of aqueous syndiotactic-rich PNIPAM solutions have been rarely reported, although this is in part very important for wide applications of isotactic-rich PNIPAMs as self-assembling materials [146]–[149].

Although, there is no report on the self-assembling behavior of syndiotactic-rich PNIPAM, some research groups reported intriguing behaviors of syndiotactic-rich PNIPAMs. Hirano et al. established the polymerization method of syndiotactic-rich PNIPAMs and demonstrated that the intrapolymer hydrogen bonding between the amide groups in the syndiotactic arrangement was formed in the dehydrated state after the coil-globule transition [63], [135]. Furthermore, Mori et al. reported that the number of a cooperative unit, defined as the number of the monomer unit

exhibiting simultaneous dissociation of the bound water molecules from the polymer chains after the coil-globule transition, increased in the syndiotactic-rich poly(*N*-*n*-propylacrylamide) (PNNPAM) compared to those in other stereoregulataed PNIPAMs [150].

In this chapter, the phase separation dynamics of aqueous solutions of PNIPAM with different stereoregularities (atactic and syndiotactic-rich) were investigated by using dye-sensitized laser T-jump experiments. The phase separation mechanisms of aqueous syndiotactic-PNIPAM solutions were then discussed in terms of the hydrophobicity in the dehydrated state of the polymer. The results obtained by differential scanning calorimetry (DSC) and dynamic light scattering (DLS) measurements for the polymer solutions were also discussed based on a diffusion-controlled aggregation model.

5.2 Sample preparations and experimental procedures

5.2.1 Sample preparations

N-Isopropylacrylamide (NIPAM) (Wako Pure Chemicals Co., Ltd., 98%) as a monomer was recrystallized twice from *n*-hexane (wako, > 96%). 2,2'-Azobis(isobutyronitrile) (AIBN) (Wako Pure Chemicals Co., Ltd., > 98%) as a polymerization initiator was recrystallized from methanol (Wako Pure Chemicals Co., Ltd., > 99.8%). Acetone (> 99.5%), 1-butanol (> 99.0%), tetrahydrofuran (THF, > 99.5%), and diethyl ether (> 99.5%), all purchased from Wako Pure Chemicals Co., Ltd., and tri-*n*-butylborane (*n*-Bu_3B), 3-methyl-3-pentanol (3Me3PenOH), and 2,6-di-*t*-butyl-4-methylphenol, supplied from Aldrich Co., Ltd. were used without further purification for the polymerization reactions described below.

Atactic PNIPAM was synthesized by a free radical polymerization in 1-butanol at 60 °C for 4 h using a 1.76 M (M = mol/dm^3) NIPAM monomer and a 9.55 mM AIBN initiator. The polymer was purified by repeated reprecipitation of the acetone solution of the polymer to *n*-hexane.

Typical polymerization procedures for syndiotactic-rich PNIPAM are as follows [63], [151]–[153]: NIPAM and 3Me3PenOH were dissolved in toluene. The polymerization of the

monomer was initiated by adding a THF solution of *n*-Bu_3B to the solution and allowed to heat at 60 °C. The concentrations of the reactants are shown in Table 1-1. The reaction was terminated after 24 h by adding a small amount of a THF solution of 2,6-di-*t*-butyl-4-methylphenol. The reaction mixture was poured into a large amount of diethyl ether, and the precipitated polymers were collected by filtration and, then, dried *in vacuo*.

5.2.2 Characterizations of PNIPAM samples

The number-averaged molecular weights (M_n) and polydispersities (M_w/M_n) of the samples were determined by using size exclusion chromatography (SEC) (HLC 8220 instrument, Tosoh Co., flow rate of 0.35 mL min^{-1}) equipped with TSK gels (SuperHM-H, Tosoh Co.) using *N*,*N*-dimethylformamide containing 0.1 M of LiBr as an eluent at 40 °C. The SEC chromatogram shown in Figure 5-1 was calibrated with standard polystyrene samples (Polymer Laboratories, Amherst, MA). The ^1H NMR spectra of the polymers in DMSO-d_6 at 140 °C were measured on a JEOL ECP-400 spectrometer (400 MHz). The meso diad (m) : racemo diad (r) ratios of the PNIPAM samples were determined based on the peak area ratio of the methylene protons at 1.3 ppm and 1.7 ppm for the meso diad to that at 1.5 ppm for the racemo diad of the ^1H NMR spectra of the polymers [63]. For examples, the ^1H NMR spectra of r-54 and r-68 are shown in Figure 5-2. Each peak is attributed as follows: methyl protons of the isopropyl group at δ = 1.1, methylene protons of the polymer backbone for the meso diad at δ = 1.3 and 1.7, methylene protons of the polymer backbone for the racemo diad at δ = 1.5, methine proton of the isopropyl group at δ = 3.8, and amide proton of the isopropyl group at δ = 6.7[138]. The clouding points of the polymers in water (T_c) were evaluated by the same manner with those described in §2.2.2. Table 5-1 shows the data of the PNIPAM samples. The samples are abbreviated on the basis of the content of the racemo diads in the polymers: For instance, PNIPAM with r = 60 is abbreviated as r-60.

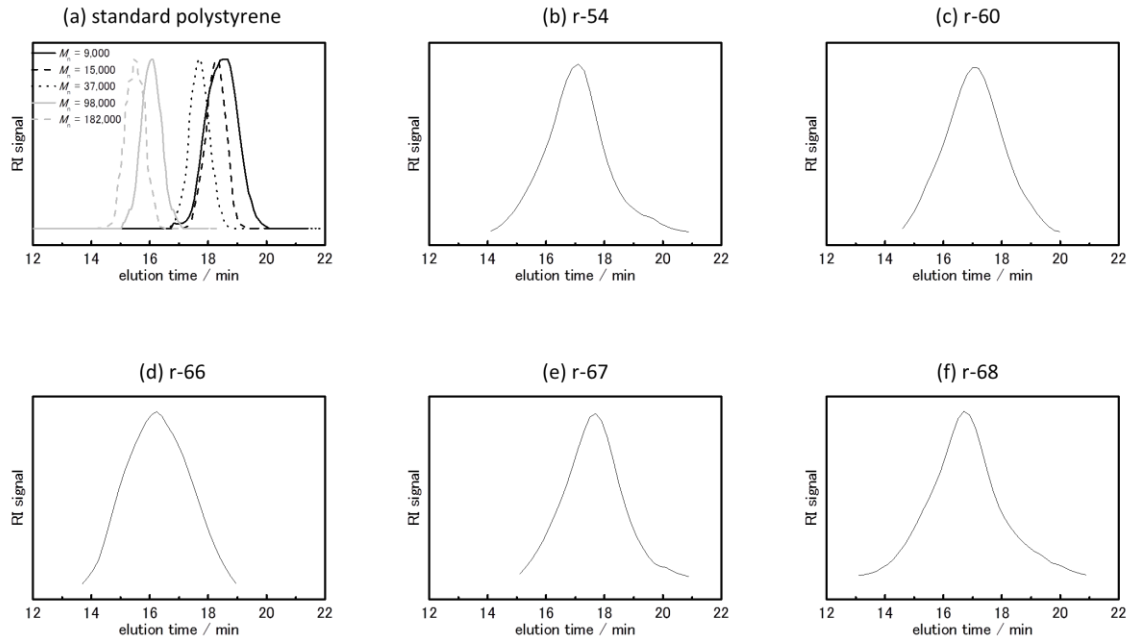

Figure 5-1. SEC chromatograms of (a) standard polystyrene samples (solid black line: M_n = 9,000, dashed black line: M_n = 15,000, doted black line: M_n = 37,000, solid gray line: M_n = 98,000, and dashed gray line: M_n = 182,00), (b) r-54, (c) r-60, (d) r-66, (e) r-67, and (f) r-68. These chromatograms were measured at 40 °C using *N*,*N*-dimethylformamide containing 0.1 M of LiBr as an eluent.

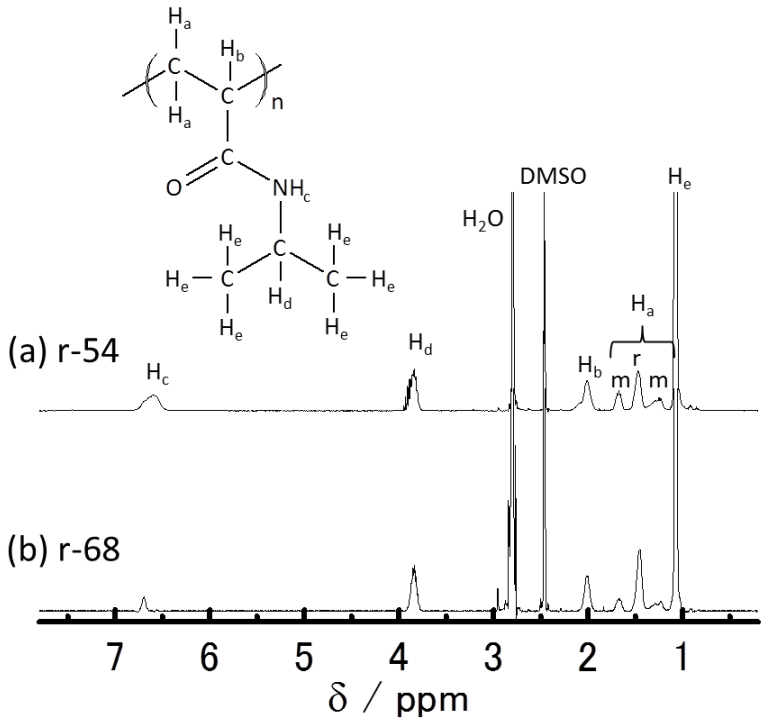

Figure 5-2. ^{1}H NMR spectra of (a) r-54 and (b) r-68. These spectra were measured in DMSO-d_6 at 140 °C.

Table 5-1. Concentration of reactants for radical polymerization and fundamental properties of the sample polymers. M_w; weight-averaged molecular weight, M_n; number-averaged molecular weight, *m*: meso diad ratio, *r*: racemo diad ratio, T_c: cloud point.

Sample name	[NIPAM] (M)	[*n*-Bu_3B] (M)	[3Me3PenOH] (M)	M_n (1)	M_w / M_n (1)	*m* : *r* (2)	T_c(°C) (3)
r-54	1.0	0.10	–	31,000	2.1	46 : 54	32
r-60	0.5	0.10	1.0	36,000	1.5	40 : 60	32
r-66	1.0	0.05	2.0	61,000	2.3	34 : 66	33
r-67	0.5	0.10	2.0	20,000	2.0	33 : 67	33
r-68	0.5	0.05	2.0	33,000	2.0	32 : 68	34

(1) Determined by size exclusion chromatography (SEC)

(2) Determined by ^{1}H NMR.

(3) Determined by turbidimetry in a 1.0 wt% aqueous solution.

5.2.3 Laser-induced T-jump method

In this chapter, two types of laser-induced temperature jump techniques were employed: (i) a direct method by which water as a solvent was heated by infrared laser light and (ii) a dye-sensitized laser-heating method using a dye as a molecular heater. In the dye-sensitized laser T-jump technique, 0.50 mM of crystal violet was added to a sample solution. The instrumental setups were the same as those described in chapter 2.

5.2.4 Differential scanning calorimetry (DSC)

DSC measurements were performed by a DSC micro calorimeter (Mettler-Toledo) with a cell volume of 100 μL at the heating rate of 1.0 ºC min^{-1} in the range of 25-40 ºC under elevated pressure (> 1.1 x 10^5 Pa).

5.2.5 Dynamic light scattering (DLS)

The hydrodynamic radius (R_h) distributions of the polymers in water were measured by

dynamic light scattering (DLS) (Otsuka Electronics, FDLS-3000) at 25 °C. A 100 mW laser (λ = 532 nm) was used as an incident beam, and the scattering angle was set 90°.

5.3 Results and Discussion

5.3.1 Sensitivity of phase separation to laser-induced T-jump

Figure 5-3 shows a representative time profile of optical transmittance ($T(t)$) obtained by the method (i) for syndiotactic-rich PNIPAM (r-68, black line) at a concentration of 5.0 wt%. The results on an atactic PNIPAM (r-54, gray line) solution (5.0 wt%) are also shown in the figure as a reference. These two polymers have similar molecular weights and, thus, the effects of the stereoregularity of the polymer on the phase separation dynamics can be discussed. As seen in the figure, $T(t)$ observed for r-54 decreases immediately after a T-jump and reaches a quasi-equilibrium state after 200 ms, where the transmittance approaches a constant value. The sharp drop of $T(t)$ is due to an increase in the turbidity of the solution by phase separation. The $T(t)$ curve observed for r-54 can be well fitted by a single exponential function, $T(t) = A \exp(-t/\tau_{ps}) + B$, and the fit by a single exponential function provides the phase separation time constant (τ_{ps}) to be 77 ms. In the case of r-68, on the other hand, the transmittance keeps constant after a T-jump even at laser power being set the same with that for the experiments for r-54. The results strongly demonstrate that phase separation of an aqueous r-68 solution requires a higher T-jump.

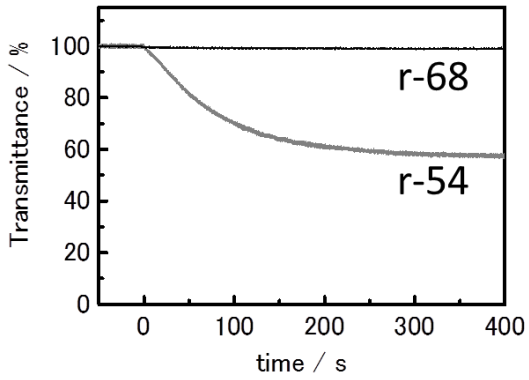

Figure 5-3. Typical examples of the time courses of the transient transmittance $T(t)$ in aqueous r-68 (black line) and r-54 (gray line) solutions (5.0 wt%).

Since the direct *T*-jump method (i) could not induce phase separation of aqueous syndiotactic-rich PNIPAMs solutions, the dye-sensitized *T*-jump method (ii) was employed. Figure 5-4 shows typical examples of the time courses of the transient transmittance $T(t)$ obtained by the method (ii) at several laser fluences as heating pulses: from 0.10 to 0.39 J·cm^{-2}. As seen in the figure, the laser fluence dependences of $T(t)$ observed for aqueous highly syndiotactic-rich PNIPAMs (c: r-66, d: r-67, and e: r-68) solutions were essentially different from those for r-54 and r-60 (Figures 5-4a and b, respectively). The $T(t)$ values of highly syndiotactic-rich PNIPAMs recovers relatively faster at the laser fluence lower than 0.18 J·cm^{-2}. According to the figure, the lowest laser energies inducing phase separation of aqueous r-54, r-60, r-66, r-67, and r-68 solutions were evaluated to be 0.10, 0.11, 0.16, 0.17, and 0.16 J·cm^{-2}, respectively. On the basis of these results, it is concluded that aqueous solutions of syndiotactic-rich PNIPAMs with the racemo diad contents of 66% or > 66% require higher T-jumps for phase separation.

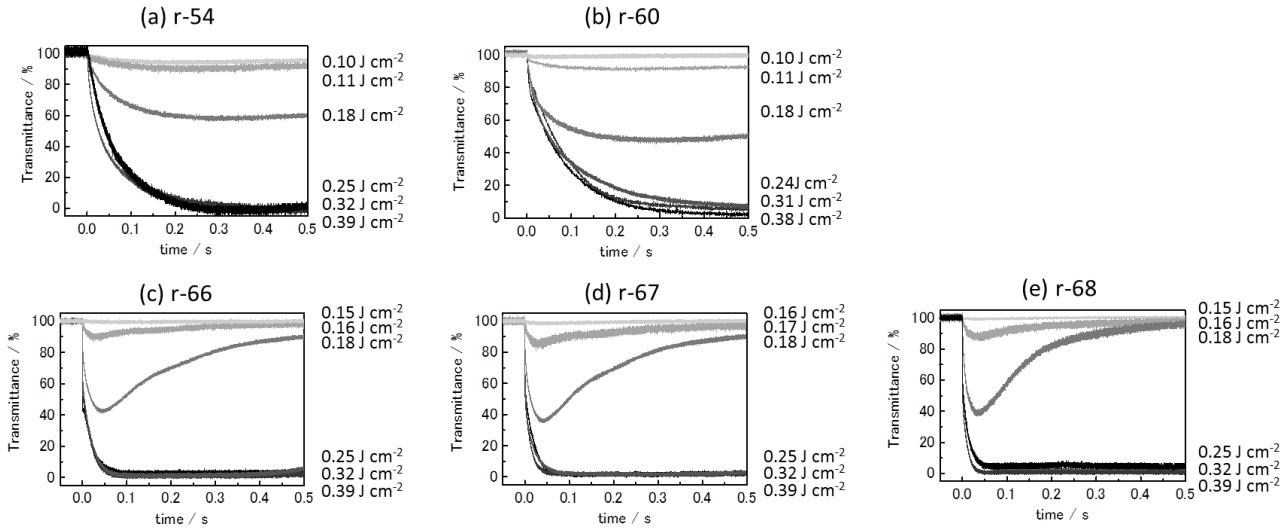

Figure 5-4. Typical examples of the time courses of the transient transmittance $T(t)$ in aqueous (a) r-54, (b) r-60, (c) r-66, (d) r-67, and (e) r-68 solutions (5.0 wt%) in the presence of crystal violet (0.50 mM) as a function of an incident heating laser pulse energy.

5.3.2 Phase separation rate

The phase separation time constants (τ_{ps}) of aqueous syndiotactic-rich PNIPAM solutions were systematically determined by the method (ii) as a function of the polymer concentration (0.50

~ 7.0 wt%). Figure 5-5a shows representative results on r-68. Each decay curve can be well fitted by a single exponential function. In the figure, it is demonstrated that the decay of $T(t)$ becomes faster with increasing the polymer concentration. Interestingly, $T(t)$ decay becomes abruptly sharp above the polymer concentration at > 1.5 wt%. The similar behaviors with those for r-68 were also observed for other highly syndiotactic-rich PNIPAMs as shown in Figure 5-5c and d. By contrast, time decay of the transmittance observed for r-54 and r-60 becomes gradually faster with increasing the polymer concentration as seen in Figures 5-5b and 5-5c, respectively.

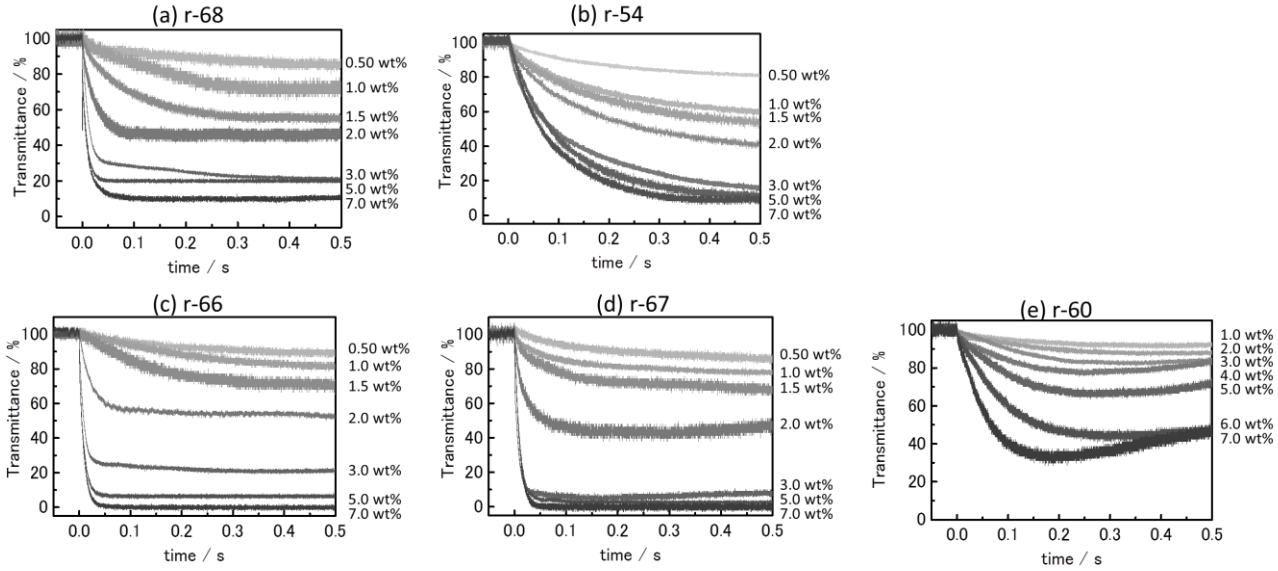

Figure 5-5. Typical examples of the time courses of the transient transmittance $T(t)$ in aqueous (a) r-68, (b) r-54, (c) r-66, (d) r-67, and (e) r-60 solutions in the presence of crystal violet (0.50 mM) as a function of the polymer concentration (0.50 – 7.0 wt%).

In Figure 5-6a, the τ_{ps} values are plotted against the polymer concentrations for both aqueous r-54 (open symbols) and r-68 solutions (filled symbols). The figure clearly shows that these two samples exhibit different dynamic behaviors and, in the low concentration region (0.50 ~ 1.5 wt%), the time constants observed for r-54 and r-68 are close with each other (τ_{ps} = 150 ~200 ms). In the high concentration region (2.0 ~ 7.0 wt%), by contrast, r-68 exhibits much faster phase separation (τ_{ps} = 10 ~ 30 ms) than r-54 (τ_{ps} = 50 ~ 100 ms). It should be pointed out here that τ_{ps} becomes constant when the polymer concentration is higher than a critical value (1.5 wt%). Similar behaviors to those in Figure 5-6a are also observed for the other highly syndiotactic-rich

PNIPAMs, r-67 and r-66, as shown in Figures 5-6b and c, while r-60 shows similar phase separation time constants to those of r-54. It is important to point out that the critical solution concentration showing an accelerated phase separation time constant is common for all of the highly syndiotactic-rich PNIPAMs studied in the present experiments: 1.5 wt%. Such behavior is a key to understand the phase separation mechanisms of the polymer solutions as discussed in §5.3.6.

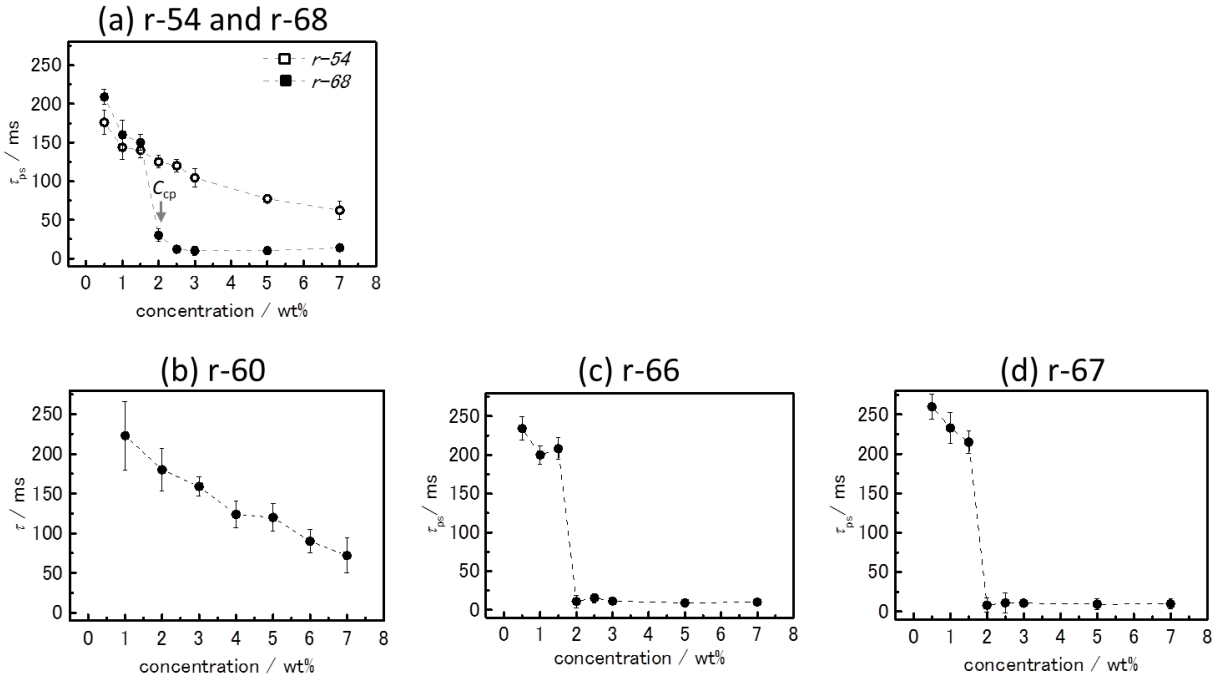

Figure 5-6. Phase separation time constants as a function of the polymer concentration (0.50 – 7.0 wt%) in aqueous (a) r-54 (open circles) and r-68 (filled circles), (b) r-60, (c) r-66, and (d) r-67 solutions in the presence of crystal violet (0.50 mM).

5.3.3 Quantitative analysis

The τ_{ps} values ranging from 200 to 10 ms evaluated in the present study is worth being discussed theoretically. As described in §3.3.5, The growth time is then given by eq. (3-1),

$$t = \frac{3}{4}\left(N_{glo} \times M_w - M_w\right)\frac{\eta}{N_A kTc} \qquad (3\text{-}1)$$

where N_{glo} is the number of the polymer chains in a single polymer-rich domain. Based on the relations described in §3.3.5, the average number of the polymer chains in a single polymer-rich

micro-domain ($N_{glo} = \langle M_{agg} \rangle / M_w$) in *r-54* and *r-68* solutions are estimated to be 2000 and 1900, respectively. Then, using eq. (3-1), the growth time of a polymer-rich microdomain in *r-54* and *r-68* solutions at 1.0 and 5.0 wt% are estimated to be ≈ 15 (1.0 wt%) and 3.0 ms (5.0 wt%), respectively. These calculated values for *r-54* are somewhat smaller than the τ_{ps} values obtained by the experiments (τ_{ps} = 70 ~ 200 ms). This suggests that the aggregation of globules takes place through numbers of collisions of globules; the aggregation is growth-controlled process. This model is applicable to *r-68* solution at 1.0 wt%. On the other hand, in case of *r-68* solution at 5.0 wt%, τ_{ps} value is 10 ms, which is very close to the calculated value (3.0 ms). This means that every collision of globules of *r-68* at 5.0 wt% results in aggregation; aggregation takes place efficiently.

5.3.4 DSC experiments

Figure 5-7 shows the heat capacity changes during phase transition/separation of aqueous r-54, r-60, and r-68 solutions (1.0 wt%) at a heating rate of 1.0 °C/min. With an increase in the syndiotacticity of the polymer, the endothermic peak resulting from dehydration of the polymer chains becomes significantly sharper and shifts to a higher temperature. The thermodynamic parameters determined by the DSC measurements are summarized in Table 5-2. The number of the cooperative units n_{coop}, which is defined by the number of the monomer unit undergoing dissociation of the bound water molecules from the polymer chains, can be calculated by the ratio of the van't Hoff enthalpy (ΔH_v) to the calorimetric enthalpy (ΔH_c) [150], [154]. Obviously seen in Table 5-2, the n_{coop} value roughly increases with an increase in the syndiotacticity. The results indicate that the cooperativity of dehydration, which is defined as the length of the sequential polymer chains exhibiting simultaneous dissociation of the bound water molecules, increases with increasing the racemo diad content.

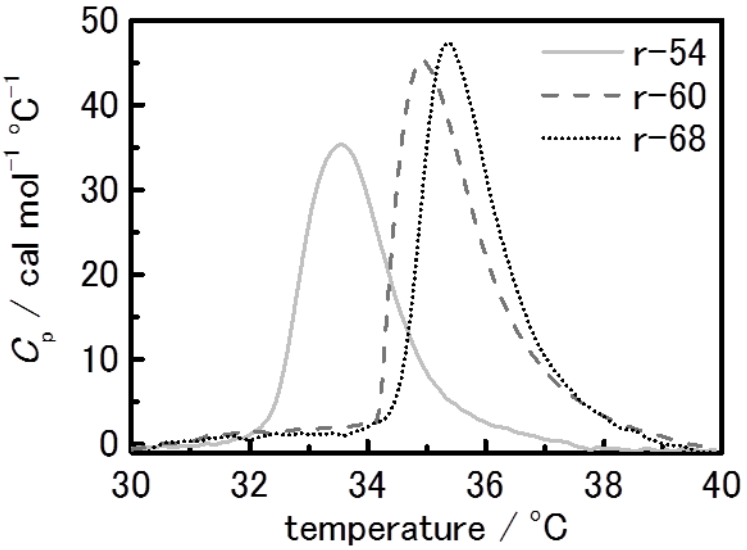

Figure 5-7. Heat capacity changes during phase transition/separation (30 – 40 °C) of aqueous r-54 (solid curve), r-60 (dashed curve), and r-68 (dotted curve) solutions (1.0 wt%). Heating rate = 1.0 ^{o}C min^{-1}.

Table 5-2. Thermodynamic parameters during phase transition/separation (30 – 40 °C) of aqueous r-54, r-60 and r-68 solutions (1.0wt%).

Sample name	T_p / ^{o}C[(1)]	$\Delta T_{1/2}$ / ^{o}C[(2)]	ΔH_c / cal mol^{-1}[(3)]	ΔH_v / kcal mol^{-1}[(4)]	n_{coop}[(5)]
r-54	33.6	1.68	68.8	5.34	77
r-60	34.9	1.54	82.5	6.29	76
r-68	35.4	1.42	79.3	7.01	88

(1) Temperature of the endothermic peak. (2) Full-width at half maximum of the endothermic peak. (3) calorimetric enthalpy. (4) van't Hoff enthalpy calculated by the equation $\Delta H_v = 4R\,T_p^2/\Delta T_{1/2}$ (R: gas constant) (5) Number of the cooperative units, $n_{coop} = \Delta H_v/\Delta H_c$.

5.3.5 Cloud points and hysteresis

Figure 5-8 shows the transmittance curves of aqueous (a) r-54, (b) r-60, and (c) r-68 solutions as a function of temperature. The black and gray curves show the transmittance changes upon heating and cooling, respectively. The T_c increased with increasing the racemo diad content in the polymer. Furthermore, with increasing the racemo diad content, the hysteresis in the T-dependent transmittance between heating and cooling processes became larger. These tendencies

are in good agreement with the results reported previously [63]. As Zhang et al. reported, formation of intra- or inter-polymer hydrogen bonding in a collapsed state above T_c causes to keep association of the polymers even at a temperature below T_c, resulting in the hysteresis. Thus, the large hysteresis in an aqueous syndiotactic PNIPAM solution implies that syndiotactic-rich PNIPAM possibly forms the intrapolymer hydrogen bonding in the dehydrated state.

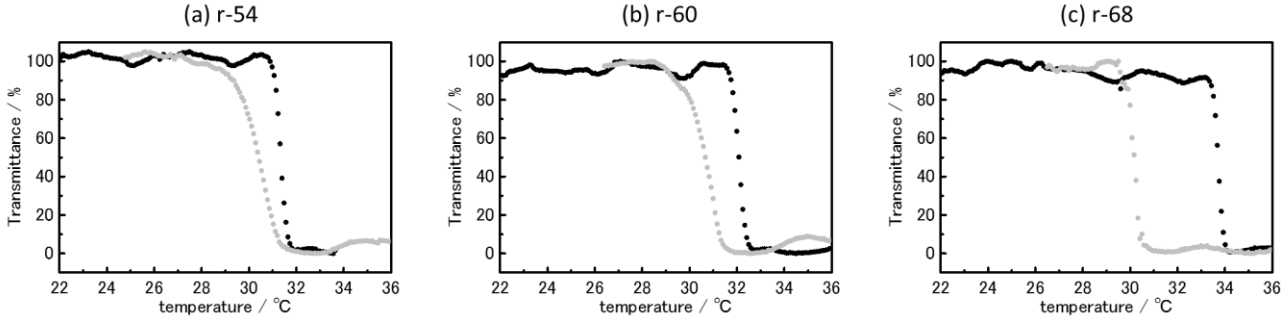

Figure 5-8. Temperature dependences of the optical transmittance at 532 nm for the aqueous (a) r-54, (b) r-60, and (c) r-68 solutions. The black and gray curves show the transmittance changes upon heating and cooling, respectively. Heating and cooling rate = 0.2 ^{o}C min^{-1}.

5.3.6 DLS experiments

To investigate the polymer structures in an aqueous solution, the hydrodynamic radii (R_h) of each syndiotactic-rich PNIPAM at several concentrations ranging from 0.50 to 7.0 wt% were evaluated based on dynamic light scattering (DLS) experiments. Figure 5-9 shows the concentration dependences of the R_h distributions for highly syndiotactic-rich PNIPAMs (a: r-68, b: r-67, and c: r-66). In the low concentration region (0.50 ~ 1.5 wt%), a single peak was observed, indicating the polymer chains were not entangled with one another. Above 2.0 wt%, by contrast, two peaks were observed, demonstrating interpolymer entanglement. Thus, the common critical polymer concentration (1.5 wt%) can be confirmed for both dynamic behaviors (phase separation rate) and static structures (entanglements). Below and above the critical polymer concentration, both dynamic and static characteristics mentioned above change considerably as described in §5.3.2 and 5.3.5. Obviously, such polymer entanglements in an aqueous solution are the origin of the acceleration of the phase separation rate observed for highly syndiotactic-rich PNIPAMs. On

the basis of these findings, the phase separation mechanisms for highly syndiotactic-rich PNIPAMs are discussed in §5.3.6.

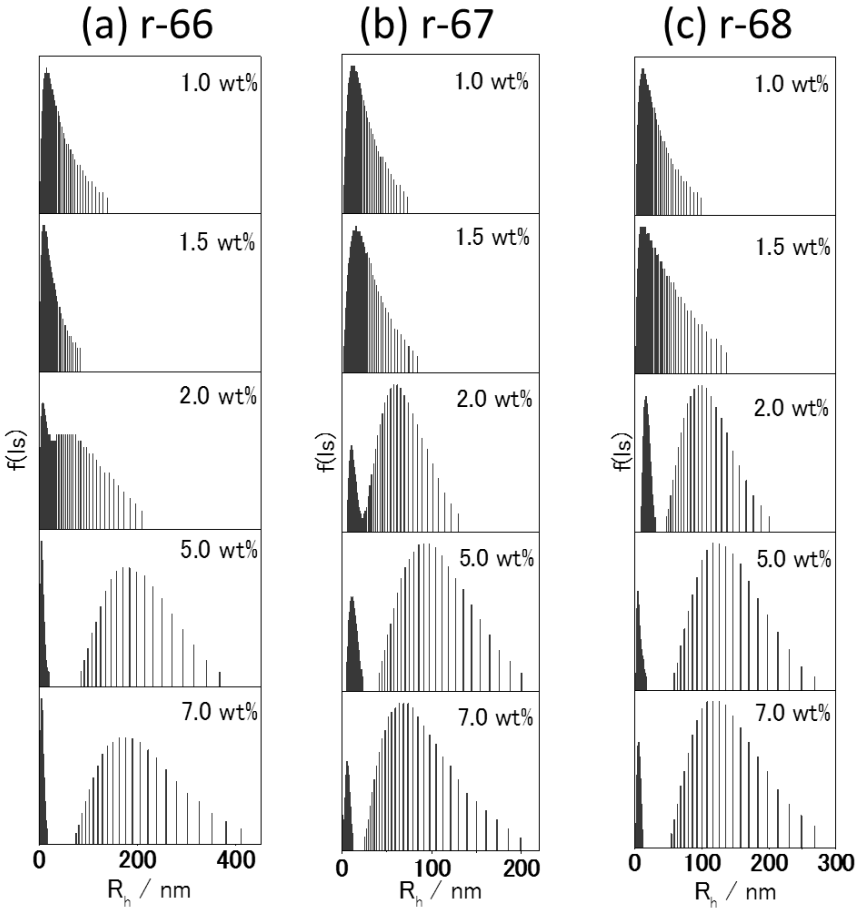

Figure 5-9. Hydrodynamic radius distributions of a: r-66, b: r-67, and c: r-68 in aqueous solutions at room temperature as a function of the polymer concentration (0.50 – 7.0 wt%). The concentration of sample solution is given in the figure.

5.3.7 Mechanisms of phase separation for aqueous highly syndiotactic-rich PNIPAM solutions

An aqueous syndiotactic-rich PNIPAM solution exhibited curious phase separation behaviors, showing less sensitive phase separation by a near-infrared laser *T*-jump and acceleration of phase separation at a high polymer concentration observed by a dye-sensitized *T*-jump. In this section, the origin of such experimental results is discussed and the phase separation mechanisms of an aqueous syndiotactic-rich PNIPAM solution are proposed: Figure 5-10.

First, the insensitive nature of phase separation in an aqueous syndiotactic-rich PNIPAM solution to temperature by the laser-induced T-jump technique can be explained in terms of the stability of an NIPAM-dimer in aqueous solution. Katsumoto et al. have studied the stability of an NIPAM-dimer in an aqueous solution on the basis of molecular dynamics calculations and predicted that a racemo-NIPAM-dimer (r-DNIPAM) is more stable than a meso-NIPAM-dimer (m-DNIPAM), because of the lower hydration free energy and larger conformational entropy of r-DNIPAM compared to those of m-DNIPAM [61]. Thus, it requires a higher T-jump for dissociation of the bound water molecules from the syndiotactic-rich PNIPAM and for the conformational change of the syndiotactic-rich PNIPAM chain.

Second, the origin of acceleration of the phase separation rate observed for syndiotactic-rich PNIPAM at a high concentration is worth discussing in terms of the hydrophobicity of the polymer in the dehydrated state. As already described in §5.3.3, syndiotactic-rich PNIPAM shows highly cooperative dehydration of the amide groups upon thermal phase transition. Furthermore, as seen in the results of transmittance measurements, intrapolymer hydrogen bonding formation proceeds between adjacent monomeric units in the dehydrated state in an aqueous syndiotactic PNIPAM solution. Mori et al. also have reported formation of the intrapolymer hydrogen bonding in the dehydrated state in an aqueous syndiotactic-rich poly(*N*-*n*-propylacrylamide) (PNNPAM) solution as revealed by the FT-IR spectrum of the polymer [150]. The highly cooperative dehydration and formation of the intrapolymer hydrogen bonding make the dehydrated polymer chains more hydrophobic. As a result, aggregation (phase separation) of the syndiotactic-rich polymer becomes faster compared to that of the atactic polymer.

Third, the mechanisms of the specific concentration dependence of the phase separation rate observed for the syndiotactic-rich PNIPAMs are worth discussing based on the results of the laser T-jump and DLS measurements. In a higher concentration region ($\geq$ 2.0 wt%), polymer chains formed aggregates even at room temperature (before phase separation). Under such situation, phase separation occurs through two ways; i) shrinkage of the aggregates formed before phase separation,

and ii) diffusion of single globules and aggregation of them (normal phase separation). Although there were two ways of phase separation at the high concentration region, the $T(t)$ was fitted by single exponential function. In the present study, phase separation dynamics is characterized by optical transmittance (i.e. Rayleigh light scattering). It is well known that the Rayleigh scattering intensity is proportional to the third power of the diameter of particles. Therefore, at the high concentration region, shrinkage of the aggregates was mainly observed as the signal of phase separation. The shrinkage underwent much faster than normal phase separation due to high hydrophobicity. This process is independent of concentration because diffusion of the polymer chains in the solution is not necessary for phase separation.

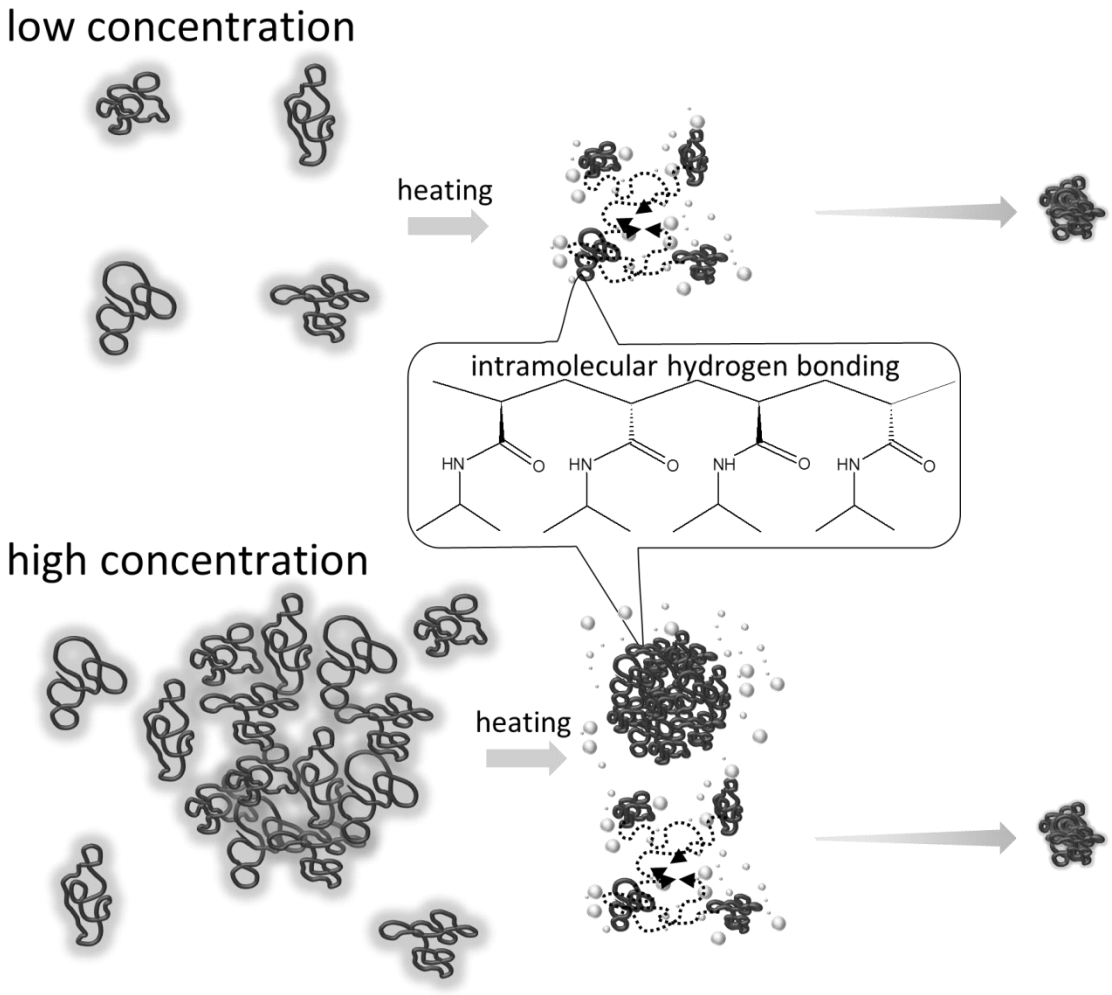

Figure 5-10. Schematic illustration of the phase separation mechanisms of an aqueous syndiotactic-rich PNIPAM solution.

5.4 Conclusions

In the present study, the phase separation dynamics of aqueous PNIPAMs solutions with various syndiotacticities ranged in 54 - 68 % was investigated by using a dye-sensitized laser-induced T-jump technique. To induce phase separation of aqueous highly syndiotactic-rich PNIPAM solutions by the laser-induced T-jump technique, higher T-jump was required compared to that of r-54 and r-60. The phase separation rates of aqueous highly syndiotactic-rich PNIPAM solutions evaluated by the dye sensitized T-jump method became considerably fast when the solution concentration was higher than a critical value (1.5 wt%), while those of r-54 and r-60 became gradually fast with increasing the polymer concentration. By combining the results of laser-induced T-jump and DLS measurements, it was revealed that acceleration of the phase separation rate was induced by entanglement of the polymer chains. Furthermore, the cooperativity of the dehydration process increased with increasing the racemo diad content as revealed by DSC and optical transmittance measurements.

Based on these results, it is demonstrated that in a high polymer concentration region, syndiotactic-rich PNIPAM exhibits rapid phase separation due to the high hydrophobicity of the polymer chain originated by cooperative formation of the intrapolymer hydrogen bonding.

The present findings indicate that the phase separation processes vary and can be accelerated by increasing the syndiotacticity of the polymer even though the polymer structures in solution before phase transition are similar to those of an aqueous atactic PNIPAM solution.

Chapter 6| Conclusions

In this thesis, the phase separation dynamics of aqueous poly(*N*-isopropyl acrylamide) (PNIPAM) solutions was studied using a laser-induced temperature jump technique combined with time-resolved photometry. The phase separation rate of an aqueous PNIPAM solution was investigated as a function of the following three important factors: the PNIPAM concentration, the molecular weight of PNIPAM, and the stereoregularity of PNIPAM. The roles of these factors in controlling the phase separation behaviors were also studied on the basis of dynamic light scattering (DLS), differential scanning calorimetry (DSC), and single molecule fluorescence imaging (SMI) techniques.

In the present study, two types of laser-induced T-jump technique were employed: (i) a direct method in which water as the solvent was heated by infrared laser light and (ii) a dye-sensitized laser-heating method using a dye as a molecular heater. The laser-induced T-jump methods mentioned above were used to analyze the phase separation dynamics of aqueous PNIPAM solutions by observing the relaxation process from the heated solution to a state of thermal equilibrium. Since the heat generated by absorption of the pulsed laser beam in the water or dye molecule is within a short time (≈ 10 ns), the thermal relaxation process of the solution could be observed with a high temporal resolution.

The most fundamental factors governing the phase separation behavior of an aqueous PNIPAM solution are the concentration and molecular weight of the polymer as demonstrated by their effects on the cloud point (T_c) and the viscosity of the polymer solution as well as on the hydration structure of the polymer. Aggregation of the polymer chains in solution above T_c proceeds successively through the diffusion and collision of the PNIPAM globules and interpolymer entanglements. The concentration and molecular weight of PNIPAM play crucial roles in these processes as described in chapter 3. The time constant for phase separation, τ_{ps}, decreases with

increasing polymer concentration and levels-off at a certain constant value (≈ 40 ms) and at a certain polymer concentration (C_c) irrespective of the molecular weight of the polymer. DLS measurements indicate that the polymer chains are entangled with each other above C_c and, hence, phase separation of the polymer solution proceeds without polymer diffusion. Therefore, the τ_{ps} value is independent of the polymer concentration above C_c and converges to a certain value. With regard to the molecular weight dependence of the phase separation rate, it was demonstrated that there is an optimum molecular weight for the fast phase separation of an aqueous PNIPAM solution. This finding provides a valuable insight into the development of PNIPAM-based functional materials with quick thermo-response times. In the conclusion to chapter 3, it was revealed that controlling the solution concentration and the molecular weight of PNIPAM allowed the phase separation rate of the solution to be accelerated. Also, it was demonstrated that the initial structure of the polymer chain below T_c has a strong influence on the phase separation dynamics.

Generally, the structures of polymers in solution are also determined by the balance between the hydrophobicity and hydrophilicity of the polymer and, therefore, there are many reports on synthetic polymers having various hydrophobic/hydrophilic parts in the main and/or side chains. The hydrophobic/hydrophilic balance of PNIPAM can be controlled by the stereoregularity of the polymer, which is very important for the present study. In chapter 4, it was shown that phase separation of aqueous PNIPAM solutions can be accelerated by a slight increase in the isotacticity of the polymer from a meso diad ratio (*m*) of 46 % to 48~55 %. For isotactic-rich PNIPAM, a SMI technique demonstrated the formation of polymer networks even below T_c. Such polymer network formation has not previously been observed by Raman spectroscopy and DLS measurements. The formation of polymer networks is considered to be the origin of the acceleration of phase separation in aqueous isotactic-rich PNIPAM solutions. Furthermore, “frozen” polymer networks similar to physical gels were observed for isotactic-rich PNIPAM samples above T_c. The results obtained by FCS experiments satisfactorily corroborate this model and provide important information on the

phase separation mechanism. Although the formation mechanisms of polymer networks are complicated and still remain unclear, precise control of the polymer stereoregularity will open new channels toward the design and development of stimuli-responsive-polymer-based smart materials.

In chapter 5, the phase separation dynamics of aqueous PNIPAM solutions with various syndiotacticities ranging from 54 to 68 % were investigated using a dye-sensitized laser-induced T-jump technique, with which a higher T-jump than that obtained with the direct method could be generated. To induce phase separation in aqueous highly syndiotactic-rich PNIPAM solutions, a higher T-jump is required compared to that for aqueous r-54 and r-60 solutions, indicating that phase separation in the former is less favorable than in the latter. The phase separation rates of aqueous highly syndiotactic-rich PNIPAM solutions become considerably faster when the polymer concentration is higher than a critical value (1.5 wt%), while those of r-54 and r-60 become gradually faster with increasing polymer concentration. DLS measurements of aqueous highly syndiotactic-rich PNIPAM solutions revealed the formation of entangled polymers above the critical concentration (2.0 wt%). Furthermore, the cooperativity of the dehydration process increased with the increasing racemo diad content in PNIPAM as revealed by the present experiments. Transmittance analysis as a function of temperature showed that, with increasing racemo diad content, the hysteresis in the T-dependent transmittance curves between the heating and cooling processes becomes larger. This indicates that syndiotactic-rich PNIPAM possibly forms intrapolymer hydrogen bonding in the dehydrated state. Based on these results, the following phase separation model for aqueous highly syndiotactic-rich PNIPAM solutions is proposed; in high polymer concentration regions, syndiotactic-rich PNIPAM exhibits rapid phase separation due to the high hydrophobicity of the polymer chain originating from the cooperative formation of intrapolymer hydrogen bonding. The present findings indicate that the phase separation processes vary and can be accelerated by increasing the syndiotacticity of the polymer even though the initial polymer structure below T_c is similar to those in an atactic PNIPAM solution.

In conclusion, this thesis reveals that the phase separation rate of an aqueous PNIPAM solution is very sensitive to the concentration, molecular weight, and stereoregularity of the polymer. In this thesis, three main conclusions are reached:

1) Phase separation of an aqueous PNIPAM solution is accelerated with increasing polymer concentration.

2) There is an optimum molecular weight of PNIPAM for rapid phase separation in an aqueous solution.

3) Phase separation in an aqueous solution is accelerated by having PNIPAM with high stereoregularity.

The dynamic aspects of the phenomena are well correlated with the static aspects. Entanglement of the polymer chains formed at high polymer concentrations play an important role in the phase separation dynamics: the phase separation time constant levels-off at a certain concentration. Phase separation of aqueous highly syndiotactic-rich PNIPAM solutions becomes considerably faster when the polymer chains are entangled below T_c. Cooperative dehydration of PNIPAM in an aqueous solution, defined by simultaneous dissociation of the bound water molecules from the sequential polymer chains, and subsequent formation of intrapolymer hydrogen bonding also results in rapid phase separation of aqueous highly syndiotactic-rich PNIPAM solutions. Furthermore, it was demonstrated that formation of microscopic inter-chain networks even below T_c in an aqueous isotactic-rich PNIPAM solution is the origin of rapid phase separation in solution.

It was demonstrated that precise control of the primary structural properties of a thermo-responsive polymer, such as its molecular weight, stereoregularity as well as of the sequence of co-monomer units in the copolymer, are of primary importance in achieving rapid thermal phase separation in an aqueous polymer solution [155]. These factors are also very

important in governing the polymer structure and its properties in solution. For example, a random copolymer between *N*-isopropyl acrylamide (NIPAM) and *N*,*N*-diethylacrylamide (DEA) in an aqueous solution exhibits a lower T_c compared to those of the corresponding homopolymers [156]–[159]. Such unusual behavior is responsible for the strong hydrogen bonding between the N-H groups in NIPAM and the C=O groups in DEA [156]. According to the present study, such intra- and/or inter-polymer interactions/associations would accelerate the phase separation of an aqueous PNIPAM solution. By accumulating knowledge about the phase separation dynamics as a function of the primary structure of the polymer in solution, it should be possible to develop a new model predicting the phase separation rates based on the fundamental structural and solution properties of thermo-responsive polymers. In conclusion, the present study and further investigation of the phase separation dynamics as a function of various primary factors controlling phase separation will open new channels toward the design and development of stimuli-responsive-polymer-based smart materials.

References

[1] P. J. Lemstra, “Macromolecular Reaction Engineering, the Chain-of-Knowledge Approach,” *Macromol. Reac. Eng.*, 1, 15–24, (2007).

[2] V. Srivastava and R. Srivastava, “Advances in Automotive Polymer Applications and Recycling,” *Int. J. Innov. Res. Sci. Eng. Technol.*, 2, 744–746, (2013).

[3] I. D. W. Samuel, “Polymer Electronics,” *Phil. Trans. R. Soc. Lond.*, A, 193–210, (2000).

[4] G. Akovali, *Advances in Polymer Coated Textiles*. Smithers Rapla Technology, (2012).

[5] C. Silvestre, D. Duraccio, and S. Cimmino, “Food packaging based on polymer nanomaterials,” *Prog. Polym. Sci.*, 36, 1766–1782, (2011).

[6] S. Ebnesajjad and K. Modjarrad, *Handbook of Polymer Applications in Medicine and Medical Devices*. Elsevier, (2014).

[7] A. Patil and M. S. Ferritto, “Polymers for personal care and cosmetics: Overview,” *ACS Symp. Ser.*, 1148, 3–11, (2013).

[8] P. K. Chidambaram and R. Ramakrishanan, “Manufacturing, Testing of Polymer Nanocomposite and Analysis of Tennis Racket Frame,” *Int. J. Eng. Tech. Innov.*, 4, 59–67, (2014).

[9] M. A. Ward and T. K. Georgiou, “Thermoresponsive polymers for biomedical applications,” *Polymers*, 3, 1215–1242, (2011).

[10] C. Peter and K. Kremer, “Multiscale simulation of soft matter systems – from the atomistic to the coarse-grained level and back,” *Soft Matter*, 5, 4357, (2009).

[11] L.-T. Yan and X.-M. Xie, “Computational modeling and simulation of nanoparticle self-assembly in polymeric systems: Structures, properties and external field effects,” *Prog. Polym. Sci.*, 38, 369–405, (2013).

[12] Y. Zhao, “Light-Responsive Block Copolymer Micelles,” *Macromolecules*, 45, 3647–3657, (2012).

[13] Q. Yan, Y. Xin, R. Zhou, Y. Yin, and J. Yuan, “Light-controlled smart nanotubes based on the orthogonal assembly of two homopolymers.,” *Chem. Commun.*, 47, 9594–9596, (2011).

[14] Y. Osada and J.-P. Gong, “Soft and Wet Materials: Polymer Gels,” *Adv. Mater.*, 10, 827–837, (1998).

[15] L. F. Boesel, C. Greiner, E. Arzt, and A. del Campo, “Gecko-Inspired Surfaces: A Path to Strong and Reversible Dry Adhesives,” *Adv. Mater.*, 22, 2125–2137, (2010).

[16] Y. Zhang, S. Furyk, D. E. Bergbreiter, and P. S. Cremer, “Specific Ion Effects on the Water Solubility of Macromolecules: PNIPAM and the Hofmeister Series,” *J. Am. Chem. Soc*, 127, 14505–14510, (2005).

[17] H. G. Schild, “POLY(*N*-ISOPROPYLACRYLAMIDE): EXPERIMENT, THEORY AND APPLICATION,” *Prog. Polym. Sci.*, 17, 163–249, (1992).

[18] M. Heskins and J. E. Guillet, “Solution Properties of Poly(*N*-isopropylacrylamide),” *J. Macromol. Sci. Chem*, A2, 1441–1455, (1968).

[19] C. Chevillard and L. D. P. Chimie, “Phase separation of aqueous solution of methylcellulose,” *Colloid Polym. Sci.*, 275, 537–545, (1997).

[20] Y. Maeda, H. Yamauchi, and T. Kubota, “Confocal micro-raman and infrared spectroscopic study on the phase separation of aqueous poly(2-(2-methoxyethoxy)ethyl (meth)acrylate) solutions.,” *Langmuir*, 25, 479–482, (2009).

[21] J. Seuring and S. Agarwal, “Polymers with upper critical solution temperature in aqueous solution,” *Macromol. Rapid Commun.*, 33, 1898–1920, (2012).

[22] F. Liu and M. W. Urban, “Recent advances and challenges in designing stimuli-responsive polymers,” *Prog. Polym. Sci.*, 35, 3–23, (2010).

[23] H. Yang, H. Zhu, M. M. R. M. Hendrix, N. J. H. G. M. Lousberg, G. De With, a. C. C. Esteves, and J. H. Xin, “Temperature-triggered collection and release of water from fogs by a sponge-like cotton fabric,” *Adv. Mater.*, 25, 1150–1154, (2013).

[24] D. Roy, J. N. Cambre, and B. S. Sumerlin, “Future perspectives and recent advances in stimuli-responsive materials,” *Prog. Polym. Sci.*, 35, 278–301, (2010).

[25] K. Kataoka, K. S. Glenn, M. Yokoyama, T. Okano, and Y. Sakurai, “Block copolymer micelles as vehicles for drug delivery,” *J. Control. Release*, 24, 119–132, (1993).

[26] Y. Kumashiro, M. Yamato, and T. Okano, “Cell attachment-detachment control on temperature-responsive thin surfaces for novel tissue engineering.,” *Ann. Biomed. Eng.*, 38, 1977–1988, (2010).

[27] E. Gil and S. Hudson, “Stimuli-reponsive polymers and their bioconjugates,” *Prog. Polym. Sci.*, 29, 1173–1222, (2004).

[28] O. H. Kwon, A. Kikuchi, M. Yamato, Y. Sakurai, and T. Okano, “Rapid cell sheet detachment from Poly(*N*-isopropylacrylamide)-grafted porous cell culture membranes,” *Cell*, 15–17, (1999).

[29] Z. Tang and T. Okano, “Recent development of temperature-responsive surfaces and their application for cell sheet engineering,” *Regen. Biomater.*, 1, 91–102, (2014).

[30] D. L. Huber, R. P. Manginell, M. a Samara, B.-I. Kim, and B. C. Bunker, “Programmed adsorption and release of proteins in a microfluidic device.,” *Science*, 301, 352–4, (2003).

[31] D. J. Beebe, J. S. Moore, J. M. Bauer, Q. Yu, R. H. Liu, C. Devadoss, and B.-H. Jo, “Functional hydrogel structures for autonomous flow control inside microfluidic channels,” *Nature*, 404, 588–590, (2000).

[32] J. S. Lee, W. Zhou, F. Meng, D. Zhang, C. Otto, and J. Feijen, “Thermosensitive hydrogel-containing polymersomes for controlled drug delivery.,” *J. Control. Release*, 146, 400–8, (2010).

[33] J. E. Chung, M. Yokoyama, M. Yamato, T. Aoyagi, Y. Sakurai, and T. Okano, “Thermo-responsive drug delivery from polymeric micelles constructed using block copolymers of poly(*N*-isopropylacrylamide) and poly(butylmethacrylate).,” *J. controlled release : official journal of the Controlled Release Society*, 62, 115–27, Nov-1999.

[34] K. Kataoka, A. Harada, and Y. Nagasaki, “Block copolymer micelles for drug delivery:

design, characterization and biological significance.," *Adv. Drug Deliv. Rev.*, 47, 113–131, (2001).

[35] M. Nakayama, "Thermoresponsive polymeric materials for drug delivery systems," *Drug Deliv. Syst.*, 23, 627–636, (2008).

[36] J. Kost and R. Langer, "Responsive polymeric delivery systems.," *Adv. Drug Deliv. Rev.*, 46, 125–148, (2001).

[37] D. Schmaljohann, "Thermo- and pH-responsive polymers in drug delivery.," *Adv. Drug Deliv. Rev.*, 58, 1655–1670, (2006).

[38] A. Kikuchi and T. Okano, "Pulsatile drug release control using hydrogels," *Adv. Drug Deliv. Rev.*, 54, 53–77, (2002).

[39] V. Aseyev, H. Tenhu, and F. M. Winnik, "Non-ionic Thermoresponsive Polymers in Water," *Adv. Polym. Sci.*, 242, 1–34, (2012).

[40] J. Seuring, F. M. Bayer, K. Huber, and S. Agarwal, "Upper Critical Solution Temperature of Poly (*N*-acryloyl glycinamide) in Water : A Concealed Property," *Macromolecules*, 45, 374–384, (2012).

[41] P. Flory and J. Osterheld, "Intrinsic viscosities of Polyelectrolytes. Poly(acrylic acid)," *J. Phys. Chem.*, 58, 653–661, (1954).

[42] N. Shimada, H. Ino, K. Maie, M. Nakayama, A. Kano, and A. Maruyama, "ureido-derivatized polymers based on both poly (allylurea) and poly (l-citrulline) exhibit UCST-type phase transition behavior under physiologically relevant conditions," *Biomacromolecules*, 12, 3418–3422, (2011).

[43] T. Aoki, K. Nakamura, K. Sanui, A. Kikuchi, T. Okano, Y. Sakurai, and N. Ogata, "Adenosine-induced changes of the phase transition of poly (6-(acryloyloxymethyl) uracil) aqueous solution," *Polymer Journal*, 31. 1185–1188, 1999.

[44] H. Schafer-Soenen, R. Moerkerke, H. Berghmans, and R. Koningsveld, "Zero and Off-Zero Critical Concentrations in Systems Containing Polydisperse Polymers with Very High Molar Masses . 2 . The System Water-Poly(vinyl methyl ether)," *Macromolecules*, 30, 410–416, (1997).

[45] Y. Maeda, "IR Spectroscopic Study on the Hydration and the Phase Transition of Poly(vinyl methyl ether) in Water," *Langmuir*, 17, 1737–1742, (2001).

[46] B. Sun, H. Lai, and P. Wu, "Integrated microdynamics mechanism of the thermal-induced phase separation behavior of poly(vinyl methyl ether) aqueous solution.," *J. Phys. Chem. B*, 115, 1335–46, (2011).

[47] Y. Maeda, T. Nakamura, and I. Ikeda, "Change in Solvation of Poly(*N*,*N*-diethylacrylamide) during Phase Transition in Aqueous Solutions As Observed by IR Spectroscopy," *Macromolecules*, 35, 10172–10177, (2002).

[48] L. Shen and G. Zhang, "Formation of Mesoglobules By Poly(*N*,*N*-Diethylacrylamid)," *Chinese J. Polym. Sci.*, 27, 561–567, (2009).

[49] C. Hashimoto, A. Nagamoto, T. Maruyama, N. Kariyama, Y. Irisa, A. Ikehata, and Y. Ozaki,

"Hydration States of Poly(*N*-isopropylacrylamide) and Poly(*N*,*N*-diethylacrylamide) and Their Monomer Units in Aqueous Solutions with Lower Critical Solution Temperatures Studied by Infrared Spectroscopy," *Macromolecules*, 46, 1041–1053, (2013).

[50] M. Itakura, K. Inomata, and T. Nose, "Aggregation behavior of poly (*N*,*N*-diethylacrylamide) in aqueous solution," *Polymer.*, 41, 8681–8687, (2000).

[51] X. Pang and S. Cui, "Single-chain mechanics of poly(*N*,*N*-diethylacrylamide) and poly(*N*-isopropylacrylamide): comparative study reveals the effect of hydrogen bond donors.," *Langmuir*, 29, 12176–82, (2013).

[52] D. G. Lessard, M. Ousalem, and X. X. Zhu, "Effect of the molecular weight on the lower critical solution temperature of poly(*N*,*N*-diethylacrylamide) in aqueous solutions," *Can. J. Chem.*, 79, 1870–1874, (2001).

[53] Y. Lu, K. Zhou, Y. Ding, G. Zhang, and C. Wu, "Origin of hysteresis observed in association and dissociation of polymer chains in water.," *Phys. Chem. Chem. Phys.*, 12, 3188–3194, (2010).

[54] C. S. Biswas, V. K. Patel, N. K. Vishwakarma, V. K. Tiwari, B. Maiti, P. Maiti, M. Kamigaito, Y. Okamoto, and B. Ray, "Effects of Tacticity and Molecular Weight of Poly(*N* -isopropylacrylamide) on Its Glass Transition Temperature," *Macromolecules*, 44, 5822–5824, (2011).

[55] Y. Grohens, L. Hamon, G. Reiter, a. Soldera, and Y. Holl, "Some relevant parameters affecting the glass transition of supported ultra-thin polymer films," *Eur. Phys. J. E*, 8, 217–224, (2002).

[56] Y. Grohens, M. Brogly, C. Labbe, M.-O. David, and S. Jacques, "Poly(methyl methacrylate) at Interfaces," *Langmuir*, 14, 2929–32, (2002).

[57] A. Razavi and J. L. Atwood, "Preparation and crystal structures of the complexes (n5-C5H4CPh2-n5-C13H8)MCl2 (M = Zr, Hf) and the catalytic formation of high molecular weight tacticity syndiotctic polypropylene," *J. Organomet. Chem.*, 459, 117–123, (1993).

[58] S. Cimmino, E. Di Pace, E. Martuscelli, and C. Silvestre, "Syndiotactic polystyrene: crystallization and melting behaviour," *Polymer*, 32, 1080–1083, (1991).

[59] H. Tsuji, Y. Tezuka, S. K. Saha, M. Suzuki, and S. Itsuno, "Spherulite growth of l-lactide copolymers: Effects of tacticity and comonomers," *Polymer*, 46, 4917–4927, (2005).

[60] C. Derosa and F. Auriemma, "Structure and physical properties of syndiotactic polypropylene: A highly crystalline thermoplastic elastomer," *Prog. Polym. Sci.*, 31, 145–237, (2006).

[61] Y. Katsumoto, N. Kubosaki, and T. Miyata, "Molecular approach to understand the tacticity effects on the hydrophilicity of poly(*N*-isopropylacrylamide): solubility of dimer model compounds in water.," *J. Phys. Chem. B*, 114, 13312–13318, (2010).

[62] E. Autieri, E. Chiessi, A. Lonardi, G. Paradossi, and M. Sega, "Conformation and dynamics of poly(*N*-isopropyl acrylamide) trimers in water: A molecular dynamics and metadynamics simulation study," *J. Phys. Chem. B*, 115, 5827–5839, (2011).

[63] T. Hirano, H. Miki, M. Seno, and T. Sato, “Effect of polymerization conditions on the syndiotactic-specificity in radical polymerization of *N*-isopropylacrylamide and fractionation of the obtained polymer according to the stereoregularity,” *Polymer*, 46. 5501–5505, (2005).

[64] B. Ray, Y. Okamoto, M. Kamigaito, M. Sawamoto, K. Seno, S. Kanaoka, and S. Aoshima, “Effect of Tacticity of Poly(*N*-isopropylacrylamide) on the Phase Separation Temperature of Its Aqueous Solutions,” *Polym. J.*, 37, 234–237, (2005).

[65] Y. Maeda, T. Higuchi, and I. Ikeda, “Change in Hydration State during the Coil−Globule Transition of Aqueous Solutions of Poly(*N*-isopropylacrylamide) as Evidenced by FTIR Spectroscopy,” *Langmuir*, 16, 7503–7509, (2000).

[66] Y. Maeda, H. Yamamoto, and I. Ikeda, “Phase Separation of Aqueous Solutions of Poly(*N*-isopropylacrylamide) Investigated by Confocal Raman Microscopy,” *Macromolecules*, 36, 5055–5057, (2003).

[67] Y. Maeda, T. Nakamura, and I. Ikeda, “Changes in the Hydration States of Poly(*N*-*n* -propylmethacrylamide) and Poly(*N*-isopropylmethacrylamide) during Their Phase Transitions in Water Observed by FTIR Spectroscopy,” *Macromolecules*, 34, 8246–8251, (2001).

[68] Y. Maeda, “Hydration of temperature-responsive polymers observed by IR spectroscopy,” *Macromol. Symp.*, 303, 63–70, (2011).

[69] Y. Ono and T. Shikata, “Hydration and dynamic behavior of poly(*N*-isopropylacrylamide)s in aqueous solution: a sharp phase transition at the lower critical solution temperature.,” *J. Am. Chem. Soc.*, 128, 10030–1, (2006).

[70] T. Shoji, R. Nohara, N. Kitamura, and Y. Tsuboi, “A method for an approximate determination of a polymer-rich-domain concentration in phase-separated poly(*N*-isopropylacrylamide) aqueous solution by means of confocal Raman microspectroscopy combined with optical tweezers,” *Anal. Chim. Acta*, 854, 118–121, (2015).

[71] H. Kojima and F. Tanaka, “Cooperative Hydration Induces Discontinuous Volume Phase Transition of Cross-Linked Poly(*N*-isopropylacrylamide) Gels in Water,” *Macromolecules*, 43, 5103–5113, (2010).

[72] Y. Okada and F. Tanaka, “Cooperative Hydration, Chain Collapse, and Flat LCST Behavior in Aqueous Poly(*N*-isopropylacrylamide) Solutions,” *Macromolecules*, 38, 4465–4471, (2005).

[73] M. Füllbrandt, E. Ermilova, A. Asadujjaman, R. Hölzel, F. F. Bier, R. von Klitzing, and A. Schönhals, “Dynamics of linear poly(*N*-isopropylacrylamide) in water around the phase transition investigated by dielectric relaxation spectroscopy.,” *J. Phys. Chem. B*, 118, 3750–9, (2014).

[74] P. G. De Gennes, “Kinetics of collapse for a flexible coil,” *J. Phys. Lettres*, 46, 639–642, (1985).

[75] A. Y. Grosberg and D. V Kuznetsov, “Single-chain collapse or precipitation - kinetic diagram

of the states of a polymer-solution," *Macromolecules*, 26, 4249–4251, (1993).

[76] A. Y. Grosberg, S. K. Nechaev, and E. I. Shakhnovich, "The role of topological constraints in the kinetics of collapse of macromolecules," *J. Phys. Fr.*, 49, 2095–2100, (1988).

[77] B. Sun, Y. Lin, P. Wu, and H. W. Siesler, "A FTIR and 2D-IR Spectroscopic Study on the Microdynamics Phase Separation Mechanism of the Poly (*N*-isopropylacrylamide) Aqueous Solution," *Macromolecules*, 41, 1512–1520, (2008).

[78] K. Kubota, S. Fujishige, and I. Ando, "Solution properties of poly(*N*-isopropylacrylamide) in water," *Polym. J.*, 22, 15–20, (1990).

[79] M. M. I. Press and F. M. Winnik, "Fluorescence Studies of Aqueous Solutions of Poly (*N*-isopropylacrylamide) below and above Their LCST," *Macromolecules*, 23, 233–242, (1990).

[80] Y. Matsumura and K. Iwai, "Fluorescence Probe Studies of Thermosensitive −Isopropylacrylamide Copolymers in Aqueous Solutions," *Polymer*, 46, 10027–10034, (2005).

[81] K. Van Durme, G. Van Assche, and B. Van Mele, "Kinetics of Demixing and Remixing in Poly(*N*-isopropylacrylamide)/Water Studied by Modulated Temperature DSC," *Macromolecules*, 37, 9596–9605, (2004).

[82] P. V. Yushmanov, I. Furó, and I. Iliopoulos, "Kinetics of Demixing and Remixing Transitions in Aqueous Solutions of Poly(*N*-isopropylacrylamide): A Temperature-Jump 1H NMR Study," *Macromol. Chem. Phys.*, 207, 1972–1979, (2006).

[83] J. Xu, Z. Zhu, S. Luo, C. Wu, and S. Liu, "First observation of two-stage collapsing kinetics of a single synthetic polymer chain," *Phys. Rev. Lett.*, 96, 1–4, (2006).

[84] A. Suzuki and T. Tanaka, "Phase transition in polymer gels induced by visible light," *Nature*, 346, 345–347, (1990).

[85] Y. Tsuboi, Y. Yoshida, N. Kitamura, and K. Iwai, "Phase transition dynamics of fluorescent-labeled poly(*N*-isopropylacrylamide) in aqueous solution as revealed by time-resolved spectroscopy combined with a laser T-jump technique," *Chem. Phys. Lett.*, 468, 42–45, (2009).

[86] Y. Tsuboi, Y. Yoshida, K. Okada, and N. Kitamura, "Phase separation dynamics of aqueous solutions of thermoresponsive polymers studied by a laser T-jump technique.," *J. Phys. Chem. B*, 112, 2562–2565, (2008).

[87] H. Inoue, K. Katayama, K. Iwai, A. Miura, and H. Masuhara, "Conformational relaxation dynamics of a poly(N-isopropylacrylamide) aqueous solution measured using the laser temperature jump transient grating method.," *Phys. Chem. Chem. Phys.*, 14, 5620–7, (2012).

[88] X. Ye, Y. Lu, L. Shen, Y. Ding, S. Liu, G. Zhang, and C. Wu, "How Many Stages in the Coil-to-Globule Transition of Linear Homopolymer Chains in a Dilute Solution?," *Macromolecules*, 40, 4750–4752, (2007).

[89] Y. Lu, X. Ye, J. Li, C. Li, and S. Liu, "Kinetics of laser-heating-induced phase transition of poly(*N*-isopropylacrylamide) chains in dilute and semidilute solutions.," *J. Phys. Chem. B*,

115, 12001–12006, (2011).

[90] L. Stryer, “Fluorescence Spectroscopy of Proteins,” *Science*, 162, 526–533, (1968).

[91] P.J. Sadkowski and G.R. Fleming, “The influence of solvent—solute interaction on radiationless processes: Excited state dynamics of 1,8-anilinonaphthalene sulphonate and related molecules,” *Chem. Phys.*, 54, 79–89, (1980).

[92] PerkinElmer, “An Introduction to fluorescence spectroscopy,” *Microchem. J.*, 65, 353, (2000).

[93] D. J. McDougall, “Some factors influencing fluorescence in minerals,” *Am. Mineral.*, 37, 427–437, (1952).

[94] A. Stelmaszewski, “The contribution of fluorescence to measurements of light scattering in oil-in-water emulsions,” *Oceanologia*, 53, 549–564, (2011).

[95] K. Belsrey and M. G. Sceats, “The overtone oh stretching raman spectrum of liquid water,” *Chem. Phys. Lett.*, 70, 504–507, (1980).

[96] Y. Matsumura and K. Iwai, “Synthesis and thermo-responsive behavior of fluorescent labeled microgel particles based on poly(*N*-isopropylacrylamide) and its related polymers,” *Polymer*, 46, 10027–10034, (2005).

[97] Y. Matsumura and K. Iwai, “Thermo-responsive behavior and microenvironments of poly(*N*-isopropylacrylamide) microgel particles as studied by fluorescent label method,” *J. Colloid Interface Sci.*, 296, 102–109, (2006).

[98] D. H. Turner, G. W. Flynn, and S. K. Lundberg, “Dimerization of Proflavin by the Laser Raman Temperature-Jump Method,” *Nature*, 235, 215–217, (1972).

[99] D. H. Turner, G. W. Flynn, N. Sutin, and J. V. Beitz, “Laser Raman Temperature-Jump Study of the Kinetics of the Triiodide Equilibrium. Relaxation Times in the 10-8-10-7 Second Range,” *J. Am. Chem. Soc*, 1078, 1554–1559, (1972).

[100] J. Frank and J. F. Holzwarth, “Application of Iodine-laser Temperature Jump to an Irreversible Enzyme Reaction,” *J. Chem. Soc. Faraday Trans.*, 90, 3201–3202, (1994).

[101] C. M. Phillips, Y. Mizutani, and R. M. Hochstrasser, “Ultrafast thermally induced unfolding of RNase A.,” *Proc. Natl. Acad. Sci. U. S. A.*, 92, 7292–7296, (1995).

[102] R. H. Callender, R. B. Dyer, R. Gilmanshin, and W. H. Woodruff, “Fast events in protein folding: the time evolution of primary processes.,” *Annu. Rev. Phys. Chem.*, 49, 173–202, (1998).

[103] R. Gilmanshin, R. H. Callender, and R. B. Dyer, “The core of apomyoglobin E-form folds at the diffusion limit.,” *Nat. Struct. Biol.*, 5, 363–365, (1998).

[104] R. M. Ballew, J. Sabelko, and M. Gruebele, “Direct observation of fast protein folding: the initial collapse of apomyoglobin.,” *Proc. Natl. Acad. Sci. U. S. A.*, 93, 5759–5764, (1996).

[105] R. Gilmanshin, S. Williams, R. H. Callender, W. H. Woodruff, and R. B. Dyer, “Fast events in protein folding: relaxation dynamics of secondary and tertiary structure in native apomyoglobin.,” *Proc. Natl. Acad. Sci. U. S. A.*, 94, 3709–3713, (1997).

[106] R. Callender, “Probing protein dynamics using temperature jump relaxation spectroscopy,”

Curr. Opin. Struct. Biol., 12, 628–633, (2002).

[107] I. P. Clark, G. M. Greetham, M. Towrie, and A. W. Parker, "Developing a temperature-jump apparatus for the Ultra laser system," *LASERS Sci. Facil. Program.*, 169–170, (2009).

[108] G. Pabst, M. Rappolt, and H. Amenitsch, "X-ray kinematography of temperature-jump relaxation probes the elastic properties of fluid bilayers," *Langmuir*, 16, 8994–9001, (2000).

[109] J. A. Curcio and C. C. Petty, "The near infrared absorption spectrum of liquid water," *J. Opt. Sos. Am. A*, 41, 302–304, (2011).

[110] D. Madge and M. W. Windsor, "Picosecond internal conversion in crystal violet," *Chem. Phys. Lett.*, 24, 144–148, (1974).

[111] S. Kirincic, "Viscosity of aqueous solutions of poly(ethylene glycol)s at 298.15 K," *Fluid Phase Equilib.*, 155, 311–325, (1999).

[112] O. Borodin, D. Bedrov, and G. D. Smith, "Concentration Dependence of Water Dynamics in Poly(Ethylene Oxide)/Water Solutions from Molecular Dynamics Simulations," *J. Phys. Chem. B*, 106, 5194–5199, (2002).

[113] R. Hoogenboom, H. M. L. Thijs, M. J. H. C. Jochems, B. M. van Lankvelt, M. W. M. Fijten, and U. S. Schubert, "Tuning the LCST of poly(2-oxazoline)s by varying composition and molecular weight: alternatives to poly(*N*-isopropylacrylamide)?," *Chem. Commun.*, 5758–5760, (2008).

[114] Y. Akagi, T. Katashima, Y. Katsumoto, K. Fujii, T. Matsunaga, U. Chung, M. Shibayama, and T. Sakai, "Examination of the Theories of Rubber Elasticity Using an Ideal Polymer Network," *Macromolecules*, 44, 5817–5821, (2011).

[115] R. Pamies, K. Zhu, A.-L. Kjøniksen, and B. Nyström, "Thermal response of low molecular weight poly-(*N*-isopropylacrylamide) polymers in aqueous solution," *Polym. Bull.*, 62, 487–502, (2008).

[116] E. E. Dormidontova, "Influence of End Groups on Phase Behavior and Properties of PEO in Aqueous Solutions," *Macromolecules*, 37, 7747–7761, (2004).

[117] Y. Isobe, D. Fujioka, S. Habaue, and Y. Okamoto, "Efficient Lewis acid-catalyzed stereocontrolled radical polymerization of acrylamides.," *J. Am. Chem. Soc*, 123, 7180–7181, (2001).

[118] B. Ray, Y. Isobe, K. Morioka, S. Habaue, and Y. Okamoto, "Polymerization in the Presence of Lewis Acid," *Society*, 543–545, (2003).

[119] B. Ray, Y. Isobe, K. Morioka, S. Habaue, Y. Okamoto, M. Kamigaito, and M. Sawamoto, "Synthesis of Isotactic Poly(*N*-isopropylacrylamide) by RAFT Polymerization in the Presence of Lewis Acid," *Macromolecules*, 36, 543–545, (2003).

[120] J. F. Quinn, E. Rizzardo, and T. P. Davis, "Ambient temperature reversible addition–fragmentation chain transfer polymerization," *Chem. Commun.*, 1044–1045, (2001).

[121] C. Schilli, "Novel Precursors for Polymer-Protein Conjugate Synthesis via Reversible Addition-Fragmentation Chain Transfer Polymerization," 2003.

[122] S. Fujishige, K. Kubota, and I. Ando, "Phase Transition of Aqueous Solutions of

Poly(N-isopropylacrylamide) and Poly(N-isopropylmethacrylamide)," *J. Phys. Chem.*, 93, 3311–3313, (1989).

[123] R. Gomes de Azevedo, L. P. N. Rebelo, A. M. Ramos, J. Szydlowski, H. C. de Sousa, and J. Klein, "Phase behavior of (polyacrylamides + water) solutions: concentration, pressure and isotope effects," *Fluid Phase Equilib.*, 185, 189–198, (2001).

[124] M. Heskins and J. E. Guillet, "Solution Properties of Poly(*N*-isopropylacrylamide)," *J. Macromol. Sci. Chem*, A2, 1441–1455., (1968).

[125] A. Milewska, J. Szydlowski, and L. P. N. Rebelo, "Viscosity and ultrasonic studies of poly(*N*-isopropylacrylamide)-water solutions," *J. Polym. Sci. Part B Polym. Phys.*, 41, 1219–1233, (2003).

[126] F. Afroze, E. Nies, and H. Berghmans, "Phase transitions in the system poly(*N*-isopropylacrylamide)/water and swelling behaviour of the corresponding networks," *j. Mol. Struct.*, 554, 55–68, (2000).

[127] L. P. N. Rebelo, Z. P. Visak, H. C. De Sousa, J. Szydlowski, R. Gomes De Azevedo, a. M. Ramos, V. Najdanovic-Visak, M. N. Da Ponte, and J. Klein, "Double critical phenomena in (water + polyacrylamides) solutions," *Macromolecules*, 35, 1887–1895, (2002).

[128] B. Chu, Q. Ying, and A. Y. Grosberg, "Two-Stage Kinetics of Single-Chain Collapse. Polystyrene in Cyclohexane," *Macromolecules*, 28, 180–189, (1995).

[129] Y. Nakamura, N. Sasaki, and M. Nakata, "Chain Aggregation Process of Poly(methyl methacrylate) in the Mixed Solvent," *Macromolecules*, 35, 1365–1372, (2002).

[130] Y. Tsuboi, M. Nishino, T. Sasaki, and N. Kitamura, "Poly(*N*-isopropylacrylamide) microparticles produced by radiation pressure of a focused laser beam: a structural analysis by confocal Raman microspectroscopy combined with a laser-trapping technique.," *J. Phys. Chem. B*, 109, 7033–9, (2005).

[131] M. Ishikawa, H. Misawa, N. Kitamura, and H. Masuhara, "Poly(*N*-isopropylacrylamide) Microparticle Formation in Water by Infrared Laser-Induced Photo-Thermal Phase Transition.," *Chem. Lett.* 481–484, 1993.

[132] P. C. Ashok and K. Dholakia, "Optical trapping for analytical biotechnology," *Curr. Opin. Biotechnol.*, 23, 16–21, (2012).

[133] T. Sugiyama, K. I. Yuyama, and H. Masuhara, "Laser trapping chemistry: From polymer assembly to amino acid crystallization," *Acc. Chem. Res.*, 45, 1946–1954, (2012).

[134] A. Ashkin, "Acceleration and Trapping of Particles by Radiation Pressure," *Phys. Rev. Lett.*, 24, 156–159, (1970).

[135] A. Ashkin, "Applications of laser radiation pressure.," *Science*, 210, 1081–1088, (1980).

[136] J. S. Park and K. Kataoka, "Comprehensive and accurate control of thermosensitivity of poly(2-alkyl-2-oxazoline)s via well-defined gradient or random copolymerization," *Macromolecules*, 40, 3599–3609, (2007).

[137] H. Y. Liu and X. X. Zhu, "Lower critical solution temperatures of *N*-substituted acrylamide," *Polymer*, 40, 6985, (1999).

[138] A. K. Dasmahapatra, G. Kumaraswamy, and H. Nanavati, “Collapse transition in random copolymer solutions,” *Macromolecules*, 39, 9621–9629, (2006).

[139] M. Siu, C. He, and C. Wu, “Formation of Mesoglobular Phase of Amphiphilic Copolymer Chains in Dilute Solution: Effect of Comonomer Distribution,” *Macromolecules*, 36, 6588–6592, (2003).

[140] T. Hirano, A. Ono, H. Yamamoto, T. Mori, Y. Maeda, M. Oshimura, and K. Ute, “Effect of composition and stereoregularity on phase-transition behavior of aqueous *N*-ethylacrylamide/*N*-*n*-propylacrylamide copolymer solutions,” *Polymer*, 54, 5601–5608, (2013).

[141] B. Xue, L. Gao, Y. Hou, Z. Liu, and L. Jiang, “Temperature controlled water/oil wettability of a surface fabricated by a block copolymer: Application as a dual water/oil on-off switch,” *Adv. Mater.*, 25, 273–277, (2013).

[142] K. Nishi, T. Hiroi, K. Hashimoto, K. Fujii, Y. Han, T.-H. Kim, Y. Katsumoto, and M. Shibayama, “SANS and DLS Study of Tacticity ffects on Hydrophobicity and Phase Separation of Poly(*N*‑isopropylacrylamide),” *Macromolecules*, 46, 6225–6232, (2013).

[143] B. Ray, Y. Isobe, K. Matsumoto, S. Habaue, Y. Okamoto, M. Kamigaito, and M. Sawamoto, “RAFT Polymerization of N-Isopropylacrylamide in the Absence and Presence of Y(OTf)3: Simultaneous Control of Molecular Weight and Tacticity,” *Macromolecules*, 37, 1702–1710, (2004).

[144] S. J. Lord, H. D. Lee, and W. E. Moerner, “Single-molecule spectroscopy and imaging of biomolecules in living cells.,” *Anal. Chem.*, 82, 2192–203, (2010).

[145] Y. Katsumoto and N. Kubosaki, “Tacticity Effects on the Phase Diagram for Poly (*N*-isopropylacrylamide) in Water,” *Macromolecules*, 41, 5955–5956, (2008).

[146] S. Nakano, T. Ogiso, R. Kita, N. Shinyashiki, S. Yagihara, M. Yoneyama, and Y. Katsumoto, “Thermoreversible gelation of isotactic-rich poly(*N*-isopropylacrylamide) in water.,” *J. Chem. Phys.*, 135, 114903, (2011).

[147] B. Ferse, S. Richter, F. Eckert, A. Kulkarni, C. M. Papadakis, and K.-F. Arndt, “Gelation mechanism of poly(*N*-isopropylacrylamide)-clay nanocomposite hydrogels synthesized by photopolymerization.,” *Langmuir : the ACS journal of surfaces and colloids*, 24. 12627–35, 04-Nov-2008.

[148] F. Wang, Y. Shi, S. Luo, Y. Chen, and J. Zhao, “Conformational Transition of Poly(*N*‑isopropylacrylamide) Single Chains in Its Cononsolvency Process: A Study by Fluorescence Correlation Spectroscopy and Scaling Analysis,” *Macromolecules*, 45, 9196, (2012).

[149] R. Raccis, R. Roskamp, I. Hopp, B. Menges, K. Koynov, U. Jonas, W. Knoll, H.-J. Butt, and G. Fytas, “Probing mobility and structural inhomogeneities in grafted hydrogel films by fluorescence correlation spectroscopy,” *Soft Matter*, 7, 7042, (2011).

[150] J.-F. Lutz, D. Neugebauer, and K. Matyjaszewski, “Stereoblock Copolymers and Tacticity Control in Controlled/ Living Radical Polymerization,” *J. Am. Chem. Soc*, 125, 6986–6993, (2003).

[151] S. Hietala, M. Nuopponen, K. Kalliomäki, and H. Tenhu, "Thermoassociating Poly (*N*-isopropylacrylamide) A-B-A Stereoblock Copolymers," *Macromolecules*, 41, 2627–2631, (2008).

[152] M. Nuopponen, K. Kallioma, A. Laukkanen, H. Tenhu, and S. Hietala, "A – B – A Stereoblock Copolymers of *N* -Isopropylacrylamide," *J. Polym. Sci. Part A Polym. Chem.*, 46, 38–46, (2007).

[153] M. Nuopponen, K. Kallioma, V. Aseyev, and H. Tenhu, "Spontaneous and Thermally Induced Self-Organization of A - B - A Stereoblock Polymers of *N*-Isopropylacrylamide in Aqueous Solutions," *Macromolecules*, 41, 4881–4886, (2008).

[154] T. Mori, T. Hirano, A. Maruyama, Y. Katayama, T. Niidome, Y. Bando, K. Ute, S. Takaku, and Y. Maeda, "Syndiotactic poly(*N*-*n*-propylacrylamide) shows highly cooperative phase transition.," *Langmuir*, 25, 48–50, (2009).

[155] T. Hirano, K. Nakamura, T. Kamikubo, S. Ishii, K. Tani, T. Mori, and T. Sato, "Hydrogen-bond-assisted syndiotactic-specific radical polymerizations of *N*-alkylacrylamides: The effect of the*N*-substituents on the stereospecificities and unusual large hysteresis in the phase-transition behavior of aqueous solution of syndiotactic poly(*N*-isopropylacrylamide)," *J. Polym. Sci. Part A: Polym. Chem.*, 46. 4575–4583, (2008).

[156] T. Hirano, A. Morikami, Y. Fujioka, and K. Ute, "Effect of a combination of hexamethylphosphoramide and alkyl alcohol on the stereospecificity of radical polymerization of *N*-isopropylacrylamide," *Polymer*, 52, 629–634, (2011).

[157] T. Hirano, H. Miki, M. Seno, and T. Sato, "Direct synthesis of syndiotactic-rich poly(*N*-isopropylacrylamide) via radical polymerization of hydrogen-bond-complexed monomer," *Polymer*, 46, 3693–3699, (2005).

[158] O. B. Tiktopulo, E. I.; Bychkova, V. E.; Ricka, J.; Ptitsyn, "Cooperativity of the Coil-Globule Transition in a Homopolymer: Microcalorimetric Study of Poly(*N*-isopropylacrylamide," *Macromolecules*, 27, 2879–2882, (1994).

[159] N. Badi, D. Chan-Seng, and J. F. Lutz, "Microstructure control: An underestimated parameter in recent polymer design," *Macromol. Chem. Phys.*, 214, 135–142, (2013).

[160] Y. Maeda and M. Yamabe, "A unique phase behavior of random copolymer of *N*-isopropylacrylamide and *N*,*N*-diethylacrylamide in water," *Polymer*, 50, 519–523, (2009).

[161] H. Kojima and F. Tanaka, "Nonlinear depression of the lower critical solution temperatures in aqueous solutions of thermo-sensitive random copolymers," *J. Polym. Sci. Part B Polym. Phys.*, 51, 1112–1123, (2013).

[162] M. Keerl and W. Richtering, "Synergistic depression of volume phase transition temperature in copolymer microgels," *Colloid Polym. Sci.*, 285, 471–474, (2007).

[163] C. H. Hofmann, F. a. Plamper, C. Scherzinger, S. Hietala, and W. Richtering, "Cononsolvency revisited: Solvent entrapment by *N*-isopropylacrylamide and *N*,*N* -diethylacrylamide microgels in different water/methanol mixtures," *Macromolecules*, 46, 523–532, (2013).

Publication list

Publications

[1] Tsuboi Y., Tada T., Shoji T., Kitamura N., "Phase-Separation Dynamicsof Aqueous Poly (N-isopropylacrylamide) Solutions: Characteristic Behavior of the Molecular Weight and Concentration", *Macromolecular Chemistry and Physics*, vol. 213, pp. 1879-1884, **2012**. (Chapter 3)

[2] Tada T., Katsumoto Y., Goossens K., Uji-i H., Hofkens J., Shoji T., Kitamura N., Tsuboi Y., "Accelerating the Phase Separation in Aqueous Solutions by Slight Modification of the Polymer Stereoregularity: A Single Molecule Fluorescence Study", *The Journal of Physical Chemistry C*, vol. 117, pp. 10818-10824, **2013**. (Chapter 4)

In preparation

[3] Tada T., Hirano T., Ute K., Katsumoto Y., Shoji T., Kitamura N., Tsuboi Y., "Phase separation dynamics of aqueous syndiotactic-rich PNIPAM solutions", to be submitted (Chapter 5)

Publications (written in Japanese)

[4] 多田貴則, 喜多村 舜, 東海林 竜也, 坪井泰之、「レーザー温度ジャンプ型透過光計測法による温度応答性高分子水溶液の相分離ダイナミクス」、*高分子論文集*、DOI: 10.1295

Abstract (written in Japanese)

代表的な温度応答性高分子であるポリ(*N*-イソプロピルアクリルアミド) (PNIPAM) は水中で温度変化に応じて構造が変化するが、その構造変化には以下の 4 つの段階が含まれると考えられている。1) 室温以下の温度では、PNIPAM 鎖は水和したコイル型の構造をとり均一に溶解しており、水溶液は透明である。2) 水溶液の温度が下限臨界溶液温度（LCST、PNIPAM 水溶液の場合は ≈32 °C）を超えると、PNIPAM 鎖と水との水素結合が崩壊し脱水和が起こる。 3) 脱水和した PNIPAM 鎖は広がったコイル型から収縮したグロビュール型へと高次構造が変化する (coil-globule 転移)。4) グロビュール型の PNIPAM 鎖は拡散と鎖間の衝突を経て疎水性相互作用により凝集する結果、水リッチ相と高分子リッチ相へと相分離し、高分子リッチ相が光を散乱するため水溶液は白濁する。これらの現象に対して、構造変化に関する知見はこれまで豊富に蓄積されてきたが、現象を特徴づける重要なパラメータの一つである相分離速度に関する知見は十分に得られていない。相分離速度の解析は、相分離機構の解明に資するだけではなく、温度応答性高分子を基盤とした新規材料開発に向けた重要な指針になる。本研究では、PNIPAM 水溶液の相分離の動的過程を明らかにする手法として「レーザー温度ジャンプ型過渡透過光計測法」を導入した。その上で、相分離速度がどのような因子に依存しているのかを解明することを目的として、相分離挙動を支配する重要な因子である高分子の濃度、分子量、および立体規則性が相分離速度や高分子の高次構造に及ぼす影響を明らかにすると共に、実験結果から相分離機構を考察した。

温度ジャンプ法は集光パルスレーザー光（ヒートパルス光、波長（λ） = 1200 nm, fwhm ≈ 10 ns） による水の OH 伸縮振動の励起による局所的な熱発生に基づいている。レーザー光照射領域の温度ジャンプに要する時間はヒートパルス光のパルス幅と同程度である。相分離に伴う PNIPAM 水溶液の濁度上昇を、ヒートパルス光の中心に導入したプローブ光（λ = 532 nm）の透過光強度の時間減衰を解析することにより相分離速度を求めることができる。

第 1 章では研究の背景と目的を述べると共に、第 2 章では温度ジャンプ法等の実験手法の概略を述べた。第 3 章では、PNIPAM 水溶液の相分離速度を特徴付ける最も基本的なパラメータである PNIPAM の濃度と分子量の効果について検討した結果を述べている。分子量 28,000 ~ 93,000 の PNIPAM を用いた場合、相分離速度は分子量によらず濃度増加に伴い速くなり、ある臨界濃度以上で一定値に収束した。濃度増加に伴う相分離速度の加速は、高分子鎖間の平均距離が短くなることにより、相転移により生成したグロビュール鎖が凝集するのに必要な拡散距離が短くなり、結果的に相分離が速くなる事を明らかにした。一方、分子量 75,000～93,000 の領域においては、分子量の増加に伴い相分離速度は遅くなるが、分子量 28,000～75,000 の領域においては分子量の増加につれて相分離速度が速くなることを見出した。すなわち、PNIPAM 水溶液の相分離は分子量 75,000 程度で最速になる。高分子量領域においては、分子量の増加とともに高分子の流体力学的半径が大きくなり、

凝集する際の拡散速度は遅くなると考えられる。したがって、分子量 75,000 以上で観測された分子量増加に伴う相分離速度の増加は高分子鎖の拡散が遅くなるためであると結論できる。一方、低分子量領域における挙動については、分子量の低下により凝集する高分子のサイズが小さくなり、プローブレーザー光を散乱するまでに要する時間が長くなるため、結果的に相分離が遅く観測されたものと考えられる。

第４章においては、46%～55%の meso 二連子比（isotacticity）を有する PNIPAM を合成し、その相分離速度を比較した結果について述べている。その結果、高分子濃度によらず isotacticity の増加に伴い相分離が速くなることを明らかにした。isotactic-rich PNIPAM 水溶液は LCST 以下においてもマイクロメートルスケール以上の高分子ネットワークを形成することを単一分子蛍光イメージングにより確認し、この高分子ネットワークが凝集体の前駆体となって相分離を加速することを明らかにした。さらに、LCST 以上においては高分子リッチドメインが成長し、高分子鎖の並進拡散運動が凍結した物理ゲルを形成することも見出した。

第５章においては、meso 比を 46%から 32%まで減少させた syndiotactic-rich PNIPAM 水溶液の相分離挙動について述べている。syndiotactic-rich PNIPAM 水溶液は、ある高分子濃度以上においてのみ高速な相分離を示した。syndiotactic-rich PNIPAM はコイル鎖から脱水和する際に分子内水素結合を協同的に形成することで疎水性が高まり、その高い疎水性によって相分離が加速されることを明らかにした。また、このような現象はグロビュール鎖の拡散を経ずに高分子が凝集する高濃度領域においてのみ観測されることも明らかにした。

第６章では、本研究の結論と研究の展望について述べている。本研究では PNIPAM 水溶液の相分離速度が PNIPAM の濃度、分子量、立体規則性に大きく依存することを明らかにした。また、濃度、分子量、立体規則性が高分子鎖の構造に及ぼす影響についても調べ、相分離速度の知見と総合的に考察することにより、PNIPAM 水溶液の温度応答相分離機構を提案した。今後、本研究で得られた知見が刺激応答性高分子に基づく新規材料開発に資することを期待する。